AUBURN

SAMUEL GINN COLLEGE OF ENGINEERING

Research Report

CELLULAR CONFINEMENT APPROACH FOR THE IMPROVEMENT OF SEDIMENT BASIN EFFECTIVENESS

Submitted to

Highway Research Center

Prepared by

Jose G. Vasconcelos, Timothy D. Simpson and Jue Wang

MARCH 2018

Highway Research Center
Harbert Engineering Center
Auburn, Alabama 36849

1. **Report No.** IR-18-01	2. **Government Accession No.**	3. **Recipient Catalog No.**	
4. **Title and Subtitle** CELLULAR CONFINEMENT APPROACH FOR THE IMPROVEMENT OF SEDIMENT BASIN EFFECTIVENESS		5. **Report Date** 02/23/2018	
		6. **Performing Organization Code**	
7. **Author(s)** Jose G. Vasconcelos, Timothy D. Simpson and Jue Wang		8. **Performing Organization Report No.** IR-18-01	
9. **Performing Organization Name and Address** Highway Research Center Department of Civil Engineering 238 Harbert Engineering Center Auburn, AL 36849		10. **Work Unit No. (TRAIS)**	
		11. **Contract or Grant No.**	
12. **Sponsoring Agency Name and Address** Highway Research Center Department of Civil Engineering 238 Harbert Engineering Center Auburn, AL 36849		13. **Type of Report and Period Covered**	
		14. **Sponsoring Agency Code**	
15. **Supplementary Notes**			

16. **Abstract**

Sediment basins provide quiescent conditions that enable settling of fine particles, mitigating environmental impacts created by excessive sediment discharges. However, settled particles are susceptible to undesired resuspension if during dewatering of the basin new flows are admitted, increasing velocities, shear forces, and turbulence near the basin bottom. A very simple idea, which has never been attempted in the context of sediment and erosion control, is to create a method by which particles can settle at the bottom of basins and be shielded from background flows and turbulent eddies. This condition can be attained by means of sediment confinement, which is similar to the concept of cellular confinement systems (CCS). This study presents results from an investigation of the benefits of confinement cells as a lining strategy for the bottom of sediment basins. Characteristics of effluents in an experimental apparatus representing the bottom of sediment basins were studied for varying geometries of confinement cells and flow conditions. As anticipated, a significant decrease in effluent turbidity was reported with the use of cellular confinement cells, with smaller cell widths as a key parameter to reduce outflow turbidity. Also, a non-dimensional Resuspension Parameter RP was proposed that related well cell geometry and intra-cell flow velocity for the tested soil. Computational Fluid Dynamics modeling was used to determine which geometries were more likely to succeed in decreasing turbulence and shear within confinement cells.

17. **Key Words** Erosion, sediment, environmental impact, cellular confinement cells		18. **Distribution Statement** No restrictions.	
19. **Security Classification (of this report)** Unclassified	20. **Security Classification (of this page)** Unclassified	21. **No. of pages** 88	22. **Price**

Research Report - DRAFT

CELLULAR CONFINEMENT APPROACH FOR THE IMPROVEMENT OF SEDIMENT BASIN EFFECTIVENESS

Submitted to

Highway Research Center

Prepared by

Jose G. Vasconcelos, Timothy D. Simpson and Jue Wang

MARCH 2018

DISCLAIMERS

The contents of this report reflect the views of the authors, who are responsible for the facts and the accuracy of the data presented herein. The contents do not necessarily reflect the official views or policies of Auburn University. This report does not constitute a standard, specification, or regulation.

NOT INTENDED FOR CONSTRUCTION, BIDDING, OR PERMIT PURPOSES

Jose G. Vasconcelos

Research Supervisor

ACKNOWLEDGEMENTS

ABSTRACT

Sediment basins provide quiescent conditions that enable settling of fine particles, mitigating environmental impacts created by excessive sediment discharges. However, settled particles are susceptible to undesired resuspension if during dewatering of the basin new flows are admitted, increasing velocities, shear forces, and turbulence near the basin bottom. A very simple idea, which has never been attempted in the context of sediment and erosion control, is to create a method by which particles can settle at the bottom of basins and be shielded from background flows and turbulent eddies. This condition can be attained by means of sediment confinement, which is similar to the concept of cellular confinement systems (CCS). This study presents results from an investigation of the benefits of confinement cells as a lining strategy for the bottom of sediment basins. Characteristics of effluents in an experimental apparatus representing the bottom of sediment basins were studied for varying geometries of confinement cells and flow conditions. As anticipated, a significant decrease in effluent turbidity was reported with the use of cellular confinement cells, with smaller cell widths as a key parameter to reduce outflow turbidity. In addition, a non-dimensional Resuspension Parameter RP was proposed that related well cell geometry and intra-cell flow velocity for the tested soil. Computational Fluid Dynamics modeling was used to determine which geometries were more likely to succeed in decreasing turbulence and shear within confinement cells.

Table of Contents

LIST OF TABLES

LIST OF FIGURES

CHAPTER 1 - INTRODUCTION

1.1. SOIL EROSION: BACKGROUND, IMPACTS AND QUANTIFICATION

Soil erosion is a complex phenomenon that is also determined by interactions between the flowing water and the soil. Soil erosion is primarily influenced by the properties of the soil itself and water movement (Utley 2008). Soil erosion is a natural process that is highly variable both spatially and temporally (Nachtergaele 2002) and is increased if the natural vegetation, even if just short grasses, is removed, since exposed topsoil can be dislodged by shear forces created by water or wind. Soil types respond differently to disturbances, and can be generally categorized as cohesive and non-cohesive types. Non-cohesive soils typically tend to erode as individual grains of sediment. Cohesive soils, on the other hand, tend to erode as groups of particles, or aggregates, and its chemical constitution can be a relevant factor in erosion (Osman 1988; Langendoen 2000). A summary of research into the erosion of cohesive soils can be found in Knapen (2007).

Various types of human activities (e.g. construction projects, agricultural land use), lead to soil erosion, which in turn lead to a series of impacts. In agricultural areas, soil erosion causes adverse impacts both on-site where erosion takes place, as the in-situ soil is degraded, and to areas surrounding the eroding soil that receive potentially destructive sediment loads with rainfall. On-site impacts may include land management difficulties, with potentially damaging rills and gullies, damage to sensitive crops, and removal of nutrients from once-fertile top soil. Rills are ephemeral incisions, or shallow channels, that can be repaired by soil tilling. Gullies are larger than rills and if not addressed quickly, become relatively permanent and represent the most severe of channel erosion phenomena (Di Stefano 2013; Posen 1996). Off-site impacts could include blockages of drainage systems of natural waterways by eroded sediment, water pollution, and damage to infrastructure due to sediment-laden flooding (Posthumus et al. 2015).

One of the greatest sources of sediment created by erosion due to rainfall is linked to construction site activities. Typically, when a new plot is to be prepared for construction, the earth must be leveled to support the foundation of a structure. This process often requires significant earthwork in a system called land grading. When the earth is moved and excavated, the natural in-situ soils that were naturally compacted over time become disturbed, and individual grains or aggregates of sediment are more easily dislodged by natural processes such as wind and rains. As storms and rainfall come, a potential for damaging erosion presents itself.

Sediment particles suspended in construction site runoff are regarded as potential hazards to the environment. In particular, fine sediments may frequently carry toxic-laden particles that impact receiving water bodies and ecosystems. High sediment concentration limits sunlight penetration and may prohibit

growth of aquatic plants (Aryal & Lee 2009). These sediments can also cover fish spawning grounds and bring sediment-bound pollutants such as heavy metals, salts, and organics with negative implications for water quality preservation (Mehta et al. 1989b; Ravisangar 2001) and to aquatic species (City of Calgary 2011). Past investigations (Hunt 2001; Fan 2003; Rohrer 2004) showed that sediment from a non-compliant construction site can create a decreased Index of Biotic Integrity (IBI), and Modified Index of Well-being (MIwb), which are scientific tools to classify water pollution, as well as decreased pebble count, and limited stream aquatic life due to habitat degradation. Important research is being undertaken to understand the sources and central impacts of sediment-laden water in receiving bodies of water.

Quantifying the quality of flowing water and effluent with sediments present can be of critical significance. There are several commonly used methods of determining this character of water. Arguably, the most commonly used method of determining general water quality is obtaining its turbidity. Turbidity is an optical water quality parameter and can be determined by colored material in water such as dyes, or particles in water. Turbidity is most commonly measured in units of nephelometric turbidity units (NTU), this term comes from the process of nephelometry, which is a 90-degree light scattering technique using white light as opposed to infrared light. Turbidity measurement units, or probes, measure the degree to which light is scattered by the particles that are suspended in water or another liquid. Measuring turbidity is known as a somewhat subjective indicator of water quality (Grayson 1996). It can be difficult to directly correlate turbidity data from one measurement device to another, so consistency is necessary across a single experiment (Gippel 1989), as is illustrated in Figure 1, which shows a wide range of turbidity values.
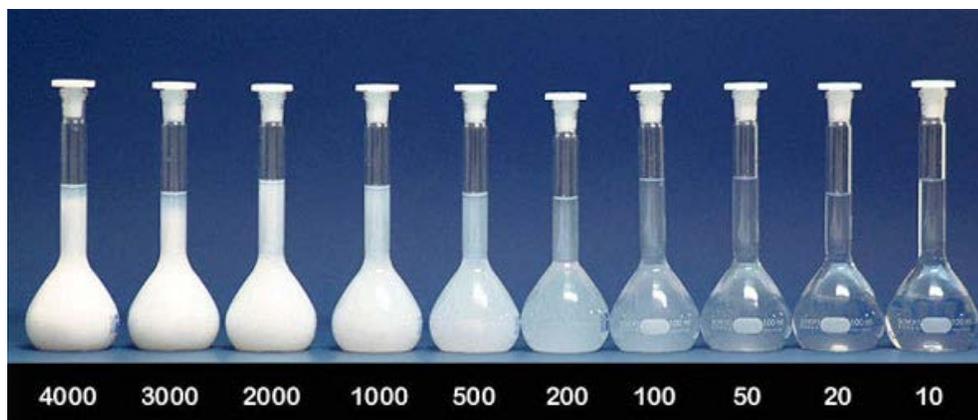
Figure 1- Turbidity standards used to calibrate turbidimeters and visualize turbidity values. Reference: Optek.com/index.asp

A primary cause of turbidity is the presence of suspended solids in water samples. Total suspended solids (TSS) is a water quality parameter that is related to turbidity and is defined as the concentration (mass per volume) of solids larger than 2 microns, whether inorganic or organic, that are suspended in water. These solids can include wastes, silts, algae, or plankton; and they all absorb light (EPA 2012b). These solids can flow into lakes or reservoirs from streams and rivers as seen in Figure 2.

Figure 2 - Water with high sediment concentration entering Tuscaloosa Lake. Reference: City of Tuscaloosa, Alabama

TSS can be directly assessed by weight once a sample of water is filtered and then dried using, for instance, the US Environmental Protection Agency (EPA) method 160.2 (EPA 1999). Although TSS measurements directly characterize the amount of suspended solids in water samples, such measurements are more time-consuming than turbidity measurements. In a comprehensive study of 5000 square kilometers of catchment area, Grayson (1996) found through general relationships across a wide range of flows that turbidity might be used as a surrogate measure of TSS. Grayson also found that there is no statistically significant difference between slopes of TSS measurements and turbidity measurements in sediment load estimation. In the study of a site in North Carolina by Line and White (2001), turbidity and TSS data taken from effluent samples indicated a relatively strong 1-to-1 relationship between turbidity and TSS. Following a best-fit line for the two variables, an $R^2 = 0.96$ linear correlation was found. Line and White also found that this relationship between TSS and turbidity decreases somewhat if there exist appreciable amounts of organic material on a site, making it soil-dependent.

1.2. Erosion and sediment control techniques

Construction sites are very prone to be sources of environmental impacts (King and Blanton 2011; Holland 2004) for various reasons, including sediment discharges generated in rainfall events. In geographical areas where precipitation is frequent or severe, or where there already exist local conditions for moderate to severe soil erosion due to poor land maintenance practices or steep slopes, careful attention must be given in deploying erosion and sediment control strategies to control such sediment discharges. Land that is disturbed by construction activities typically has soil erosion rates that are 2 to 40,000 times greater than pre-construction rates (Harbor 1999).

Several management practices (BMPs) are used to prevent sediment erosion that are widely implemented. These are referred to as erosion and sediment control (ESC) practices. These practices often involve structural devices or non-structural practices. Non-structural practices, typically including pollution prevention, storm water management, and vegetated buffers (EPA 2004), are not the focus of the present

work. Structural devices include silt fences, sand bags, fiber rolls, waterbars, collector channels, and other devices that are examples of perimeter control and protective BMPs (EPA 2012a; Parker 2014). These BMPs may deter sediment concentrated waters from having erosive impacts. Of these perimeter control devices, the silt fence is perhaps the most widely implemented to mitigate the discharge of sediment. Perimeter control BMPs will not in themselves prevent soil erosion (Harbor et a. 1995), but soil stabilization practices, such as the introduction of plant life, can be deployed to prevent initial eroding of soil.

Figure 3 - Deployed silt fences and sand bags. Reference: Bellseedstore.us(left) diversifiedlandscape.com/wp (right)

Figure 4 - Sediment-laden water from site with overwhelmed silt fence draining to sewer. Reference: environment.arlington.us/2014/07/see

Other practices temporarily detain sediment-laden runoff, and through gradual dewatering, allow for settling of sediments in quiescent conditions. These BMP's include sediment basins that may have features such as baffles installed which spread the flow across the width of the basin and increase sediment deposition within the basin (ALDOT 2014). The basic operating function of sediment basins is to temporarily store, in large volumes, surface runoff water. This water may otherwise quickly flow away from construction sites, or parking lots, or steeply sloped areas, polluting receiving waters, or causing erosion (Bidelspach and Jarrett 2004). These basins release collected water slowly, allowing for large amounts of sediment carried by the water to settle out within the basin itself, and they are useful alongside perimeter control BMPs and other practices within and around the construction site. Sediment basins vary greatly in size according to local conditions and designs. Figure 5 shows sediment basins on a larger scale, whereas Figure 6 shows the general layout for a sediment basin and a photograph of an installed basin.

Figure 5 – Sediment basin in large construction site (top). Reference: thewalkercompany.com. Sediment basin full of turbid water (bottom). Reference: mdpi.com/water
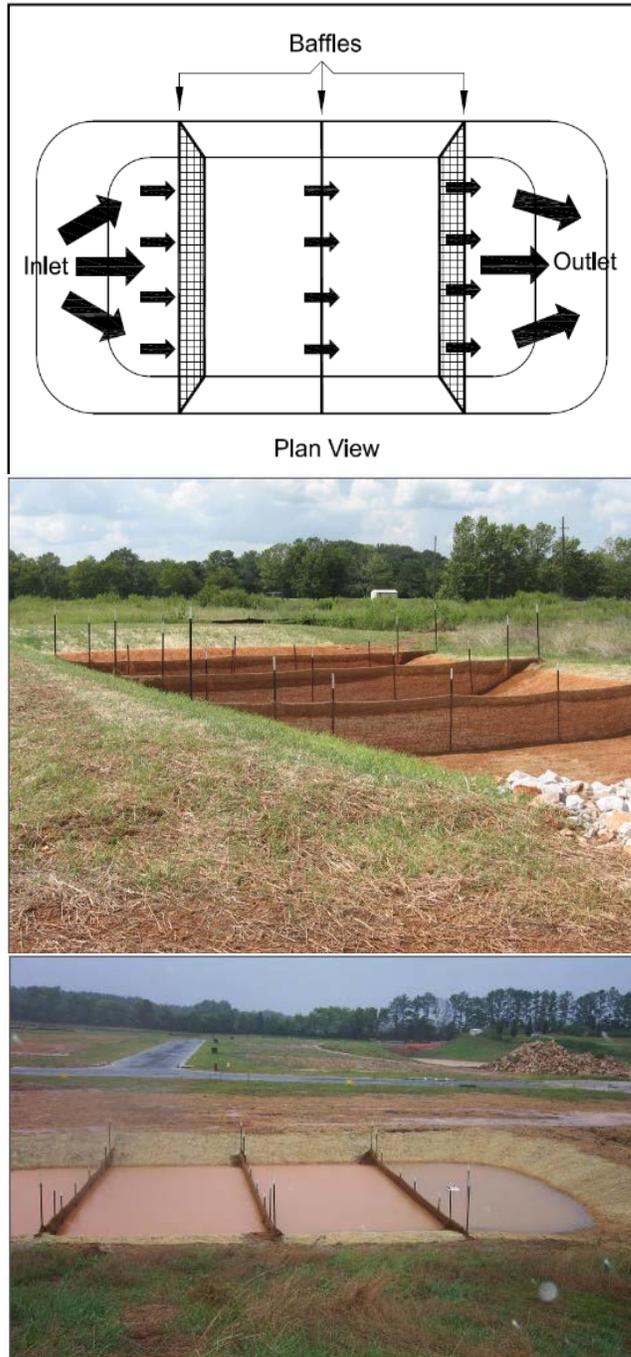
Figure 6 - General sediment basin design (top) empty sediment basin with baffles (middle) full sediment basin with baffles (bottom). Reference: ALDOT 2014

1.2. Factors influencing efficient sediment basin operation

It is important to note that even with practices to control erosion and sediment in construction sites, proper deployment, upkeep, and adequate maintenance is critical. In many cases, silt fences and sediment basins are installed incorrectly, are poorly maintained and thus have limited effectiveness. This potentially results in more problems than would have existed were there nothing in place to aid in either erosion or sediment control (Harbor 1999). If a basin is sized incorrectly, or the basin's slopes not properly managed, or outflow mechanisms not properly constructed, resulting harm could be environmentally damaging. Poor management practices could be very costly and have a negative effect on the environment. If sewerage systems become overwhelmed and clogged with sediment, or lakes and reservoirs receive excess sediment-laden flows and require dredging, these expenses can mount quickly and become staggering. Although they may not necessarily immediately affect developers or contractors, poorly installed or designed management practices may work for a short period of time before failure (Moore 1987).

The effectiveness of the operation of sediment basins depends on the settling processes of particles within them, which in turn are influenced by gravity, viscous drag, and inter-particle forces and interactions. Settling velocity is the single-most important property pertaining to sediment capture efficiency in these basins (Mehta et al. 1989a), since it influences sediment capture and effectiveness of sediments basins. Stokes law provides a mathematical approximation for the terminal velocity of an unhindered spherical object under laminar conditions. In the Stokes Equation 1 seen below, terminal velocity reached by a particle that is settling increases exponentially as the diameter of the particle increases.

$$V_S = \frac{g(s-1)d^2}{18\mu}$$

Equation 1

Where, V_s is the terminal velocity, g is the acceleration of gravity, s is the specific gravity of the suspended particle, d is the particle diameter and μ is the kinematic viscosity. Efficiency within a sediment basin is also directly correlated to the presence or absence of correctly installed and maintained protective practices upstream of the basin, such as silt fences and land management. In the field, properly functioning sediment basins have shown efficiencies of roughly 85% (Petterson 1999). This reported efficiency, however, varies among other investigations as shown in recent studies. McLaughlin et al. (2009) have shown that sediment control practices such as sediment basins removed approximately 35-60% of run-off sediments from construction sites. The efficiencies of detention basins and other erosion and sediment control measures vary per storm event length, intensity of related rainfall, topography of the site, soil type, and amount and type of vegetation coverage (Zech et al. 2014).

Basin volume is fundamental to the adequate performance of a sediment basin, and these are determined with a design rain event in consideration. A design rain event is typically the most intense rainfall a catchment area could likely experience within a certain period of years,. The longer the period, the greater the potential for a more intense rain event. Per ALDOT design standards for a sediment basin,

there is a 100m^3 requirement on volume of a basin per 4000 m^2 of disturbed area within the portion of a site that drains to the basin (ALDOT 2014). Other design considerations are displayed in the following Table 1:

Table 1 - Design criteria for a sediment basin constructed in Alabama. Reference: ALDOT 2014

Parameter	Value
Emergency Spillway	Trapezoidal spillway with non-erosive lining. 10-year, 24-hour rainfall event
Recommended Maximum Drainage Area	40,000m^2
Minimum Volume	100m^3 per 4000m^2 of drainage area
Minimum L/W Ratio	2:1
Minimum Depth	60cm
Dewatering Mechanism	Skimmer(s) or other approved basin dewatering devices
Dewatering Time	2-5 days
Baffles Required	3

However, a basin designed according to disturbed area alone may prove insufficient, depending on the site (Zech et al. 2014). A given construction site may experience such significant rainfall, or may have soil that absorbs hardly any water through infiltration, that it may require design considerations that incorporate the local conditions, going beyond the criteria given by ALDOT.

A large factor in sediment basin efficiency is the geometric ratio of effective flow length to effective flow width. It is recommended by the EPA that this ratio of effective flow length to effective flow width be greater than 2:1 (Madaras and Jarrett 2000). This ratio is used as the indicator to the flow-path length of the basin. The flow-path length of a basin is the necessary distance that the sediment-laden water must travel to the outlet of the basin. As this distance is increased, it provides more time for the sediment that is suspended in the water to settle out to the bottom of the basin, resulting in less sediment in the basins effluent. This ratio also prevents the sediment from short-circuiting the basin, and taking a direct route to the basin outlet. Chen (1975) concluded that to maximize efficiency of sediment basins, they should be constructed to be long and narrow. Recent research has emphasized that the surface area of a basin should be maximized to efficiently trap the sediment within it, and maintains that the flow length to width ratio should to be a minimum of 2:1 (ALDOT 2014).

Another method used to aid in the effectiveness of the sediment basins is the addition of a flocculant upstream in the site before the sediment basin. Flocculants act to promote aggregation, or coagulation of particles, that results in an increased settling velocity of particles of sediment that are suspended in water (McLaughlin et al. 2009). Settling velocity is the velocity with which a particle, or aggregated particles fall out of suspension in a liquid and approach the bottom of, in this case, the

sediment basin. Flocculants are currently used to reduce the transport of sediment in both construction sites and agricultural land plots (Sojka et al. 2007). The use of flocculants such as polyacrylamide (PAM) can effectively create particles that have median particle diameters of 7 to 9 times greater than untreated runoff sediment. In some cases, depending on characteristics of soil material, the use of flocculants allows for enhanced settling of suspended particles that justifies construction of smaller sized sediment basins (Kang et al. 2016).

Effluent limitation guidelines were proposed in 2009 by the EPA that regulated the effluent turbidity of sediment from construction sites (ADEM 2017). These regulations have since been removed and there are no current effluent limitations enforced by the federal government agencies (Serio, 2014). However, many local governments have enforced specific numerical limitations that construction sites and contractors must abide by. In Alabama, for example, the Alabama Departments of Environmental Management requires that effluent turbidity be less than 50 NTU's above the background turbidity levels for any waterbody with designated fish and wildlife use (Fang et al. 2015). If this limit is exceeded, the owner or contractor must halt work and address the problem until effluents are within acceptable limits (National Pollutant Discharge Elimination System 2015).

1.3. Turbulence and its impacts to sediment basin operation

Turbulence is of great significance within the context of ESC, particularly within sediment basins. Turbulence within a fluid is characterized by a chaotic environment of changes in both velocity and pressure. Hazen (1904), in developing an initial theory for particles settling in sediment basins, made a distinction between quiescent flow and turbulent flows in observations and testing of sediment basins. A non-dimensional number, called Reynolds number, provides quantification of the existence of turbulence, and the degree to which a fluid is or is not turbulent. Reynolds number is the ratio of inertial forces to the viscous forces and is a dimensionless quantity. There are functionally two general regimes in which flows exist across any context. The first is a laminar regime, which is characterized by a significantly low Reynolds number where flows are dominated by viscous forces. The second regime is turbulent flow which is characterized by a higher Reynolds number. Turbulent flows are dominated by inertial forces rather than viscous forces (Benson 2014).

Since laminar flows are controlled by viscous forces, fluid motion within a laminar flow regime will have a tendency to be smooth and move more predictably in regular paths. These regimes are bound by a Reynolds number of less than 2000. At each point in the fluid of a laminar regime, the velocity and pressure remain constant within a given layer. Laminar flow is prevalent only in situations in which a flow channel is small and/or the fluid movement is very slow or the fluid is viscous.

Turbulent flows are much more common within most civil engineering contexts. Turbulent flow regimes exist at Reynolds numbers that are greater than 2000. There is a transitionary phase when crossing from laminar to turbulent flow just under a Reynolds number of 2000; but once crossed, shear stresses at boundaries change abruptly which is an important indicator of a change of regimes (Viola and Leutheusser 2004). At the initiation of turbulent flow, eddy formation becomes visible and can be detected

in pipes with the introduction of particles such as sediment (Meisner 1963). Sediment basins are designed to minimize turbulence as much as possible. The more effectively a sediment basin avoids turbulent areas or conditions, the greater the potential for a sediment basin to effectively settle out sediments. There are, however, many conditions in which turbulent flows can arise within a sediment basin.

Sediment basins must first be equipped to minimize high flow velocities that may arise from intense rain events. If these high velocity waters are not handled properly, recirculation velocities can be established at basin surfaces that may cause the basins themselves to contribute to the sediment load of the site (Fennessey and Jarrett 1997). Turbulence acting within a basin can also act as a disruptor through turbulent diffusion that can negatively contribute to sediments settling, and lead to prolonged suspension (Graf 1971). The most common and practical measure within a basin to limit turbulence is the use of baffles. Baffles reduce the flow energy as well as reduce the turbulent forces within a basin (Thaxton 2004). The use of baffles to increase the L:W ratio also reduces short-circuiting within a basin and increase sediment trapping effectiveness in a correctly sized basin (Millen et al., 1997; Jarrett 1996). Short-circuiting within a basin is sediment-laden water taking the direct, shortest route to the outlet without adequate time in the basin for particle settling. As the purpose of a sediment basin is the removal of suspended sediments, typically providing a longer effective flow length will provide greater efficiencies of the basins, granted there are not turbulent eddies causing disruption of the particles within the basin. Eddies are chaotic disturbances and swirls in a flow field and are the fundamental basis for turbulence.

Sediments accumulate within a sediment basin when receiving runoff flows from a construction site. These flows are drained by the gradual dewatering in the basin. However, even this gradual process may potentially discharge sediment particles that were previously settled within the basin due to sediment resuspension. Sediment resuspension takes place in rivers, ponds, lakes, bays and in the massive scale of seas and oceans (Eadie, 1984). As the process involves particles once again entering suspension in the surrounding water, and not remaining in the bedform, resuspension can take place virtually anywhere sediment and conditions for turbulent eddies and vortices exist.

Sediments may become resuspended when new inflows that are admitted to a basin cause enough turbulence and agitation to dislodge fine particles within a basin. This resuspension involves creating enough velocity and shear stresses in the basin, which in turn can exceed a critical point and suspend particles that are already settled (Arulanandan et al. 1975). Significant aspects of related hydrodynamics, such as forces interacting with the basin storage water and the particles within it, also include wind over the water surface and waves, which can lead to turbulence and transport of large quantities of sediment (Krone 1979; Booth et al. 2000; Bentzen et al. 2009). The efficiency of sediment basins is thus affected by turbulence induced by a variety of sources leading to sediment resuspension.

Flow characteristics near the bed of sediment basins can also lead to resuspension of sediment particles. Bottom regions are designed to be smooth, which has been shown to yield smaller settling, or deposition rates, than in cases when there is increased small-scale roughness in the bed (Yager et al. 1993). The work of Braskeruf (2001), demonstrated that the addition of vegetation to the bottom of shallow

detention basins reduced resuspension of sediments. It was concluded that when flow velocities are low, detention time decreases with the density of vegetation due to the lack of resuspension that would otherwise take place (Jadhav and Buchberger 1995). Most sediment basins, however, do not incorporate vegetation along the bed, and NRCS (2010) only recommends establishing vegetation along the embankments of a sediment basin to protect them from erosion. Basins may also require dredging, in which accumulated sediment is collected from the basin bed, which, along with excessive amounts of sediment from runoff, is not conducive to vegetation health. Vegetation is most commonly used along embankments, channels, and ditches for stabilization purposes (UDFCD 2013, ALDOT 2014).

1.4. Summary

In summary, erosion is a natural process that causes sediment removal at much higher rates within areas in which there is exposed topsoil and disturbed vegetated cover, and these areas are very frequently created in construction sites (Perez 2014). Erosion control practices such as the use of rock, vegetation, and fiber rolls have proven extremely useful in mitigating the harm from excess sediment being dislodged from its natural locality. Sediment control practices, such as the use of sediment basins, flocculants, silt fences, and storm drain inlet protection are valuable practices that aid in limiting harm from sediment that has been previously eroded. There are helpful parameters to characterize the presence of sediment and other impurities in water, such as turbidity and TSS. Once sediment has entered a sediment control practice, it may not always escape during, using a sediment basin as an example, the slow dewatering, or draining phase. The sediment within a basin may then be subject to resuspension when flows become turbulent within a basin. Resuspension can also occur in other BMPs in construction sites, such as drainage ditches, sumps, forebays and is more widespread then within sediment basins alone. More innovation towards solutions to shield particles from turbulence and shear stresses created by water flows could be very beneficial in preventing this phenomenon of resuspension of sediments.

CHAPTER 2 - LITERATURE REVIEW

2.1. Approaches to improve sediment basin performance

The incorporation of sediment control devices within construction sites is not a recent development, however, innovation and research into many devices such the silt fence, storm drain inlet protection units, ditches and sediment basins continues to be undertaken (Perez 2014). Environmental concerns, safety hazards, protection of municipal and private property, and public sensitivity have all driven the continuation of these efforts in making sediment control devices more efficient and economical.

Sediment basins are widespread, and there has been extensive testing regarding their effectiveness to improve flow regimes and the overall performance of the basins (Jarrett 1996, Mclaughlin 2016). In a summary of guiding principles for sediment control surrounding sediment basins, Harbor (1999) developed various recommendations. These recommendations include fitting the development to site conditions, retaining as much existing vegetation as possible, minimizing bare soil exposure, using covers over disturbed areas, minimizing runoff velocity, trapping sediments on site, and designing outlets to be non-erosive, among others.

Many strategies, particularly within the basins, were successfully implemented to improve basin performance including:

- Altering the basin layout (Su et al. 2009),
- Creation forebays in which coarser sediments can settle
- Introduction of baffles (De Oliveira et al. 2011)
- Implementation of floating rafts that treat site runoff called floating treatment wetlands (Khan et al 2013; Farjood et al. 2015)
- Use of skimmers that drain from the water surface of a basin
- Optimizing inlet and outlet configurations (Bodin et al. 2012)
- Improvement of inflow channels just upstream of the sediment basins with a layer of riprap, or loose stone, to help control discharge from rain events (Fang et al. 2015).

In the seminal contribution by Hazen (1904), in which he explored particle settling, it was found that deposition increased with greater contact area between the bed of the sediment basin and the water in which the particles themselves are suspended. Increasing this contact area has been accomplished by methods such as the insertion of lamella plates, or settlers within the basins. These plates markedly increase the surface area with which particles may come into contact. Further testing has been undertaken by others regarding lamella plates (Culp et al. 1968; Yao 1973). Now, lamella settlers and clarifiers compromised of lamella plates are seeing widespread use in water purification processes.

Baffles are widely used to slow inflow velocities and thereby increase trap efficiency (Bhaduri et al. 1997). These baffles operate by means of either creating a longer flow path for sediment-laden water within a basin, or dividing the sediment basin into several bay areas by spanning the length of the basin to limit velocity of runoff inflow. Baffles, on the other hand, may perform some of both functions. Baffles act, in a sense, as general shock absorbers or dampeners to flow energies within a basin to limit turbulent flows that contribute to prolonged resuspension (Goldman et al. 1986), but there is a limit to their effectiveness. Garofalo (2012) extensively examined the effectiveness of baffles in applications varying from clarification to stormwater handling. Garofalo determined that higher numbers of baffles within a basin do not necessarily equate to greater deposition rates, rather there is a limit to their effectiveness that will not increase with excessive baffling. McLaughlin (2009) performed thorough studies of sediment basins with baffling and concluded that while solid baffles, such as those constructed of plywood, are effective in creating a longer effective flow length and increasing deposition with a basin, porous baffles such as jute and coir blankets are even more effective at improving deposition, alternatively spanning the width of the basin, and spreading the water flow over the entire width of the basin. Figure 7 and Figure 8 present sketches of solid and porous baffling strategies.
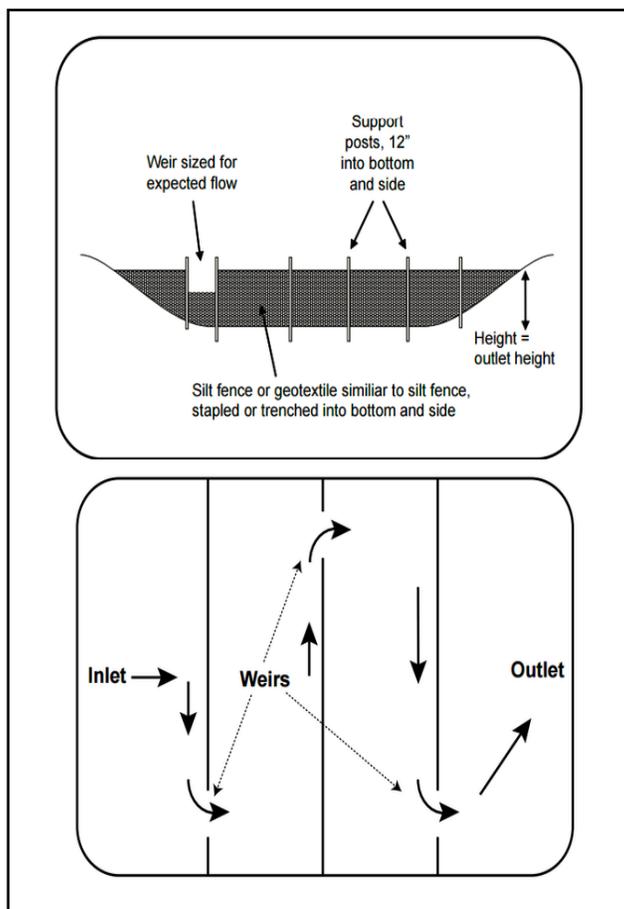
Figure 7 - Solid baffling to increase L:W ratio, cross section (top), and plan view (bottom) Reference: McLaughlin 2004
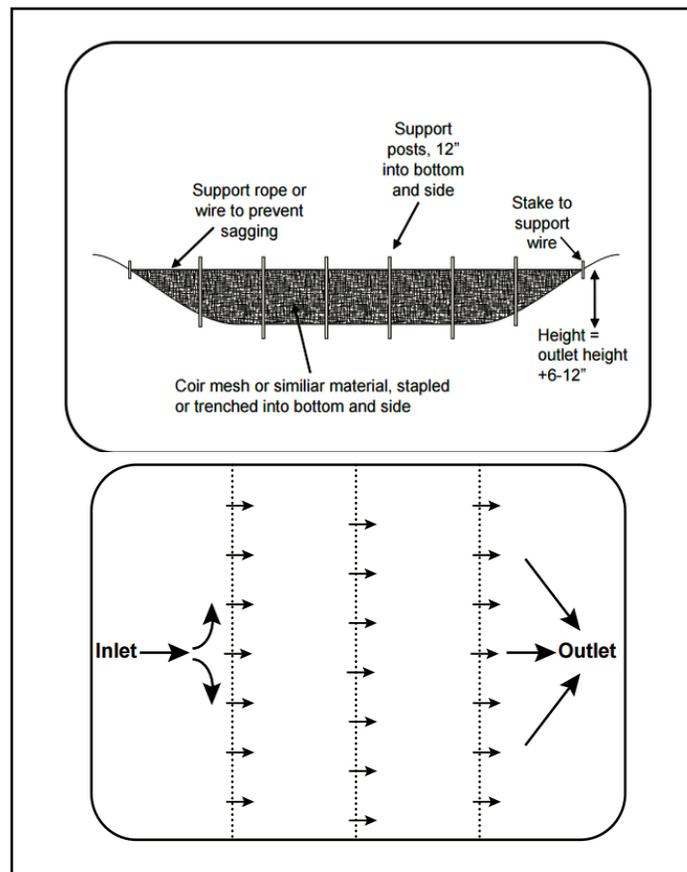
Figure 8 - Porous baffling for increased deposition, cross section (top), and plan view (bottom)
Reference: McLaughlin 2004

While there are many devices and systems used surrounding a sediment basin to help mitigate concentrated basin effluents, such as baffles and drainage skimmers, less is known about protective devices for sediments that are already settled within a basin. Most practices to limit highly turbulent effluent involve structures or flocculants before the basin, which are often necessary. However, there is limited research and testing concerning structures within a basin itself that aim to shield settled sediments from inflows, and continue to protect during draining periods. This deficit of information opens doors for some intriguing potentialities such as the effective mitigation of sediment resuspension.

2.2. Effects of bed roughness on sediment settling

An interesting new development has arisen from the practice of sediment control. The strategy to be discussed and examined in this work is that of cellular confinement. The premise of cellular confinement is to prevent resuspension of sediment particles and encourage the trapping efficiency of sediment basins by means of shielding small pockets of sediments from inflow and outflow velocities, as well as turbulent eddies.

This strategy takes the form of small structures placed in a laboratory experiment designed to mimic flow conditions at the bottom of sediment basins or draining swales leading to them. As previously discussed, turbulence is typically considered to adversely affect particle settling and cause potential resuspension. Cuthbertson et al. (1998) demonstrated experimentally that this adverse settling may not entirely be the case within the boundary layer settling region. This boundary layer is the layer nearest to the sediment within a channel or water system. Cuthbertson et al. (1998) found that the settling velocities of particles over a rough, porous bed within a turbulent flow regime were 2.5 times greater than the settling velocities in water that was quiescent. Cuthbertson et al. (1998) argued that this was due to eddies, or vortices, that captured particles from the high-speed flow area of the channel into the slower-speed flow area of the boundary layer.

In the region near a wall, or bed, of turbulent flows, bursting phenomena can be observed where slow-moving fluid is ejected outward from a wall boundary. These bursting phenomena contribute to the production of turbulence with the looping fluid structures they create (Lelouvetel et al. 2009; Robinson 1991). Such looping structures are characterized by vortices that entail sweeps and ejections that occur upstream, and downstream of the vortices, respectively. An ejection is a low-velocity fluid movement directed away from a wall, while a sweep is a high-speed fluid movement directed towards a wall (Hurther 2001; Adrian and Liu 2002). One of the first to suggest that these sweeps and ejections composing the bursting phenomena, could affect the transport of suspended sediments was Jackson (1976). Figure 9 illustrates the ejection and sweep processes over a boundary layer.
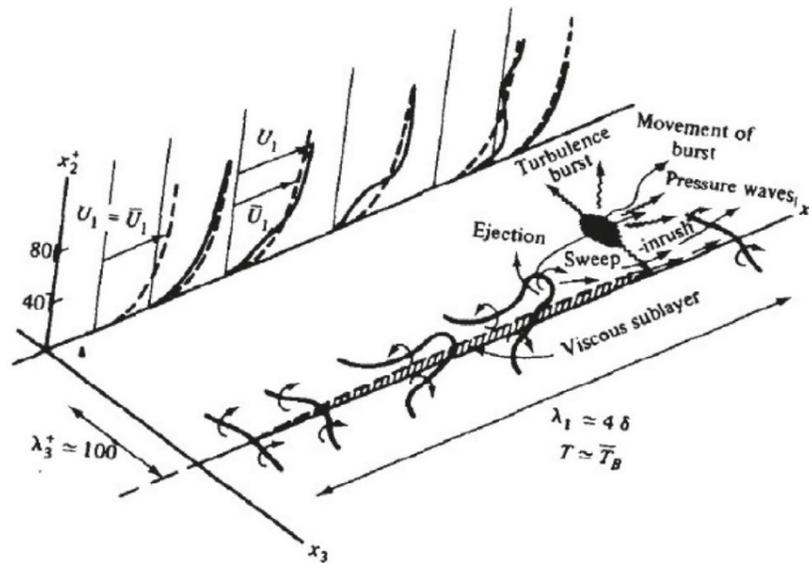
Figure 9 - Ejection, sweep, and bursting dynamics (Hinze 1979)

Marchioli and Soldati (2002) revealed that through these vortices, sweeps, and ejections provided for an efficient transfer mechanism for suspended particles. When a particle becomes caught up in a sweep toward a wall boundary (as described by Hurthur 2001), it is expected that it will continue in a sweep and approach the wall or boundary. The flow structure of the local surrounding fluid typically prevents particles

that have entered a boundary layer through a sweep to be ejected again to the fluid outside the wall layer (Pedinotti et al. 1992; Yager et al. 1993). Due to this process, deposition rates of sediment tend to be low with a hydraulically smooth bed, but with the presence of a rough boundary, i.e. through the introduction of rip-rap or gravel, deposition rates are increased substantially (He and Marsalek 2009).

2.3. Incipient motion

Sediment particles within a streambed, or any body of water, are subject to hydrodynamic forces. Incipient motion is a term used to describe a situation in which minimum conditions are met to dislodge individual sediment particles from a bed form, and its prediction is an important component in the analysis of sediment transport (Marsh et al. 2004). Groundbreaking work in incipient motion was introduced by Shields (1936) who posited a critical shear stress able to mobilize a particle relating to a specific grain size of sediment. Most investigators presently incorporate a modified form of a dimension-less parameter put forth by Shields called the Shields parameter that is seen below:

$$\tau_c^* = \frac{\tau_c}{(\rho_s - \rho)} g D_i$$

Equation 2

Where,

$$\tau_c^* = \text{Shields parameter (critical shear stress)}, \text{Pa}$$
$$\tau_c = \text{Critical shear stress at incipient motion}, \text{Pa}$$
$$\rho_s = \text{Sediment density}, \text{kg/m}^3$$
$$\rho = \text{Fluid desity}, \text{kg/m}^3$$
$$g = \text{Gravitational acceleration}, \text{m/s}^2$$
$$D_i = \text{Grain size}, \text{m}$$

Rather than provide with certainty the exact conditions for the mobilization of a specific grain size, the incipient motion determination is inherently statistical. Interactions between particles of different sizes are an important consideration as well. Larger coarse particles have a higher probability of being exposed to flow and finer particles are more likely to be sheltered by the coarse particles (Wu 2007). Incipient motion is influenced by turbulent velocities, shear forces, and bed material geometry and composition (Miller and Byrne 1966; Buffington et al. 1992).

While the Shields method investigates incipient motion by means of critical shear stress, other methods, such as Qin's (1980) equation, and Chen's (1992) method, are approaches based on critical average velocities. There have been different approaches proposed to represent the critical velocity that is associated with sediments of varying sizes. Among these methods, the method proposed by Qin (Yang 1993), is presented below:

$$U_{ck} = 0.786 \left(\frac{h}{d_{90}}\right)^{\frac{1}{6}} \sqrt{\frac{\gamma_s - \gamma}{\gamma} g d_k \left(1 + 2.5m \frac{d_m}{d_k}\right)}$$

Equation 3

$$m = 0.761 - \frac{0.680}{\left(\frac{d_{60}}{d_{10}} + 2.23\right)}$$

Equation 4

Where,

$$U_{ck} = \text{Critical average velocity for size class } k, m/s$$
$$h = \text{Flow depth, m}$$
$$d_{90} = \text{Sediment diameter under which 90\% of sample lies, m}$$
$$\gamma_s = \text{Specific weight of sediment, kN/m}^3$$
$$\gamma = \text{Specific weight of water, kN/m}^3$$
$$d_k = \text{Diameter of size class } k, \text{ m}$$
$$m = \text{Compactness of non} - \text{uniform bed material}$$
$$d_m = \text{Arithmetic mean of bed material, m}$$

2.4. INTRODUCTION TO CELLULAR CONFINEMENT STRATEGY TO IMPROVE SETTLING

Recently, He and Marsalek (2014) studied the effects of a bottom grid structure (Figure 10) with the purpose of improving suspended solids removal by introducing a downward vertical vortex force and reducing disturbances of the bottom settled sediment. This work presented an investigation focused on settling effectiveness and protection of sediments. The authors attempted to create vortex structures that would enhance settling, while simultaneously avoiding resuspension. The bottom grid structure proposed by He and Marsalek was positioned in the bottom of a settling tank that was approximately 2.5 m (L) x 1.5 m (W) x 0.4 m (D). The bottom grid structures used were similar in shape to the cellular confinement systems initially proposed by the US Army Corps of Engineers, used in the context of soil improvement and erosion control (Webster and Watkins 1977). Below, in Figure 10, are two separate bottom grid structures used for He and Marsalek's testing. Figure 11 displays the laboratory apparatus used by He and Marsalek to carry out their experiments.
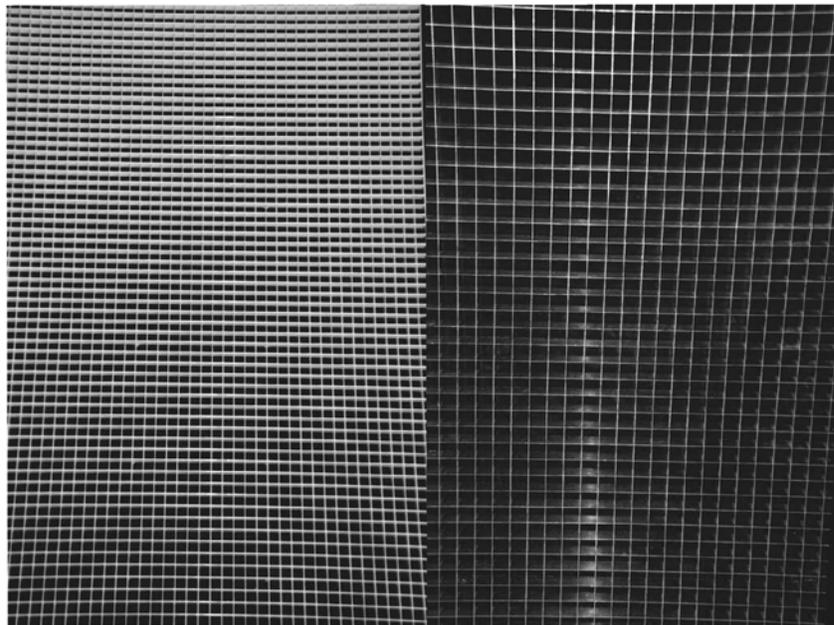
Figure 10 – Bottom grid structure from He and Marsalek (2014)
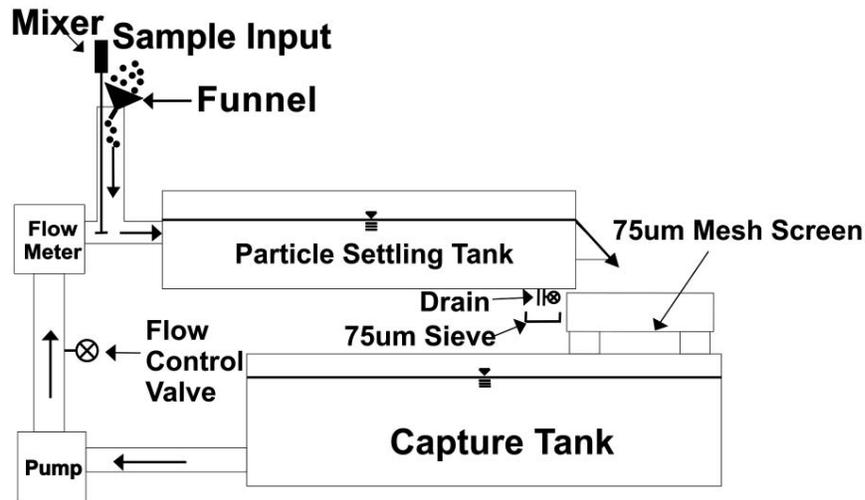
Figure 11 - Schematic of laboratory set-up used by He and Marsalek (2014)

The experimental procedure of He and Marsalek's test included adding crushed material, with small density and large size, via a funnel to a metered amount of water, mixing it in a slurry. This slurry was then pumped into a corner of the settling tank at the location of the inlet. After running its course through the settling tank, the effluent would drain from an opening at the far end of the tank. From here the sediment-laden water, to allow only for the circulation of clean water, would be filtered through a 75-micron screen before draining to the capture tank which acted as a reservoir. The particles used by He and Marsalek were not typical sediment particles, but crushed walnut shells. The shells were chosen because they are light, and would be more sensitive to flow conditions than smaller and heavier particles. These crushed shells had a density of $1.35 g/cm^3$ and ranged in size from 50 to 225 micrometers.

He and Marsalek tested the settling effectiveness of the tank with a smooth bottom, and compared this to the settling effectiveness of the tank when fitted with the bottom grid structure. It was observed that approximately a 67% particle retention rate was achieved when the particles were allowed to settle into the structure. During the smooth bottom test, approximately 26% of particles were retained within the tank. These tests were accomplished with a 6 L/s inflow to the tank. Across all the differing tests run at various inflows from 1 to 8 L/s, He and Marsalek roughly observed removal efficiencies of 10-30% greater than that of those efficiencies from a smooth tank bottom. They stated that the bottom grid structure performed better under high flow conditions until a maximum value was reached, then efficiency began to decrease due to the strong turbulence created by the fast flows within the tank. They noticed that under weak flows, the bottom grid structure provided only limited benefits, and in some instances, may decrease trapping efficiency with the disappearance of the vortices necessary to entrain the particles. He and Marsalek also developed a Computational Fluid Dynamics (CFD) model of their experiment to observe the potential hydraulic conditions created by their set-up.

While the work demonstrated the potential of cellular confinement to improve settling, some limitations were noticed in the experimentation by He and Marsalek. An examination of the laboratory set-

up of He and Marsalek (2014) itself renders some confusion as it is difficult to ascertain just how the slurry of water and crushed shells entered the tank and settled in the manner that the pictures depicted. The introduction of the slurry was also not in a location, or direction that would mimic a sediment basin, which made application of these findings more difficult the in the context of construction site ESC. In addition, He and Marsalek's work involved tests run in which there was not settled material in the tank at the onset of the test. Rather, large amounts of material were introduced during the tests and the authors determined how much of the material was retained by using the difference of the mass caught by the 75-micron screen. The latter is not an experiment in which observations can be clearly made regarding resuspension of settled sediments, which would be a primary function of an installed cellular confinement strategy. Another limitation of the work is the lack of testing with natural soil, as the authors substituted crushed walnut shells, which represents only a narrow range of potential sediment sizes that can be particularly much smaller in diameter.

The tests completed by He and Marsalek also leave some questions as to geometry for the bottom grid structure. Namely, there was no adjustment of the height of the cells, a feature that seems may prove a vital design characteristic for future implementation. There is also a lack of CFD modelling generated by He and Marsalek to verify the protection methods served to protect the sediment, or entrain it.

2.5. Knowledge gaps

To test the feasibility and effectiveness of cellular confinement strategy to ESC applications, several topics need to be addressed. The main research needs identified at this point are:

- A more definitive geometry study of the cells themselves and the ability to change, with several configurations, the geometry of the cells in the experiment to make observations concerning effective designs for optimal trapping efficiency.
- A more relevant experimental set-up and test procedures that mimic ESC conditions are necessary. These procedures include the use of actual sediment and more precise velocity measurements during experiments.
- There is also a need for more applicable numerical modelling, based on CFD, that may lead to helpful insights to the sizes of sediment particles that are able to be removed from within the confinement cells, and what the flow fields within the cells look like.

In summary, research has been able to demonstrate the relevance of sediment basins in controlling sediment discharges from construction sites. Related research to settling effectiveness showed that bottom grid structures, like cellular confinement cells, can create vortices that improve the settling characteristics of settlers. However, there are questions as to whether these alternatives are also effective methods to prevent sediment resuspension in sediment basins. A key knowledge gap is how cellular confinement geometries influence the resuspension process, how this can be quantified in terms of the turbidity and the particle size distribution of resuspended soils, and how this can be appropriately modeled to give insight into hydro-dynamic characteristics. The investigation of the author aims to address these knowledge gaps.

CHAPTER 3 - OBJECTIVES

The following work aims to perform an experimental investigation on the performance of cellular confinement strategies in preventing sediment resuspension created by shear flow forces. The experimental strategy involves using seven different geometric configurations of protection in a horizontal flume, subjected to two different ranges of flow velocities, for a total of 14 conditions. For every experimental condition, various samples were collected to characterize the turbidity of flows over time, as well as the particle size distribution of suspended particles.

The primary objective of this study is to conduct small-scale experimentation for examining effectiveness of the cellular confinement structures in reducing turbidity of effluent by limiting particle resuspension. Specific objectives include:

- Research existing erosion and sediment control practices
    - Analyze how current sediment control practices function fundamentally, and examine relevant fluid mechanics
    - Examine particle resuspension and relevancy to effluent
- Design and construct a channel to provide means for simulation of desired water inflows and turbulent effects
    - Create conditions involving both high and low shear forces on a sediment surface
- Form quantitative recommendations for potential future users of cellular confinement for sediment control by obtaining data from experiments
    - Outfit channel with instrumentation relevant to research
    - Identify relevant data that could prove insightful post experiment conduction
- Determine optimal design characteristics for maximum efficiency of cellular confinement protection
    - Experiment with confinement cell geometry
    - Create relevant parameters and metrics for data comparison
- Provide insight into potential uses of cellular confinement
    - Study feasibility of cellular confinement within a sediment basin, and other sediment control practices

CHAPTER 4 - METHODOLOGY

4.1. Experimental apparatus

The process by which the effectiveness of the cellular confinement was tested involved the creation of a channel open to the atmosphere to simulate an open channel, ditch, or a sediment basin. The constructed channel is housed in an indoor laboratory facility to discourage outdoor debris and unnecessary contamination of the channel. The channel created is 12.5-cm wide and approximately 10 meters long, built from acrylic panels with little roughness at the walls and channel bottom. This construction material, because of its transparency, also allowed for ease of viewing phenomena occurring while testing, which would not be feasible in full-scale applications. Figure 12 through 15 present a 3D modeling of the experimental apparatus and Figure 16 presents a photograph of the physical laboratory apparatus.
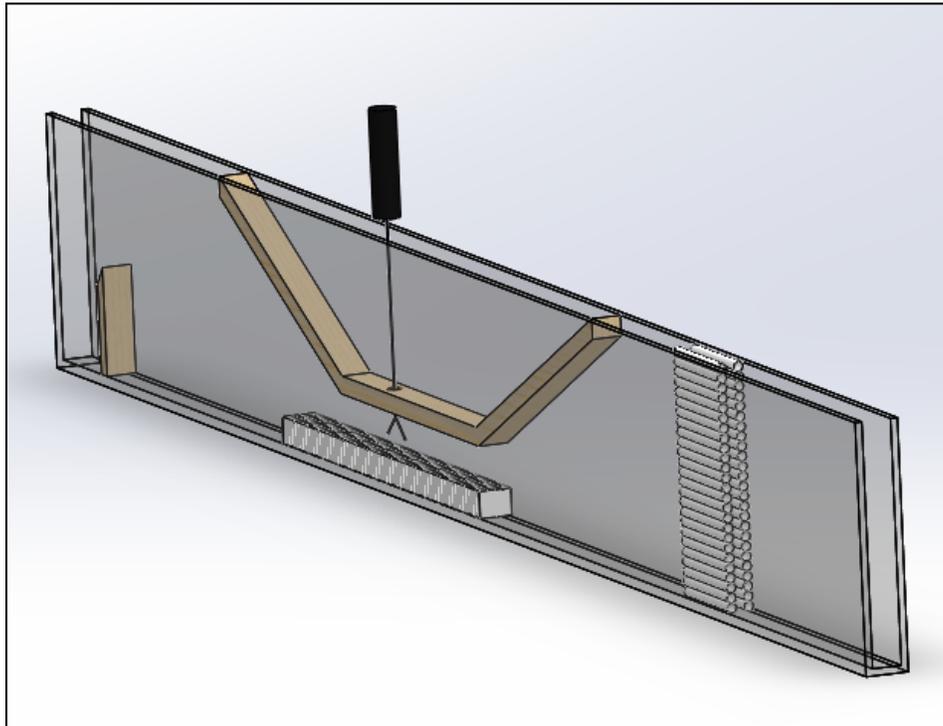
Figure 12 - 3D model of the experimental apparatus used in the
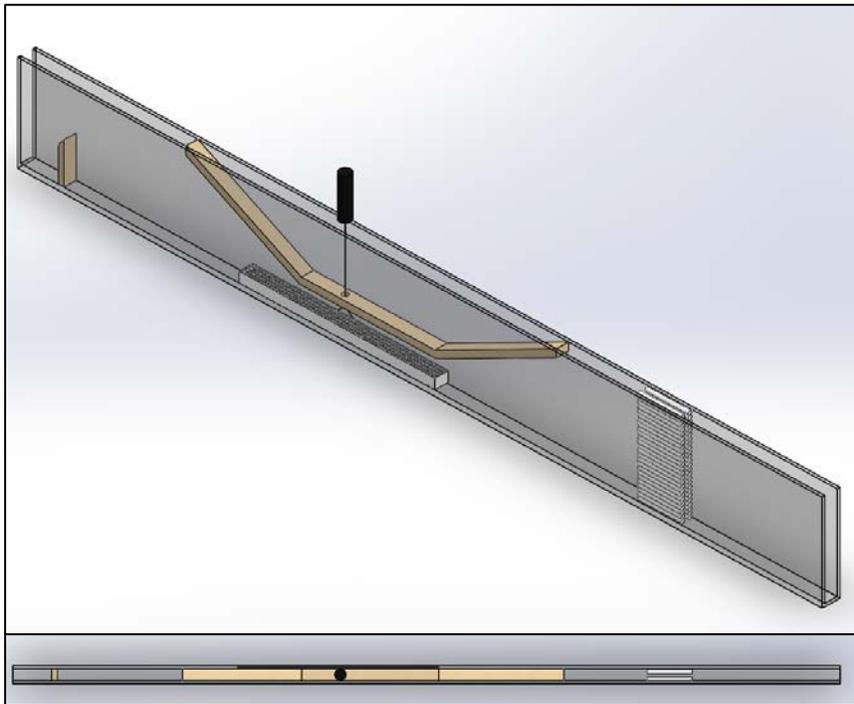
Figure 13 - Secondary view of channel (top), view of channel from directly overhead (bottom)
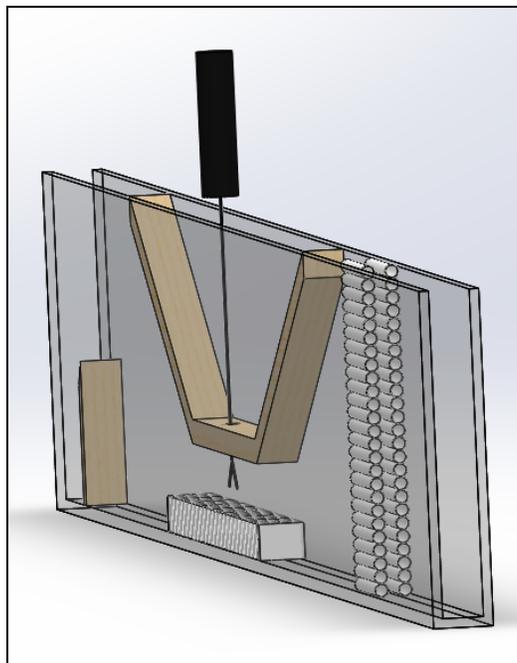
Figure 14 - 3D model view looking down the channel, nearly through flow straighteners
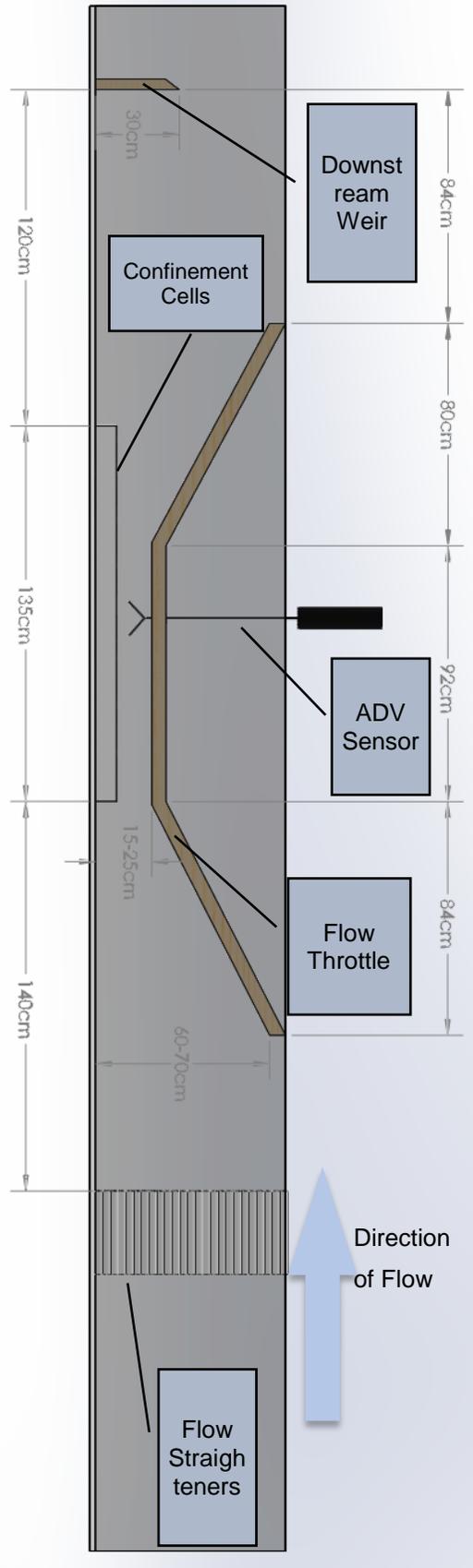
Figure 15- 3D model profile with relevant measurements
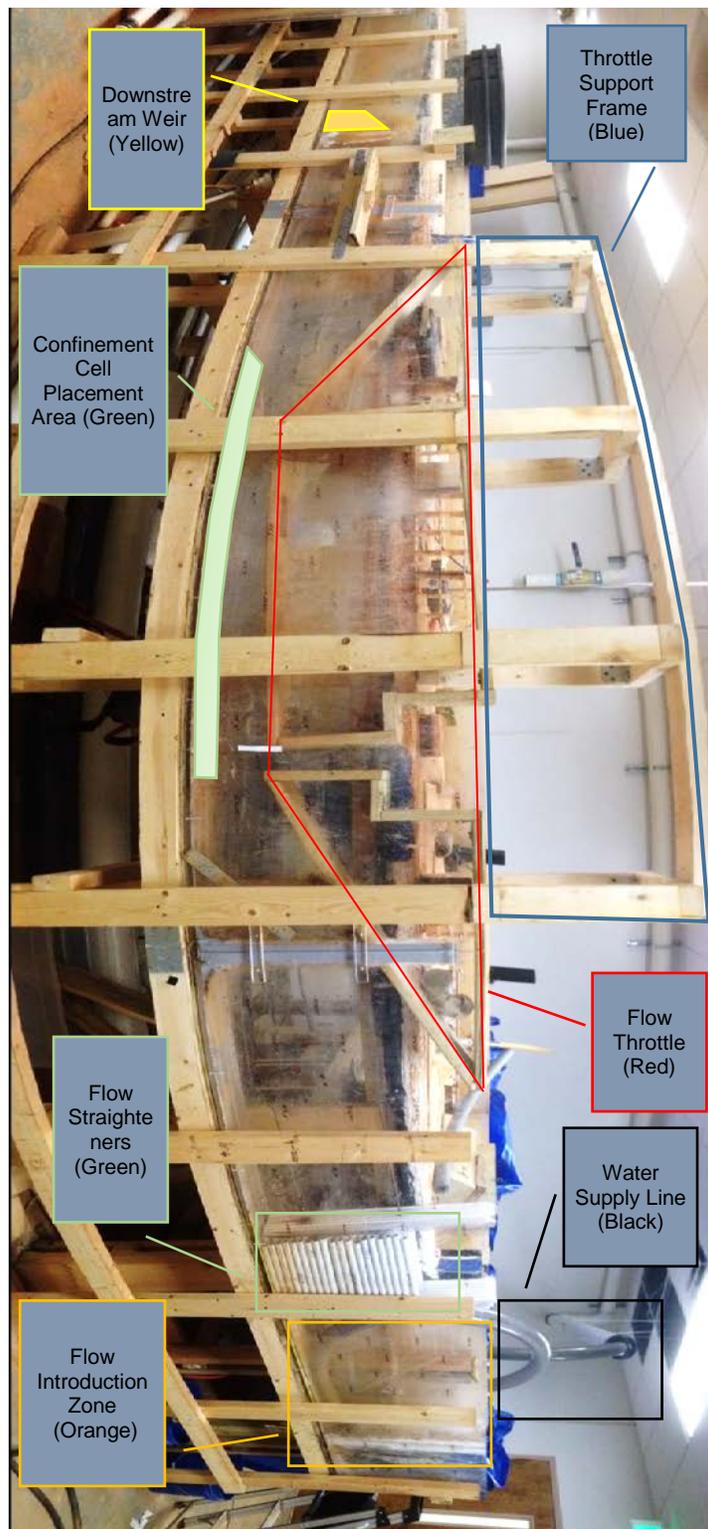
Figure 16- Laboratory open channel with flow throttle in place

The size of the channel, relative to the size of a full-scale basin or ditch also allowed for much simpler and more timely cleaning and preparation of the testing channel. The channel rested on a wooden frame that placed the bottom of the channel at 0.75-m above ground level for ease of viewing. The channel consisted of a long rectangular stretch of acrylic walls upstream and downstream of which were two large reservoirs for storage and controlled drainage of inflows. Both reservoirs were rectangular with a volume of approximately 1.0 m^3. The upstream reservoir, which lay behind the flow introduction zone from Figure 16 was independent from the channel and could be filled to capacity without drainage into the channel.

Within the upstream reservoir there was a sump pump that rested on the bottom of the tank that discharged through a 5-cm diameter flexible pipe into the upstream end of the acrylic channel. A knife gate controlled flows in the flexible pipe. Once pumped from the reservoir, the water would pass through flow straighteners at the initial section of the channel, an array of 1.25-cm diameter PVC pipes that directed flows to be parallel to the channel bottom and limited secondary currents created by the pump discharge. Once flow was conveyed to the channel it advanced 5.0-m until it passed through a 0.25-m high, horizontal sharp-crested weir. In the region upstream from the weir, all sediment addition and flow measurements were performed.

An important component of this test was modifying the system to create maximum flow velocities that were in the range of 50 cm/s. To measure it, a Nortek Vectrino Acoustic Doppler Velocimeter (ADV) sensor was used. It can sample three-dimensional velocity vectors at 25 Hz. The accuracy of the Vectrino sensor is +/- 0.5% of the measured value or +/- 1mm/s, whichever is larger. The ADV sensor was put in place 70 cm behind the leading edge of the sediment layer whether a protected test with cells was in place, or an unprotected test without them was run. Below in Figure 17 is the ADV sensor in use.
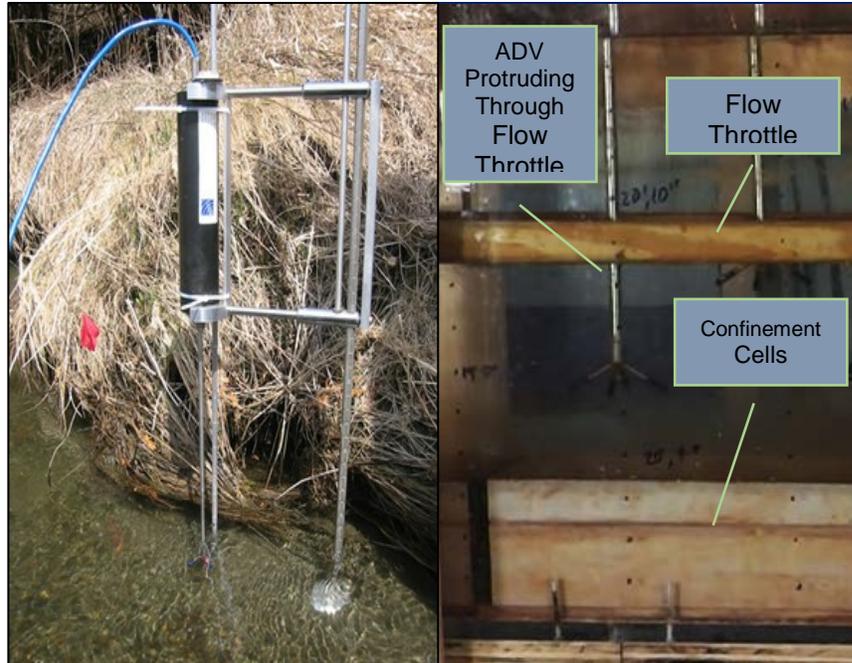
Figure 17 - Nortek Vectrino in place in natural stream (left) and our lab channel set up (right).
Reference: www.Nortek-as.com

With the pump operating at full capacity, the desired flow velocity could not be achieved in the entire channel cross section, but instead an insufficient value ranging between 17 and 19 cm/s was achieved. This range of velocities did not create the desired amount of resuspension within the time the experiment was performed, about two minutes. Run times much above two minutes resulted in increased water depth downstream of the weir, reaching a limit after which the weir discharge could be influenced by increasing water levels downstream of it.

Such design constraints prompted the creation of a flow throttle (water tunnel) downstream from the flow straighteners that decreased the effective cross-sectional area of the available flow path and increased local flow velocity near the channel bed. In order for cross-currents induced by the tunnel to not cause heavily disruptive eddies, a mild introduction to the flow throttle, incorporating a gentle leading edge of the tunnel of 30 degrees, was made. The tail end of the tunnel had a similar exit angle of 30 degrees. The flow throttle consisted of three separate wooden units: the initial throttle entrance, the throttle mid-section, and the throttle tail. The flow throttle units are displayed in Figure 18 as they rest outside of the channel.
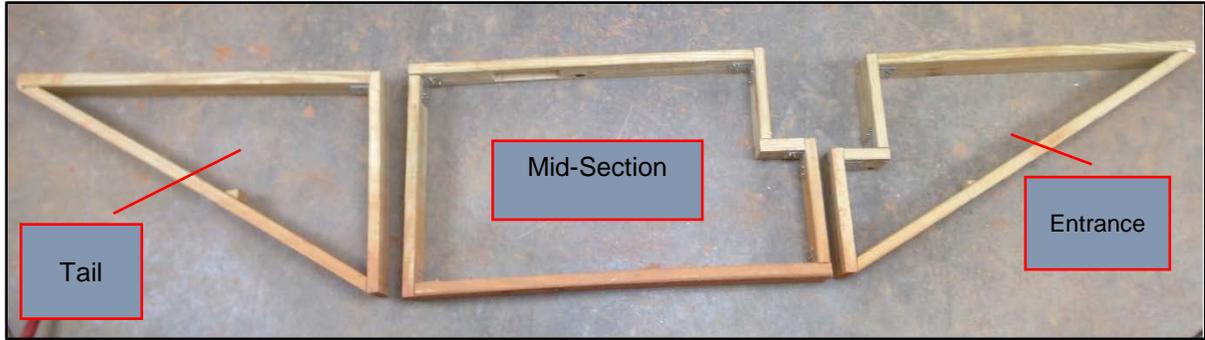
Figure 18 - Three sections of flow throttle, removed from channel.

To keep common velocity values across differing tests, the height of the flow throttle needed to be adjusted if the cell configuration was changed, or if the cells were removed entirely. The flow throttle structure was suspended from the supporting frame by threaded steel rods. These rods then fit through drilled holes in the frame, and were held in place by adjusting a nut above the support fame itself. This system created a simple and stable method of adjusting the height of the flow throttle. By adjusting the height of the throttle, achieving different flow velocities was possible for the tests. Figure 19 displays an annotated view of the channel with the flow throttle in place, along with the flow introduction zone in which the water was pumped from the reservoir. Though the flexible pipe is facing right, the inflow rebounds off the fixed boundary wall and continues downstream (to the left) towards the flow straighteners. Figure 20 contains a close-up of the confinement cell section with and without cells in place.
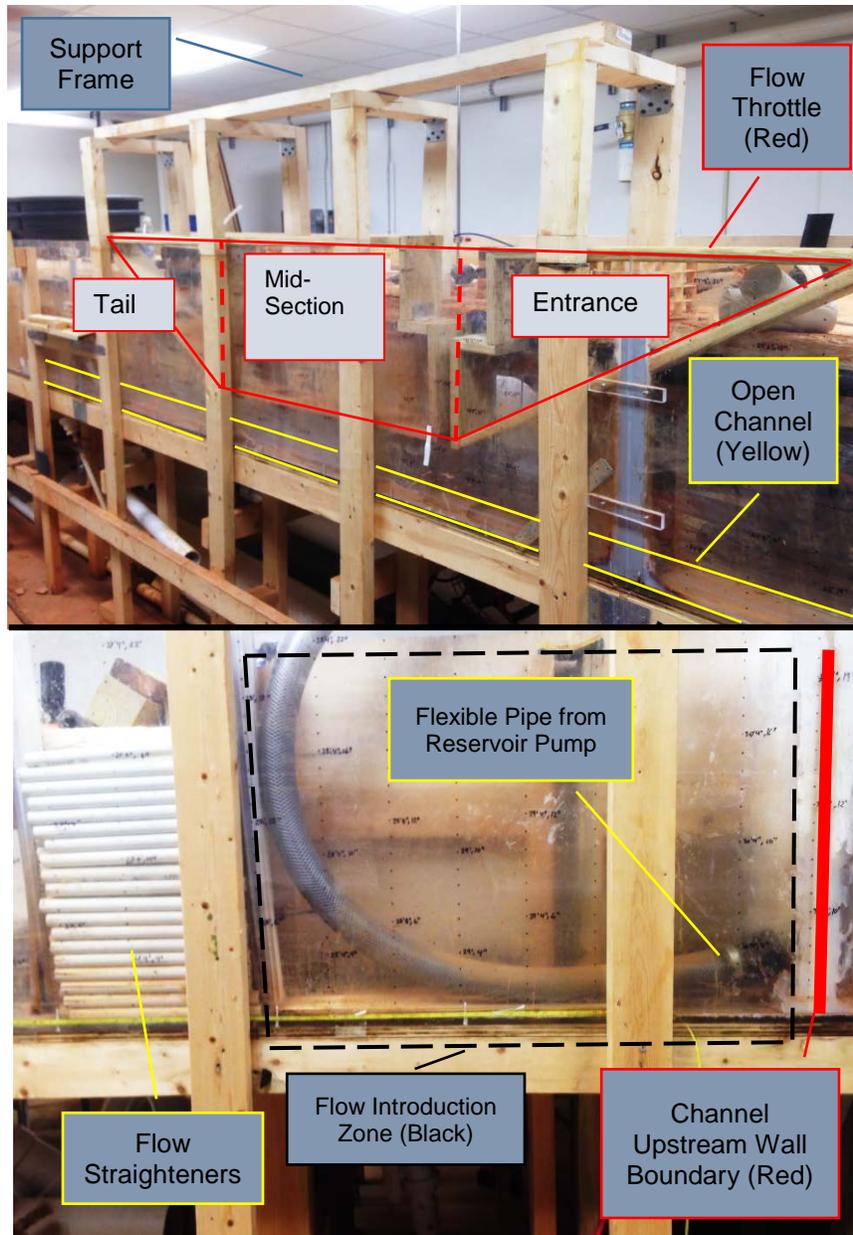
Figure 19 - Apparatus picture with flow throttle (top) and detail of flexible pipe discharge point and flow straighteners at the upstream end of the channel (bottom).
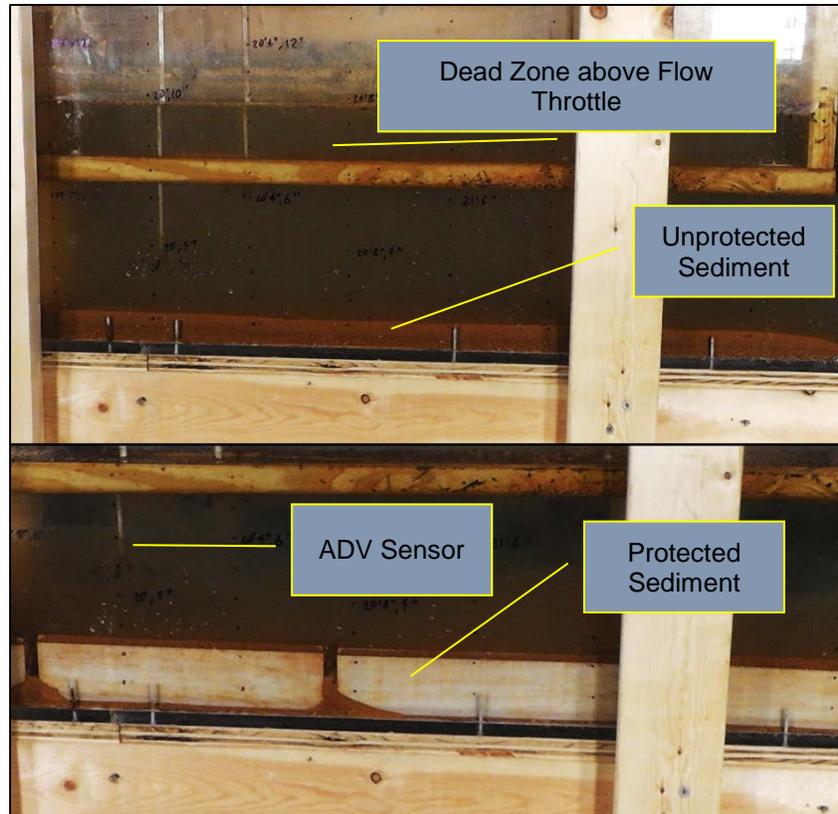
Figure 20 - Initial experimental conditions, with unprotected sediment conditions (top) and one of the protected configurations (bottom), immediately under flow throttle section.

The flow throttle was created with pinewood cut to 12.5 cm width to fit snugly inside the channel. The creation of the throttle also required the construction of the frame that would support it, allowing the throttle to be placed into the channel without shifting once flows were introduced. The placement of the throttle created an effective dead-zone, and visual observations indicated that the water velocity through the flow throttle wooden frame itself was very small, and was neglected. Finally, some slots were cut in the wooden frame to allow the positioning of the velocity sensor in the apparatus.

4.2. Experimental variables and conditions

The investigation of the efficiency of cellular confinement in preventing sediment resuspension involved a systematic evaluation of selected experimental variables, presented in Table 1. Baseline tests were performed where stream flow was influencing the bare sediment with no confinement cells in place, and such conditions are referred to as "unprotected configurations," or UP configurations. Most tests were performed with varying degrees of protection that were afforded by plastic confinement cells, 3-D printed with 1-mm thick polyethylene walls. These square cells varied in size that ranged from 2.5 to 12.0-cm in width, and from 5.0 to 7.5-cm in height. Six different "protected configurations" were considered. For both protected and unprotected configurations, two different flow rates were used, creating flow velocities that average either around 50 cm/s or 25 cm/s. Thus, a total of 14 different configurations were studied in this

investigation with the UP and protected configurations. Each configuration was performed a minimum of 3 times, or more until data converged. Over 50 tests total were performed. The results of the investigation are presented in terms of cell size, height, and flow velocity according to the terminology presented in Table 2.

Table 2 - Experimental variables used in the investigation and terminology used to refer to each testing condition

Parameter	Configuration
Cell Size	UP - Unprotected
	W3 - 2.5cm wide square
	W6 – 5.7 cm wide square
	W12 – 12.0 cm wide square
Cell Height	H5 - 5cm
	H8 - 8cm
Water flow velocity	25cm/s (low)
	50 cm/s (high)

The confinement cell units that comprised the protected configurations were each 20-cm in length. There were 5 cellular confinement units spanning over a 102-cm length immediately under the flow throttle. The cells were placed 1.4-m away from the flow straighteners. The plastic polyethylene, chosen as a construction material, had a density that was not sufficient to prevent the shear forces from causing the units to move. Narrow steel plates (10-cm wide) were attached to the cells to increase their weight. This increased the total length of the cellular confinement section to 135-cm within the channel. Below, Figure 21 through 29 display the confinement cells used for the research and their geometry configurations.

Figure 21 - Confinement cell base, largest cell configuration, W12
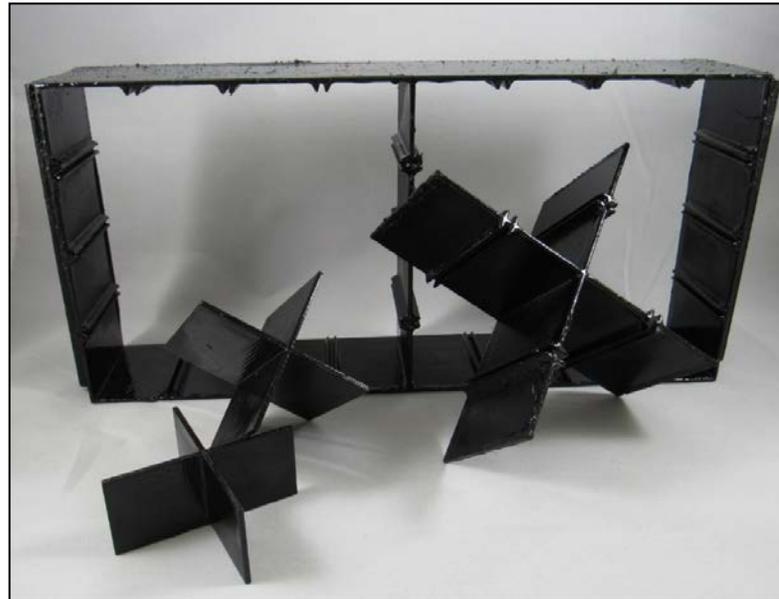
Figure 22 - W12 configuration with available smaller W6 and W3 cell components

Figure 23 - W6 cell configuration (left), W3 cell configuration (right)

Figure 25 - Horizontal W3-H5 cell configuration with steel weights on ends of cells
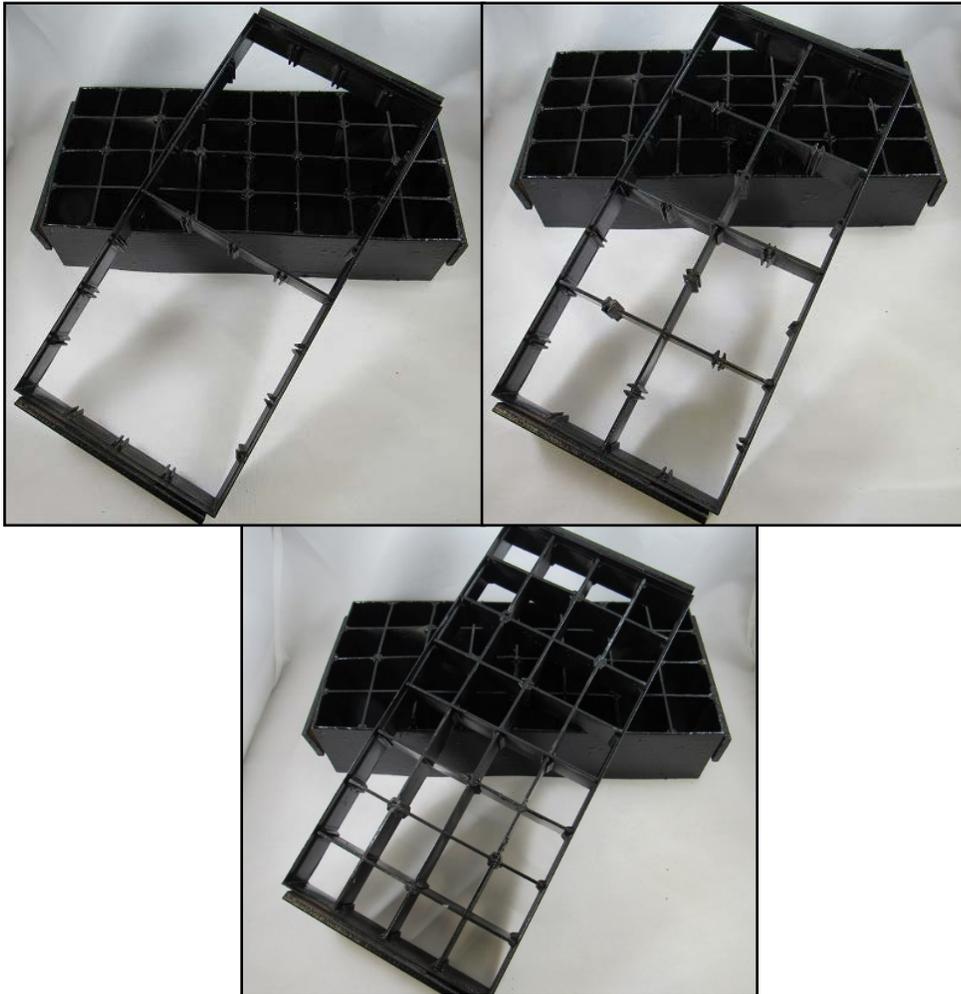
Figure 24 - Base W3-H5 confinement cells with W12-H3 resting on top (top left), W6-H3 resting atop (top right), W3-H3 resting atop (bottom)

33

Figure 26 - W3-H8 confinement cell configuration with stacked W3-H5 and W3-H3 cells

Figure 27 - W3-H8 confinement cell configuration, longitudinal
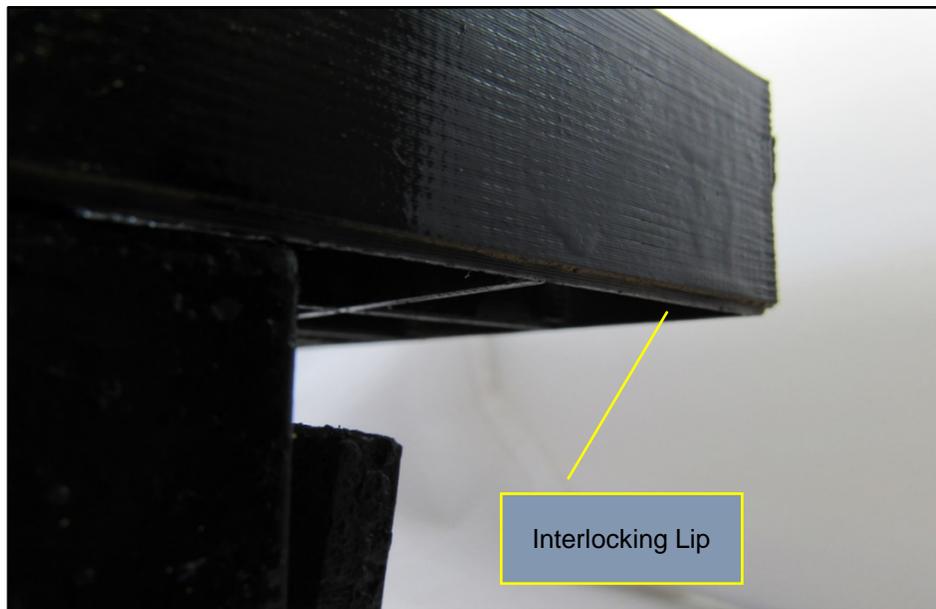
Interlocking Lip

Figure 28 - H5 and H3 interlocking lip, holding trays securely in place

Figure 29 - Varying potential cell configuration geometries

During tests, turbidity was measured in various samples using a Hach 2100Q portable turbidity meter. This sensor recorded samples in NTU with accuracy of +/- 2% of the measured value. This unit incorporates a two-detector optical system that compensates for sample color, light fluctuation, and stray light. Such measurements helped assess the impact of varying protection configurations in terms of the resulting turbidity of the effluent leaving the apparatus over time. Figure 30 shows the Hach 2100Q:

Figure 30 - Hach 2100Q turbidimeter. Reference: mwww.hach.com

The samples taken for particle size distribution (PSD) analysis required a separate procedure. These tests were accomplished by means of analysis through a Malvern Mastersizer 3000. This device uses the technique of laser diffraction to measure the size of particles by detecting scattered light intensity as the laser passes through the particulate sample. It can detect sediment particle sizes in the range of .01-3500 micrometers, or 3.5-mm. The accuracy of the system is 0.6%, and the precision/repeatability of tests are within 0.5% of each other and it samples at 10kHz during analysis. The detection limit of the Mastersizer is .01-μm Below, Figure 31, is a picture of the Mastersizer 3000:

Figure 31 - Malvern Mastersizer 3000. Reference: www.malvern.com

The sediment used in the investigation was collected from a stockpile located at the National Center for Asphalt Technology test track, at the Auburn University Erosion and Sediment Control and Testing Facility (AU-ESCTF). This sediment was taken to the geotechnical laboratory at Harbert Engineering Center to be sieved. The sediment was then sieved in a mechanical shaker. From the original sample, everything was discarded above the #8 (2.38mm) sieve. This remaining sample passing the 2.38-mm sieve was then stored to be tested in the channel to maintain fines within the sediment sample, but also to include larger diameter particles. Figure 32 presents a particle size distribution (PSD) of the soil used in the investigation, obtained with the Mastersizer. These PSD curves are not based on weights of sediment fractions, but rather relative percentages of total particle counts at each size range. This measurement method is due to the analysis that is performed using the laser diffraction machine.
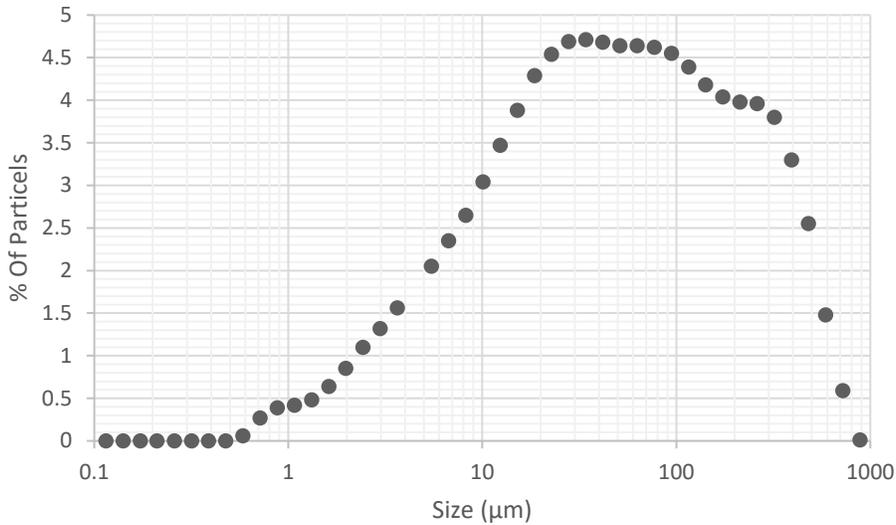
Figure 32 - Particle size distribution of the soil used in the investigations

The Mastersizer also provided a means to accurately discern the specific type of soil utilized in the present research. The following Table 3 contains relevant soil composition:

Table 3 - Soil composition before any testing - raw soil

Clay:	% Less than 2um	2.30%
Silt:	% Between 2-50um	46.36%
Very Find Sand:	% Between 50-100um	15.78%
Fine Sand:	% Between 100-250um	18.99%
Medium Sand:	% Between 250-500um	12.49%
Coarse Sand:	% Between 500-1000um	4.08%
Very Coarse Sand:	% Between 1000-2000um	0%

4.3. Experimental procedure

The following section details the systematic procedure followed to complete a single experiment in the laboratory. Before the execution of experiments, the channel and equipment were thoroughly cleaned with water, a tough-bristle brush, sponges, and mild soap. Sediment from the previous test would be washed out of the channel by way of a 2.5-cm drain in the bottom of the acrylic section that could be opened or closed at any given point by a rubber stopper. In the case of protected configuration tests, the cellular confinement cells were placed in the 135-cm isolated section of the channel. If an unprotected configuration was being tested, no confinement cells were installed within the channel. The typical experimental run involved the following steps:

1) Fill the entire channel section up to 15-cm with water. This was done using city-supplied water through a standard hose.

2) Place confinement cells in channel for experiments that involved use of protection. The cells are inserted after the tank is filled to its initial height due to the bowing of the channel walls slightly upon filling, allowing easier placement of cells.

3) Place water-tight isolating barriers above and below the 135-cm channel region in which the sediment will settle.

4) Add sediment to the 135-cm long section of the channel that was isolated with barriers. This amount of sediment was experimentally determined to yield an average settled thickness of 2.5-cm. The amount of sediment that was required for each test correlated to a mass of 3.5-kg. This sediment was distributed in five containers that were used to introduce the sediment to the channel along the isolated region.

5) Remove isolation barriers after a 24-hour settling period and pump water to fill the upstream reservoir. Isolation barriers are removed very carefully to not disturb either the cloud of unsettled fines that remained after the 24-hour settling period or the delicately settled fines within the confinement cells.

6) Install flow throttle in the channel at a predetermined height to create the needed flow velocity for the given test condition, either 25 cm/s or 50 cm/s.

7) Set up the Acoustic Doppler Velocimeter (ADV) sensor that measured flow velocities during the tests.

8) Turn on main pump to allow clean water to flow through the flow straighteners into the region where the soil was added

9) Sample weir effluent for turbidity measurements every 15 seconds after weir overflow initiates. At times of 30, 60, and 120 seconds, 500-mL samples were taken for particle size distribution testing.

10) When upstream water reservoir exhausted, cut off pump, halt sampling effluent and ADV sampling, and open drain to empty the channel. With the size of the reservoir, it was possible to run over 2-minute-long tests of approximately 50cm/s in the channel.

11) Measure and record turbidity results from samples and determine particle size distribution through further analysis. Turbidity samples were recorded immediately. Particle size distribution samples were taken to a separate facility to be analyzed.

12) Repeat entire test procedure at least 3 times to test consistency in the measurements.

13) Take desired observational documentation including photographs and sediment samples.

The procedure for the laser diffraction particle size distribution tests after the samples were collected from the channel effluent was as follows:

1) Transport samples from test channel to the Geosciences Research Laboratory at Auburn University. This laboratory housed the Malvern Mastersizer required for PSD analysis.

2) Place samples in glass beakers to prepare for evaporation of unnecessary water in sample. The samples were 500mL in volume, however, the Mastersizer required only about 10-20mL of sample with heavy sediment concentration.

3) Place Samples in oven at 75 degrees Fahrenheit for 24-hour periods until remaining sample resembles a slurry of sediment more so than turbid water.

4) Initialize laser diffraction test through Mastersizer software, producing the data desired such as count-based particle size distribution plot, and d_{50} and d_{90} determination.

5) Introduce sample to Mastersizer. If sample greater than 10mL, shake vigorously for 10 seconds then immediately sample with a pipette, then introduce to Mastersizer.

6) Once analysis complete, thoroughly clean Mastersizer to ensure accuracy of future tests.

7) Export relevant data to .csv files for data analysis in Microsoft Excel.

4.4. Summary and hypotheses

This chapter outlined the manner in which the experimentation necessary to test the feasibility of cellular confinement as a means to limit sediment resuspension was performed. The construction of relevant experimental apparatuses is also detailed such as the flow throttle, flow straighteners, and support frame. Instrumentation is discussed and pictorial information is included for the specific configurations of the confinement cells used for the testing procedure. The research question to be answered from the present work is: will the confinement cells present an effective means of sediment control through the limiting of resuspension of sediments within a channel or basin? It is hypothesized, based upon expected shielding of the sediment surface from high water velocity due to the confinement cells, that the cells will limit sediment resuspension as evidenced by reduced turbidity measured in the channel effluent. It is also hypothesized, that the reduced turbidity will demonstrate decreased scouring of the sediment surface with confinement cells in place which will provide support for future large-scale applications of this novel sediment control alternative. The null hypothesis, is that experiments performed with confinement cells in place, will produce effluent turbidities similar to, or worse, than those produced when there are no cells in place, and physical evidence will not support protection from scour. A Student's t-test was performed in order to test the null hypothesis and determine whether the data sets from the fully-protected H8-W3 configuration tests and the data from all unprotected tests were significantly different from one another. If strong statistical correlation did not exist between limited turbidity and the use of confinement cells here, it should not be found elsewhere in the data. Using an unpaired t-test with a confidence interval of 95%, a two-tailed p value of .0452 was obtained from the two raw data sets. There is therefore a 4.52% chance of observing a difference as large as the differences observed between the data sets of a UP and a H8-W3 test even if the population means were identical, or stated differently, there is a 4.52% chance that the null hypothesis is true. This relationship presents strong evidence against the null hypothesis and it is therefore rejected. The following Chapter 5 will introduce the results and analysis of the data collected from the adherence to the methodological procedures presented within Chapter 4.

CHAPTER 5 - RESEARCH RESULTS AND ANALYSIS

The key results obtained in the current research are presented in this chapter. Firstly, the velocity measurements obtained with the ADV are presented. These results are important as these velocities were the cause for the shear forces that led to sediment resuspension. Secondly, the turbidity data series collected through experimental runs is presented. This data varied according to the level of protection of sediments and velocity within the channel. Thirdly, the results obtained from particle size distribution testing of sediment particles at different locations and times in the apparatus are presented. Fourthly, residual channel sediment was examined and analysis was conducted concerning incipient motion and CFD modeling. Finally, this chapter explores the financial feasibility of implementing confinement cells as a means to limit sediment resuspension. The following sections are structured in this above sequence and detail the related findings.

5.1. VELOCITY RESULTS

The channel, with the flow throttle installed and adjusted, maintained the required velocities consistent throughout various repetitions. The supporting structure controlling the height of the flow throttle was adjusted to preserve these velocities in the desired range for each level of protection provided by the cellular confinement configurations. Velocity associated with these tests was recorded as a function of time in cm/s by the ADV sensor. The desired velocity range was 45-50 cm/s for the high-range velocity tests, and 25 cm/s for the low-range velocity tests. These values were chosen to create shear forces that could resuspend sediment particles, even with the use of cellular confinement.

Figure 33 illustrates velocity hydrographs of the various tests performed within the channel. Figure 34 displays an unprotected (UP-50) test, and two tests with maximum protection (W3-H8, or a cell width of 3.0 cm and cell height of 7.5 cm) with both 25 or 50 cm/s flow velocities. The hydrograph presents different stages of the experiment based on velocity measurements.
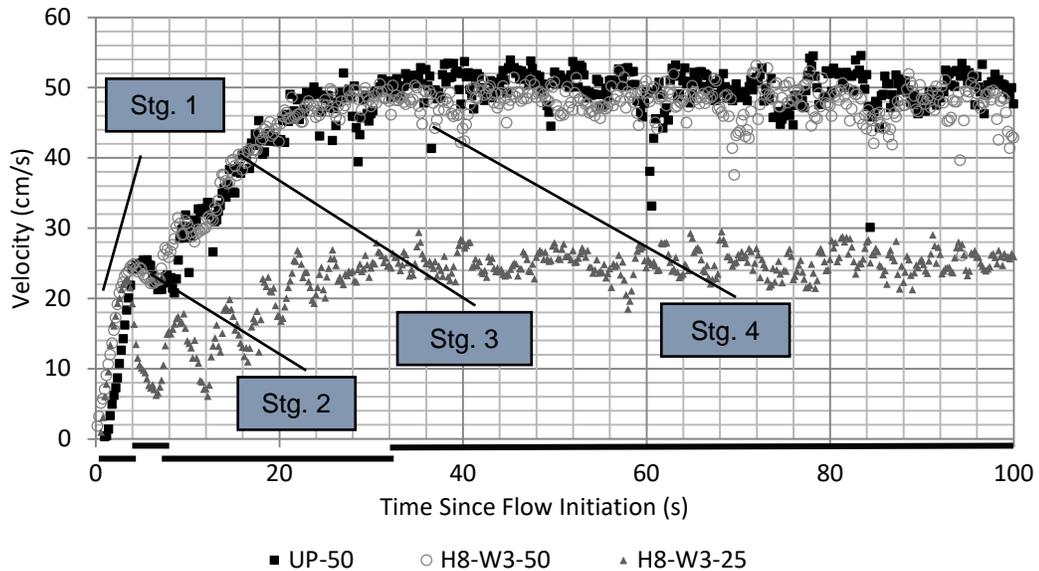
Figure 33 - Channel velocities measured with the ADV sensor

The first stage takes place within the first 5-10 seconds of the test, indicated approximately by the black time bar below the x-axis, where there is rapid water movement induced by the pump, filling the channel to the height of the weir. There is then, during the second stage at around 10 seconds, presumably due to the inertia with which the initial volume of water impacts and over-tops the weir, a rebounding of water, similar in nature to small water-hammering phenomena, after which downstream velocity continues. After the weir is over-topped, a third stage is visible that occurs within 10 to 35 seconds of each test, in which the velocity oscillates and continues to increase as steady state equilibrium is reached within the channel at around 35-40 seconds after flow initiation. This oscillation of water velocity is particularly noticeable in the UP configuration. Velocities in this third stage, as they oscillate, reflect the unsteadiness of flow conditions as the filling takes place. However, the flow velocities are not as large as flow velocities observed when steady state conditions develop. Following the filling stages, the flow of water gradually transitions into a more steady, quasi one-dimensional channel flow in stage 4 as overflows continue to be observed at the weir. In the initial stage of the overflow, the discharged sediments are essentially a cloud of non-settled particles following the 24-hour period of sediment introduction. Fluctuations of the velocity results presented by the ADV are attributed to the expected turbulence in the flow.

5.2. TURBIDITY RESULTS

Figure 34 presents a semi-log graph with the evolution of average turbidity data for tests involving unprotected configurations. An important distinction of these results is that the reported times are presented with respect to the weir overflow initiation, not the time at which the pump initiated filling. This time scale was preferred since selecting the overflow initiation as the reference time would provide a common event

regardless of the inflow rates or degree of protection provided to sediments. Figure 35 results indicate the large influence of flow velocity in shearing and resuspending unprotected soil, which is reflected in large turbidity values.
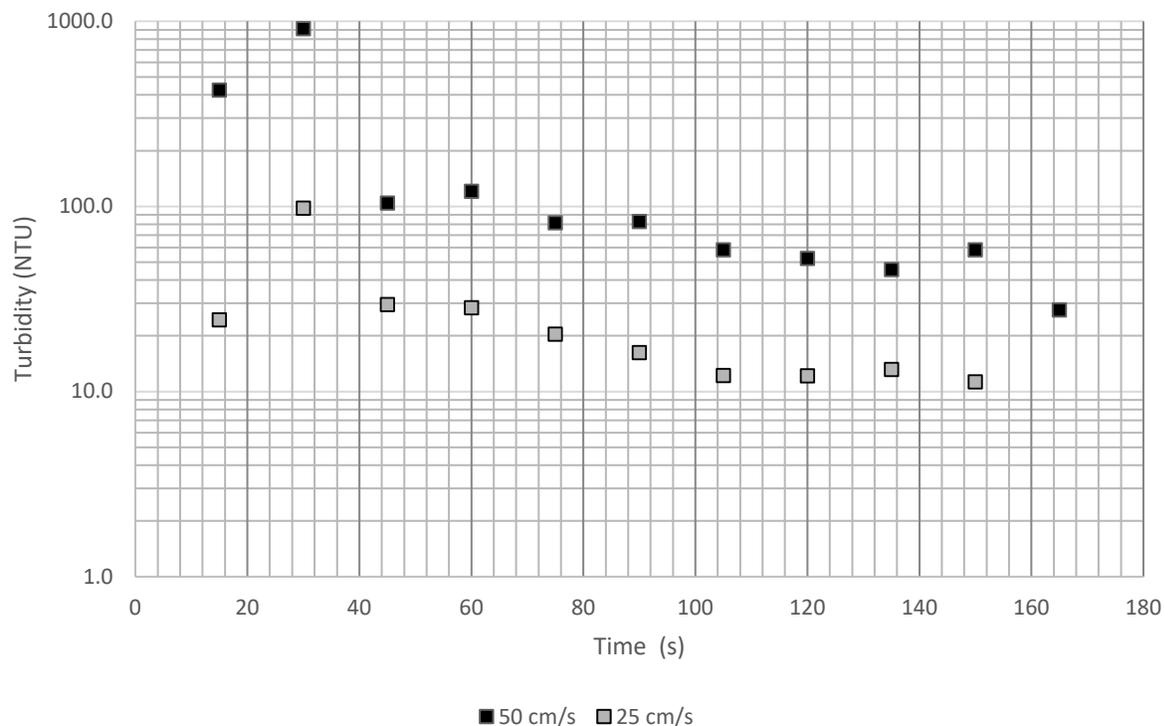
Figure 34 - Unprotected turbidity velocity comparison

The turbidity results indicated that a peak in turbidity occurs around 30 seconds after weir overflow, and is attributed to the initial flush of fine sediment particles at the top layer of settled and unprotected soils. High velocity range (50 cm/s) yielded peak turbidity around 950 NTU, while in the case of the low velocity range (~25 cm/s) peak turbidity was about an order of magnitude smaller. Following the peak, there was a gradual drop in turbidity values lasting for 60-80 seconds. It is possible that in this period there was a steady decrease in the concentration of fine sediments that were sheared by the flow. In the third and final stage, after 90-100 seconds of overflow, the turbidity levels decreased more gradually. This behavior was observed in both ranges of flow rates, as is displayed in Figure 35.

In general, the same type of results was observed in all cases involving the protected configurations, as is shown in Figure 35 and Figure 36. Turbidity results for protected cases for 50 cm/s are presented in Figure 35, and the unprotected configuration results are presented for comparison. The highest decrease in turbidity was observed with 3.0-cm wide cells. The highest cell height of 7.5 cm, which provided a 5-cm initial offset between the stream flow and the sediment level, allowed for a very significant drop in peak turbidity, to around 30 NTU peak value in the H8-+W3 configuration, which was over 30 times less than the unprotected peak turbidity. The minimum turbidity levels of the H8-W3 configuration were

around 2 NTU, which was also much smaller when compared to the minimum level obtained with the unprotected configuration of 30 NTU.
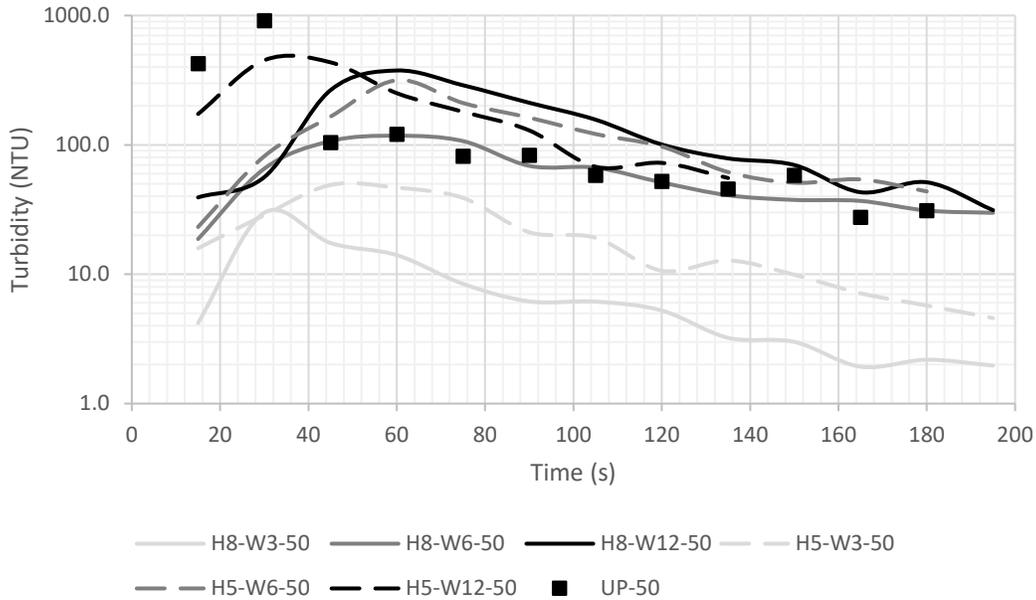
Figure 35 - Turbidity protected comparison - 50 cm/s flow velocity

The second most efficient protection configuration was also with the 3.0-cm cell sizes, but only with 5-cm cell height (H5-W3). Peak turbidity was in the range of 50 NTU, with minimum turbidity around 5 NTU. The third best condition was observed with the 5-cm width cell and 7.5-cm height (H8-W6), when the peak turbidity was a little over 100 NTU. From this point onward, the turbidity values of other protected alternatives were comparable with the unprotected case. The other protected conditions, while presenting smaller peak turbidities than the unprotected case, showed turbidity levels following the peak in the same range or above the unprotected configuration. In summary, it can be inferred that the protection configurations H5-W6, H5-W12 and H8-W12 were not effective in preventing resuspension for a 50-cm/s velocity condition.

When the velocity range was lower, the difference between unprotected and protected configurations became less noticeable. However, there were still noticeable improvements to the degree of turbidity peak reduction in several configurations. As shown in Figure 36, the greatest decrease in effluent turbidity was observed for the H8-W3 configuration. However, the peak turbidity (~30 NTU) for this configuration was in the same range as the peak observed for the high range velocity. This value was approximately 3 times smaller than the unprotected configuration, which was above 100 NTU. Following the peak turbidity value, a steady drop was observed and the final turbidity measured was below 2 NTU. For other protected configurations involving 2.5 and 5-cm cell widths (H5-W3, H8-W6 and H5-W6), the peak turbidities were in the range of 60 to 70 NTUs, which were smaller than the unprotected configuration. The

configurations with 10-cm cell sizes were in general not effective in reducing the turbidity compared to the unprotected configuration.
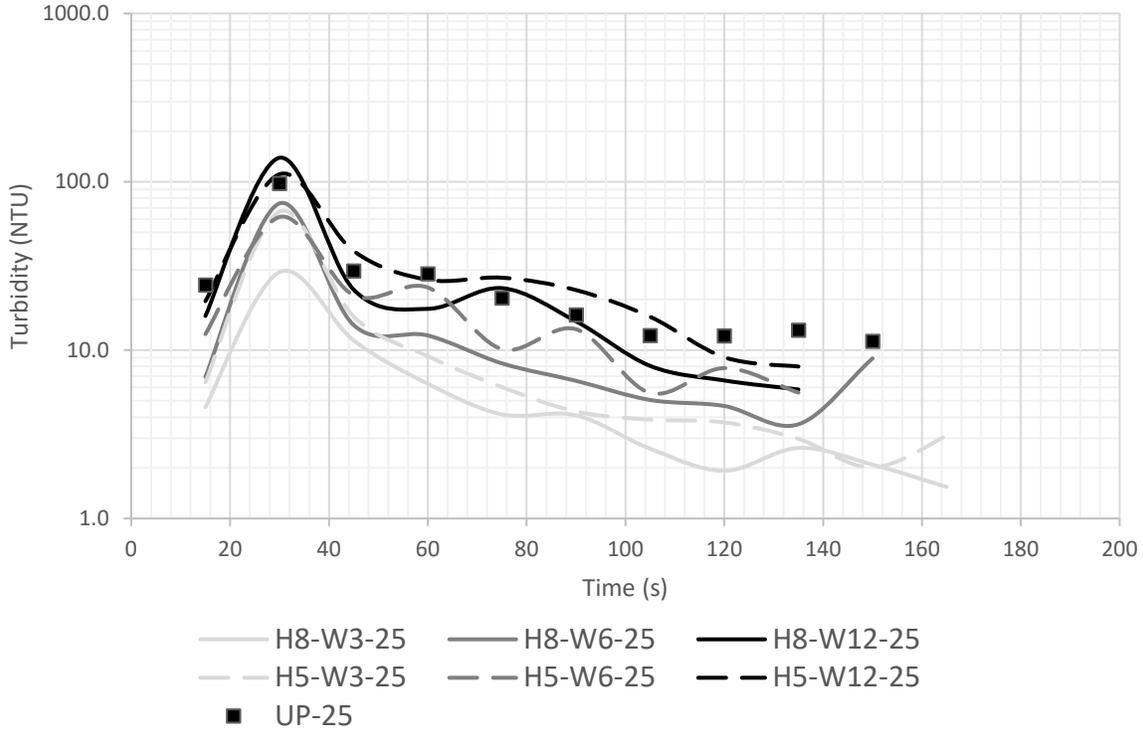
Figure 36 - Turbidity protected comparison - 25 cm/s

5.3. TURBIDITY CORRELATIONS WITH FLOW AND CELL GEOMETRY

To assist in creating an application of these findings for other cellular confinement geometries, the creation of a dimensionless parameter called Resuspension Parameter (Rp) was proposed. This parameter takes into consideration the flow velocity, cell area and height, and the kinematic viscosity of water. Equation 5 expresses this resuspension parameter, Rp:

$$R_P = \frac{V_{Channel} * (A_{Cell}/H_{Cell})}{v} \qquad \textbf{Equation 5}$$

Where,

$$R_P = \text{Resuspension Parameter}$$
$$V_{Channel} = \text{Velocity in channel, m/s}$$
$$A_{Cell} = \text{Area in cell, m}^2$$
$$H_{Cell} = \text{Height of cell wall, m}$$
$$v = \text{ Kinematic viscosity, m}^2/\text{s}$$

Figure 37 presents the values of the average turbidity over a given test in terms of the resuspension parameter for all tested conditions, and the plotted results grouped by the background flow velocity. Figure

37 is a plot of the effectiveness of each confinement cell configuration of limiting resuspension for both channel velocities based on corresponding average turbidity. There is a monotonical increase in the average turbidity with the value of Rp, also noting that both the vertical and horizontal axis of Figure 37 are logarithmic. Table 4 contains the data for the plot.

Table 4 - Resuspension parameter (R_p) values for each protected configuration

Configuration	R_p Value	
	25cm/s flow velocity	50 cm/s flow velocity
H8-W3	4,342	7,816
H5-W3	8,685	15,632
H8-W6	17,369	31,265
H5-W6	34,738	62,529
H8-W12	72,994	131,389
H5-W12	145,988	262,778
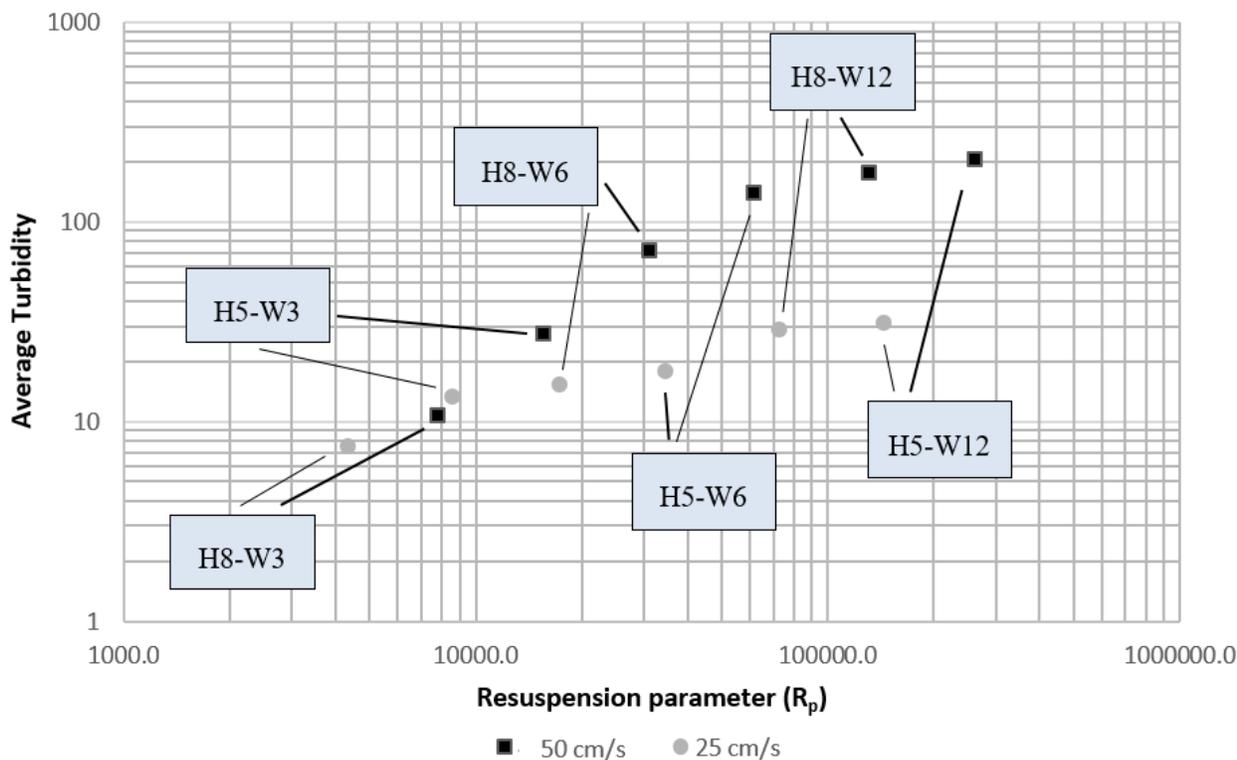
Figure 37 - Resuspension parameter vs. average turbidity with cell configurations

The protection from resuspension decreases, based on the above data, not primarily with a shorter height of the cellular confinement, but with a larger confinement cell configuration, as is perceived by the

increased value of R_P first as a function of the increased cell width (W), and second as a function of increased cell height (H). The resuspension parameter is helpful in this case for identifying ratios of cell area to cell depth that are beneficial in limiting resuspension. We can observe from Table 4 and Figure 38, that as R_P increases, the protection from resuspension for sediment particles decreases, as indicated with higher average effluent turbidity.

Presented below in Figure 38 is a similar graph, but in the place of average turbidity, peak turbidity is plotted against R_P. A relationship was formed between the two parameters with a regression line ($R^2 = .804$) incorporating all configurations according to the following Equation 6:

$$NTU_{PEAK} = 42.5 + 0.0064R_P$$

Equation 6
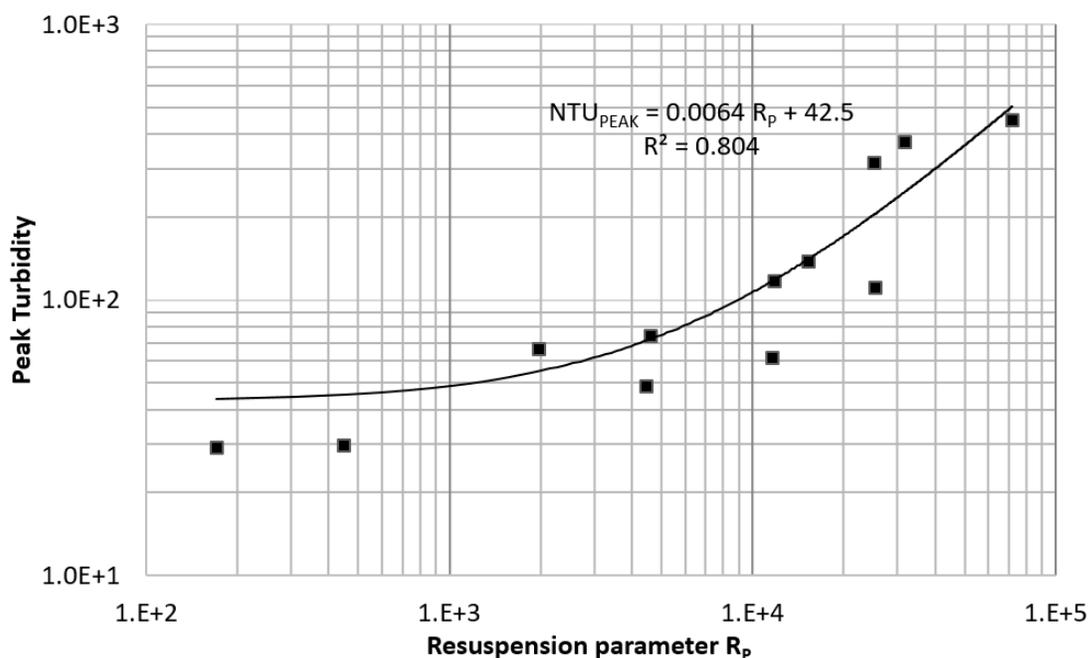
Figure 38 - Resuspension parameter vs. peak turbidity with cell configurations

The resuspension parameter could be a useful means of providing general predictions as to the relationship between cell geometry, in-cell velocities, and the anticipated turbidity that is related to the resuspension of sediment particles. The turbidity values observed are specific to the soil tested during this research. However, it is presumed that a similar relationship exists for other soils as well.

For further simplicity, height to width (H:W) cell ratios were plotted against the average turbidity results normalized by the unprotected turbidity. H:W ratios are presented below in Figure 39 according to flow velocity, resulting in the confinement configurations being plotted against their respective control scenarios of an unprotected test.
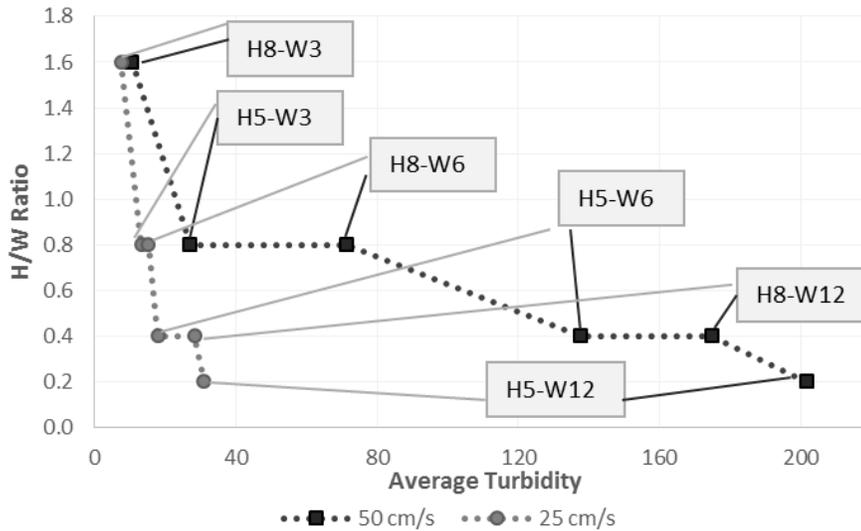
Figure 39 - 50 cm/s H:W vs. average turbidity normalized by UP

The H:W ratio data reveals the primary geometric characteristic that influenced the average turbidity was the cell width, W. However, for wider cells and greater ambient flows the height of the cell also notably effected the turbidity. Normalizing the plots against the unprotected scenarios reveals the percentage of the turbidity that a protected configuration experienced compared to the unprotected turbidity. In low flow rate situations, the confinement cells of large widths and shallow heights (e.g. H5-W12) yielded worse average turbidity, nearly 110% of the unprotected scenario turbidity. However, all other confinement cell configurations yielded lower average turbidities than the UP configuration.

5.4. PARTICLE SIZE DISTRIBUTION RESULTS

As discussed in the methodology, a laser diffraction apparatus (Mastersizer) was used to determine the particle size distribution (PSD) of sediment particles at various locations and instants during experimental runs. It is important to reiterate that these results, unlike traditional PSD results, are not based on weight of particles, but rather particle counts from various size fractions. Each sediment particle size data point corresponds to a percentage of the total sample count through the Mastersizer apparatus. The characteristics of the raw soil have been presented in Table 3 in Section 4.2.

A sequence of experimental PSD results was obtained for selected experimental conditions, in which samples of the effluent at the weir were taken at 3 different times: 30, 60, and 120 seconds after the water over-topped the weir. The following Figure 40 shows the PSD results from these time intervals during an unprotected test with a channel velocity of 50 cm/s.

48
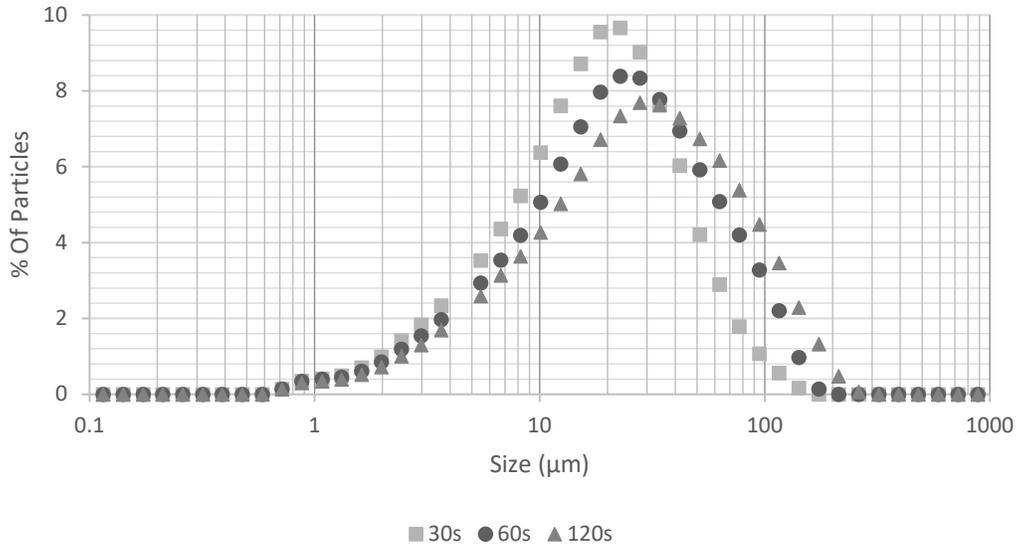
Figure 40 - PSD of UP conditions over time, 50 cm/s flow velocity

An interesting trend is noticed that may reflect the decrease in the fraction of fine sediments in the resuspended soil particles reaching the weir. The shifting of the PSD curves, progressing in time, from left to right and the gradual increase in D_{50} values of the particles in the samples indicates that, over time, larger-sized sediments become more prevalent in channel effluent. To some extent, the result is expected, since this process is similar to that of armoring in natural streams, where finer particles are swept away over time in the presence of stream velocity, then become protected more so by the larger diameter particles as time progresses. This armoring phenomenon seems to be occurring at an accelerated pace due to the experimental conditions. The statistical mode for the PSD of sediment samples collected at 30 seconds was approximately 20 microns, whereas for 60 second and 120 second samples it was 25, and 31 microns, respectively. Table 5 below consists of data from shifting D_{50} and D_{90} trends from two configurations, based on count analysis through the Mastersizer. The D_{50} and D_{90} values from the protected H8-W6-50 configuration are based on substantially smaller soil sample volumes compared to those present in the effluent of the UP test, due to the presence of the confinement cells.

Table 5 - Diameter changes across UP and H8-W6-50 configurations

Unprotected Configuration		
Time	d_{50} (microns)	d_{90} (microns)
30s	23.5	71.7
60s	31.6	94.8
120s	35.7	112
H8-W6-50 Configuration		
Time	d_{50} (microns)	d_{90} (microns)
30s	25.6	59.7
60s	28.2	61.1
120s	31.6	71.0

As observed in Table 5 with increasing d_{50} and d_{90} values, as time continues, larger particles become more prevalent in the channel effluent. The assessment of the effects of the confinement cells on the size of resuspended particles is that confinement cells prevent the resuspension of more fine particles as is most clearly noted in the progressing d_{90} trends towards larger particle diameters. A limitation of the Mastersizer apparatus is that it cannot characterize sediment PSD in samples with low turbidity, or obfuscation percentages. The Mastersizer required an obfuscation range of 14-20% to analyze a sample. Thus, tests with protection configurations and flow velocities yielding very low effluent turbidities could not be evaluated with this apparatus. A protected configuration that was examined was the H8-W6-50 case, in which 3 sets of samples from H8-W6-50 tests were analyzed and averaged to display the evolution of the PSD of channel effluent in the following Figure 41.
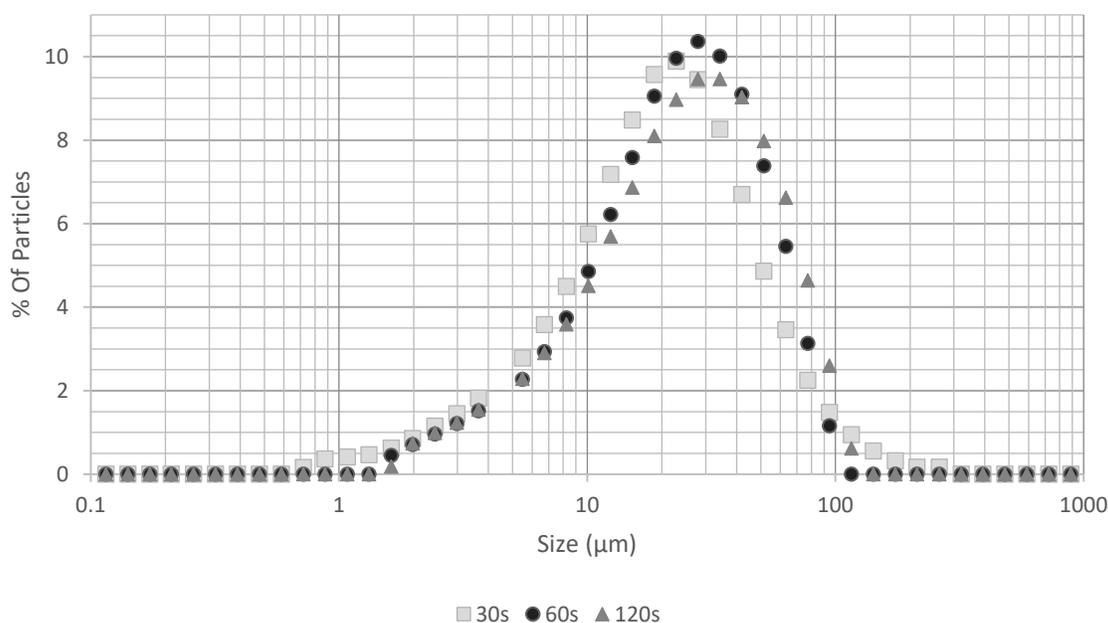
Figure 41 - PSD H8-W6-50 time progression

Figure 41 indicates that, as the tests progressed, a very slight shift in particle sizes and of general proportions of resuspended particles was detected over the weir during the protected configuration. Smaller incremental increases in D_{50} values were also measured when compared to the unprotected configuration as shown in Table 5 above. While the general proportions of resuspended particles did not change as markedly as in the unprotected configuration, the statistical mode of particle sizes varied over time, from 25-microns, into 28 microns, then, finally, 32 microns for the 30, 60 and 120 second samples, respectively. In comparison to the UP-50 PSD plot in Figure 41, which may indicate that in earlier stages of resuspension a larger proportion of the finer particles was removed and the larger particles then became exposed to shear forces, Figure 42 may indicate that the layer of fines that settled atop the coarser particles is still slowly being removed.

After several tests, including both protected and unprotected cases, a long period of time was allowed to pass before the channel was cleaned so that the sediment remaining in the channel would completely dry out. At this point, several sections of dried soils were sampled using a knife to cut into the hardened sediment layer at the bottom of the channel. The objective was to qualitatively observe how the sediments settled and what the effects were of the confinement cells on remaining sediments.

Figure 42 shows a cut section from the dried sediment of an unprotected configuration that resembled other samples taken from protected conditions. The cut-section indicates stratification of settled particles. As larger particles tend to settle with higher velocity, according to Stokes law, coarse particles were visibly more frequent in the bottom section of the dried soil sample with a gradation towards fine sediments in the upper layer of the sample.

Figure 42 - Dried sediment sample indicating stratification of particles closer to the bottom of the settled sediments

Other photographs were also taken after tests were completed, to examine the profile of the remaining sediment, both from protected and unprotected tests. Figure 43 through Figure 46 presents conditions of sediments post-tests in various protection configurations. The H5-W3 configuration presented a fairly uniform thickness of sediment within the confinement cells after the experimental runs. By comparison, the H5-W6 configuration showed more distinct variation in sediment thickness within the cellular confinement cells indicating more substantial velocities inside the cells. In the downstream half of the cells, approximately a 1 cm deep scoured depth was created where sediment had been displaced. The H8-W12 configuration, with the least protection in terms of cell area, showed dramatic displacement of sediment particles within the cells. Nearly all the sediment shifted away from the downstream half of the cell and either resuspended, or deposited on the upstream half of the cell.
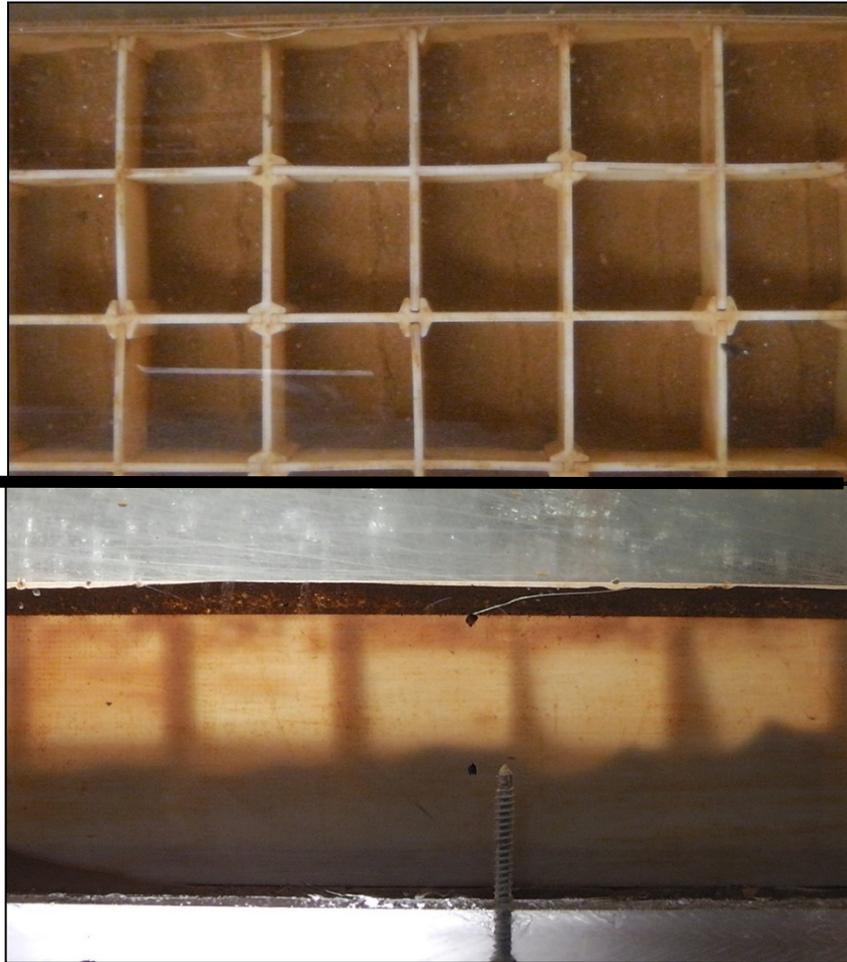
Figure 43 – Post-test configuration H5-W3-50 plan view (top) and profile with backlighting used to illustrate the sediment distribution (bottom)

As the above condition involved the smallest cell size, limited resuspension occurred when compared to other cases. However, as Figure 43 illustrates, based on the sediment movement from the downstream portion of the individual cells to the upstream portion, small vortices are forming within the confinement cells, lifting sediment from the cells at high velocities.
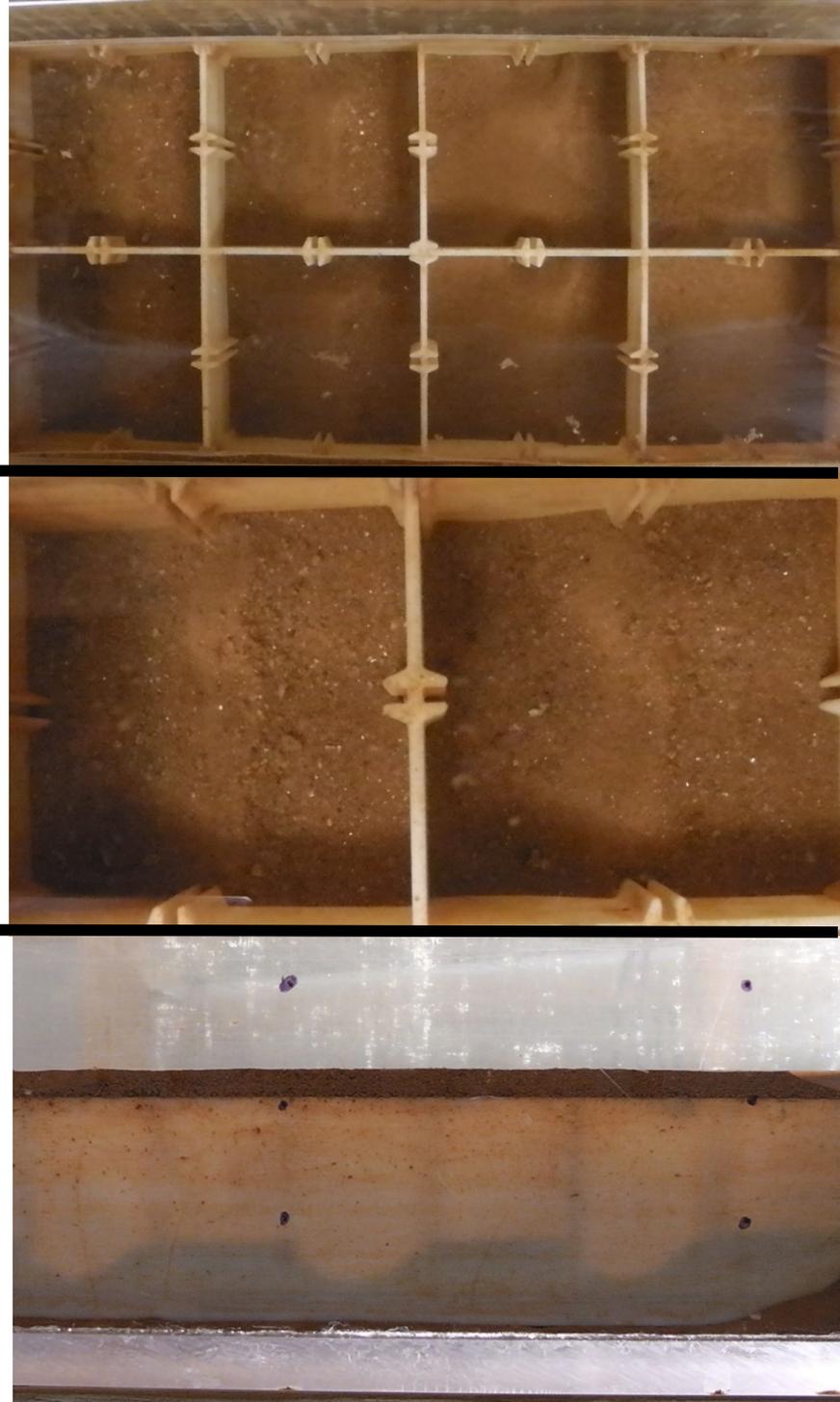
Figure 44 - Configuration H5-W6-50 plan view (top), detailed view of two cells (middle), and profile with use of backlighting (bottom)
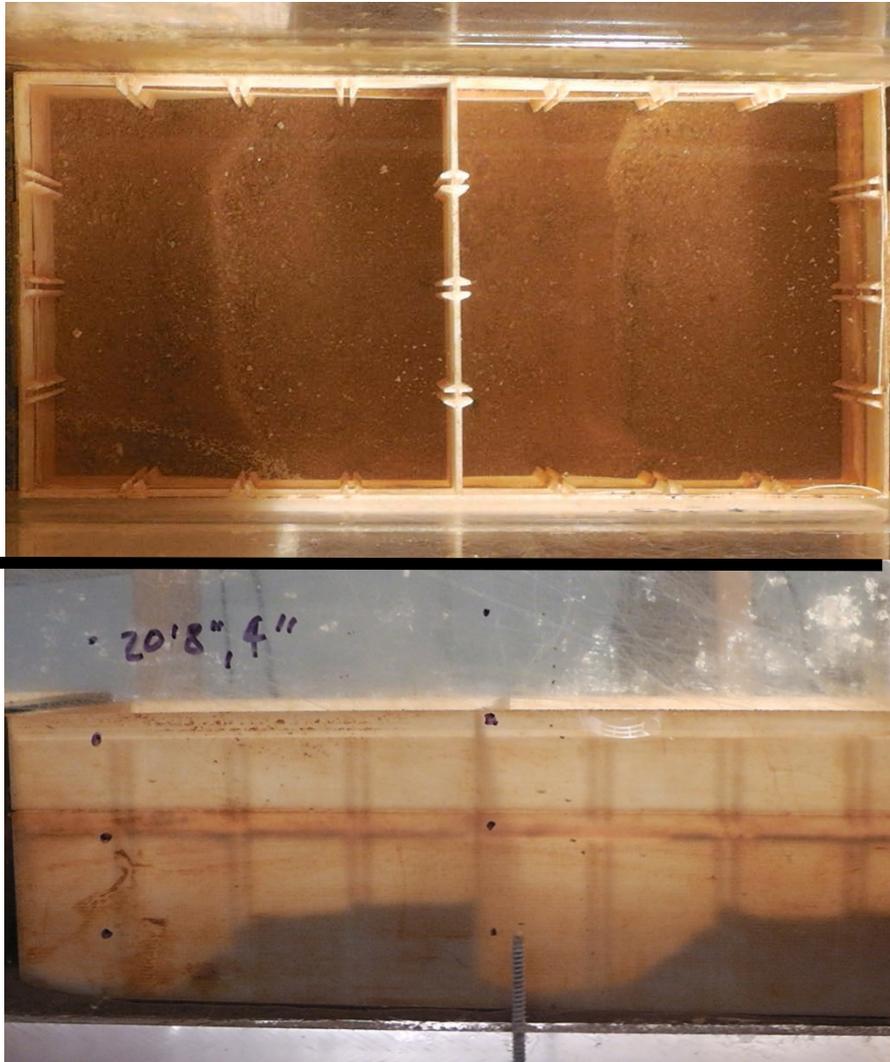
Figure 45 - Configuration H8-W12-50 plan view (top) and profile with use of backlighting (bottom)

Figure 44 and Figure 45 illustrate the punctuated effects of the vortices at the 50 cm/s channel velocity within the confinement cells as cell size increases. There is a large percentage of the sediment within the cells that is either resuspended or deposited on the upstream half of the confinement cells, while, in the case of the H8-W12 configuration, the downstream half of the cells are left nearly depleted of settled sediment.
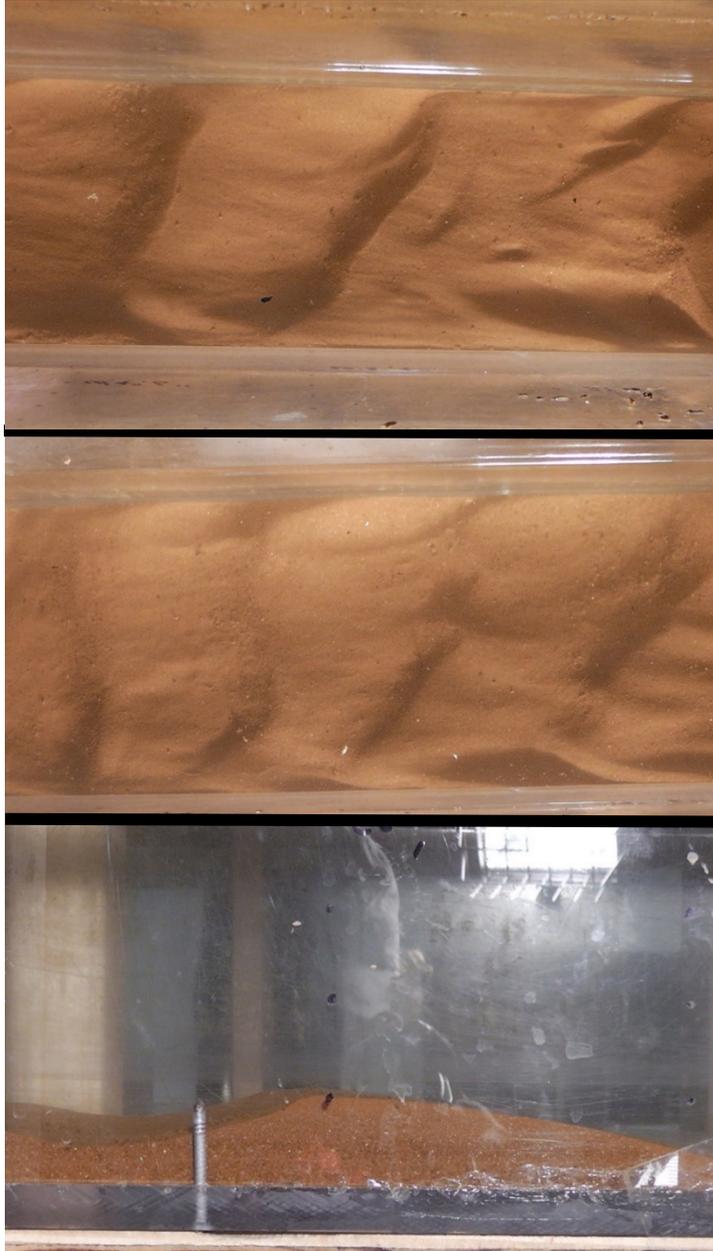
Figure 46 - Unprotected, UP-50 configuration, plan view (top and middle) and profile view (bottom)

Unprotected tests with 50 cm/s flow velocities and resultant shear forces, unlike the confinement cell configurations, produced a series of ripples throughout the entire sediment section, but most noticeably on the leading edge of the sediment. Steadily flowing water is known to create bed forms in natural channels with movable beds (Brush et al, 1966; Kennedy 1963; Andreotti 2012). Depending on flow depth, sediment properties, and velocity of fluid, these various patterns can be observed with regularity (Ashley 1990). The ripples observed in the unprotected tests formed quickly following the initial introduction moving of water and as the velocity stabilized around 50 cm/s. As the tests progressed with time, the bed forms in all cases began to slowly stabilize with either the ripples in the unprotected cases, or varying degrees of

scouring and displacement within the confinement cells, least noticeably in the H8-W3 small cell configurations.

Though the use of observational analysis proves helpful, computational fluid dynamics (CFD) modeling was used to better understand the vortices being formed within the confinement cells. A CFD model (Jue 2017) was created representing the channel and cells used in the present research through interFOAM software. This model was created with the desire of tracking velocity vector intensity and patterns inside the confinement cells by calculating the peak turbulent kinetic energy (TKE) at the soil-water interface. TKE is measured by root-mean-square (RMS) velocity fluctuations. Below, Figure 47 and Figure 48 present the velocity patterns of water for the varying confinement cell configurations, with water flowing from right to left, as with the 3D model presented in Chapter 4.
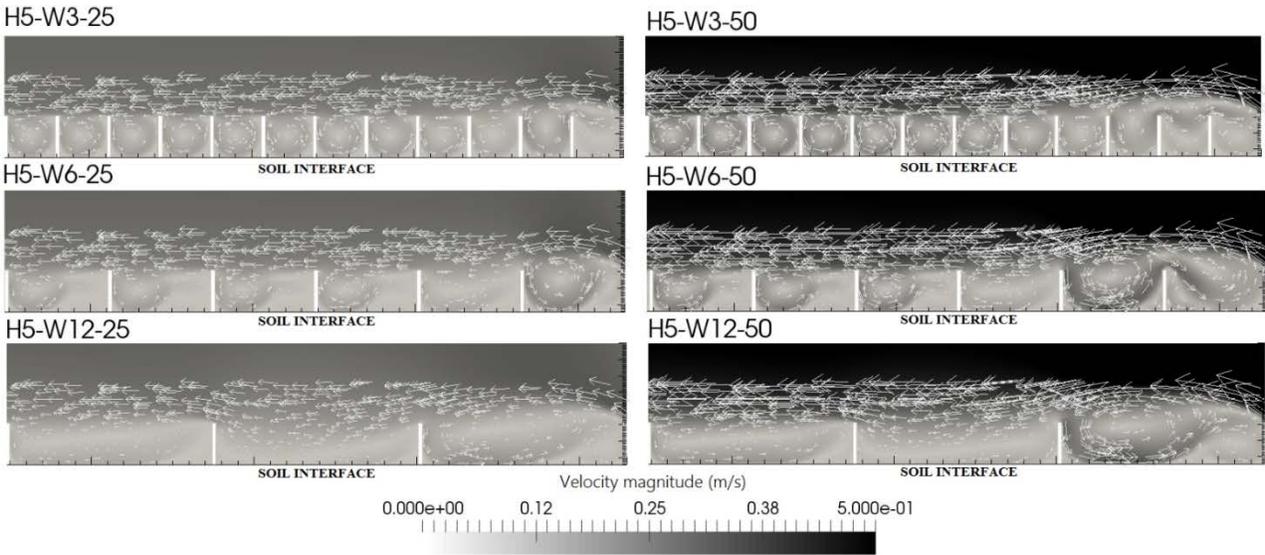
Figure 48 - Velocity patterns in H5 confinement cells through CFD model
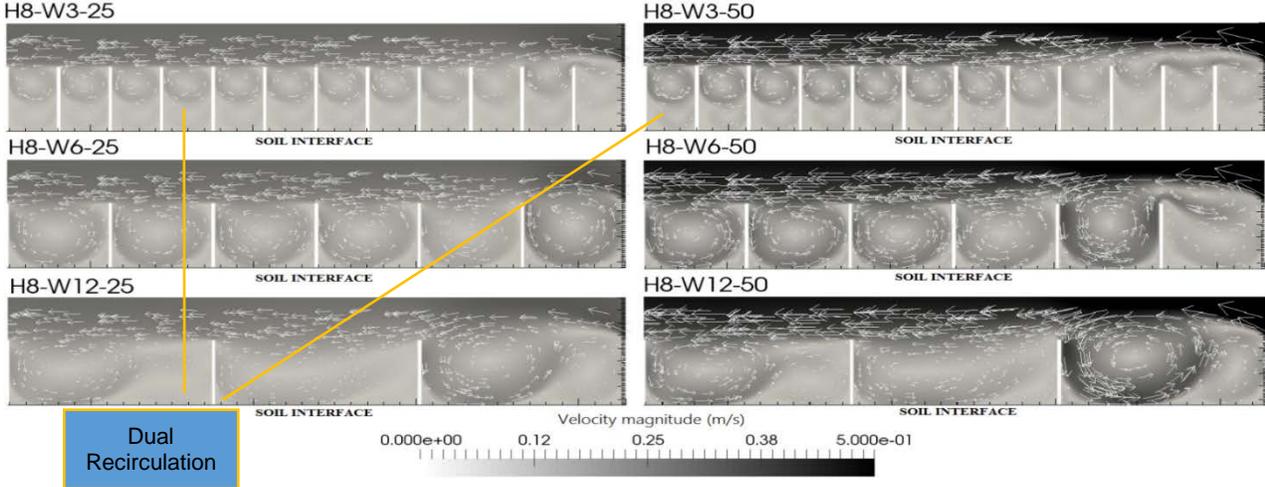
Figure 47 - Velocity patterns in H8 confinement cells through CFD model

In Figures 47 and 48, the lighter the area corresponds to smaller velocity magnitudes. Vortices, or recirculation zones are clearly seen in each cell with a counter-clockwise rotation. The above model suggests that both W6 and W12 configurations may experience flow velocities within the confinement cells that are comparable to the free stream channel velocity and should thus experience greater resuspension and limited protection from shear. The H8-W3 configurations present an interesting dual recirculation zone, due to the cell geometry in which velocities are very low.

The turbulent kinetic energy (TKE) calculations performed by Jue (2017) in interFOAM, presented below in Figure 49, indicate reduced turbulent kinetic energy for the W3 configurations (solid lines), particularly the H8-W3 configuration, with TKE from W6 and W12 configurations (dashed and doted lines) maintaining similarity.
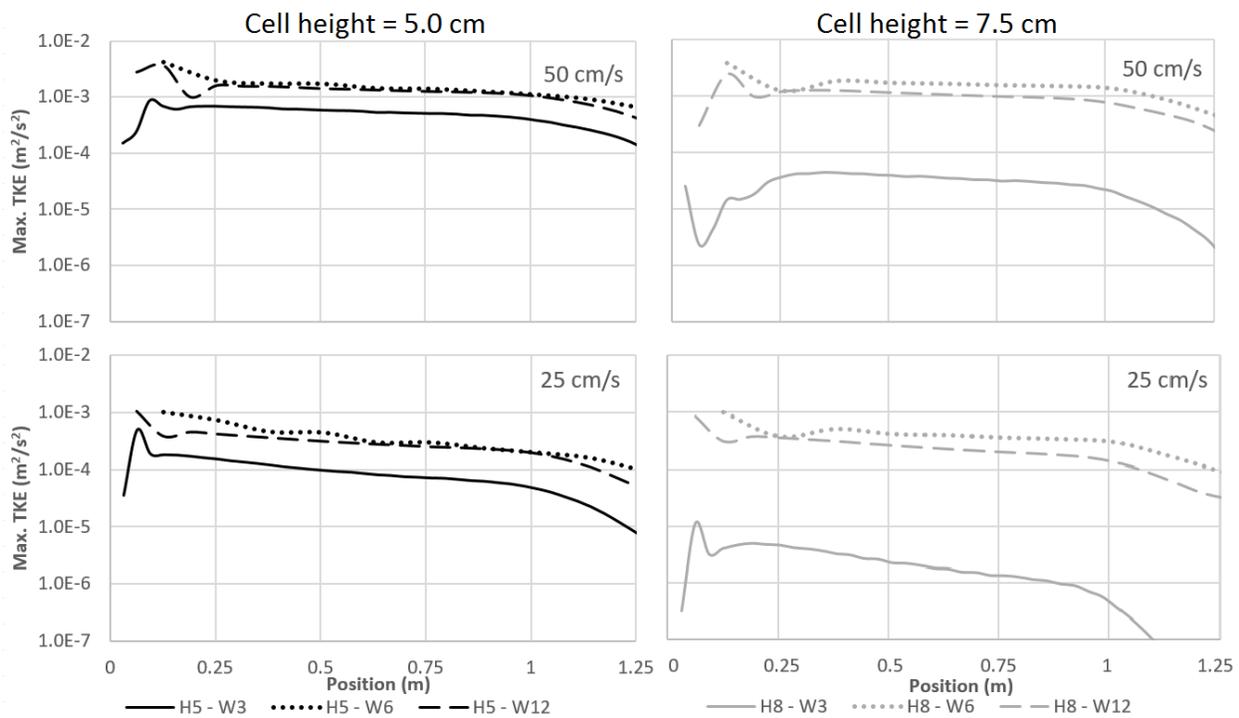
Figure 49 - Relationship between geometry, channel velocity, and maximum TKE

The computational model results, both in TKE and velocity patterns, is reflected in the turbidity measurements taken from the channel effluent, and the post-test bed form observations in the channel with the scouring of the differing test conditions.

5.6. INCIPIENT MOTION RESULTS

Qin's equation (Yang 1993) was used to obtain critical average velocity results for each particle size that was detected by the Mastersizer during PSD characterization. These critical average velocities were estimates of when a particle would begin to be dislodged from the bed form. For incipient motion analysis,

this work was constrained again to the samples that could be evaluated through the Mastersizer apparatus, namely the H8-W6-50 configuration. The associated critical velocity, U_{ck}, is shown in Table 6 below with particle diameters alongside the percentage of the volume that each particle size category corresponded to, together comprising the entirety of the sample:

Table 6 - Critical average velocity according to Qin's Eq. by particle size and sample constitution for H8-W6-50

Size (μm)	% Volume In	Uck (cm/s)
1.6	0.19	10.02
2.0	0.74	10.03
2.4	0.99	10.06
3.0	1.24	10.09
3.7	1.55	10.12
5.5	2.29	10.21
6.7	2.91	10.28
8.2	3.59	10.35
10.1	4.52	10.45
12.4	5.69	10.56
15.2	6.87	10.70
18.6	8.11	10.86
22.8	8.97	11.06
27.9	9.47	11.30
34.2	9.47	11.58
41.9	9.03	11.92
51.4	7.98	12.33
63.0	6.62	12.81
77.2	4.64	13.37
94.6	2.60	14.03
116.0	0.62	14.81

These calculation results for critical velocity are compared with the results from the CFD model created by Jue (2017), and are presented in Table 7. The in-cell average and maximum velocities were compared with the stream velocity in the following table in the case of the H8-W6-50 test:

Table 7 - Comparison of in-cell and stream velocity

H8-W6-50	
Stream Velocity (cm/s)	50
Avg. In-Cell Velocity (cm/s)	7.8
Max In-Cell Velocity (cm/s)	27

For a more general comparison, Figure 50 demonstrates the trends of average and maximum in-cell velocities with their corresponding stream velocity for all the protected cases run at 50 cm/s and 25 cm/s. In the only configuration with PSD data, the H8-W6-50, the max velocity was above U_{ck}, meaning it is statistically likely that some particles of diameter 116-µm, which were the largest particles detected for this configuration, could have been dislodged and detected in the channel effluent, as U_{ck} was exceeded. In terms of experienced in-cell velocities, the most protective condition proved to be the H8-W3 condition. The second-best performing configuration was the H5-W3, showing cell protection was primarily influenced by individual cell area.
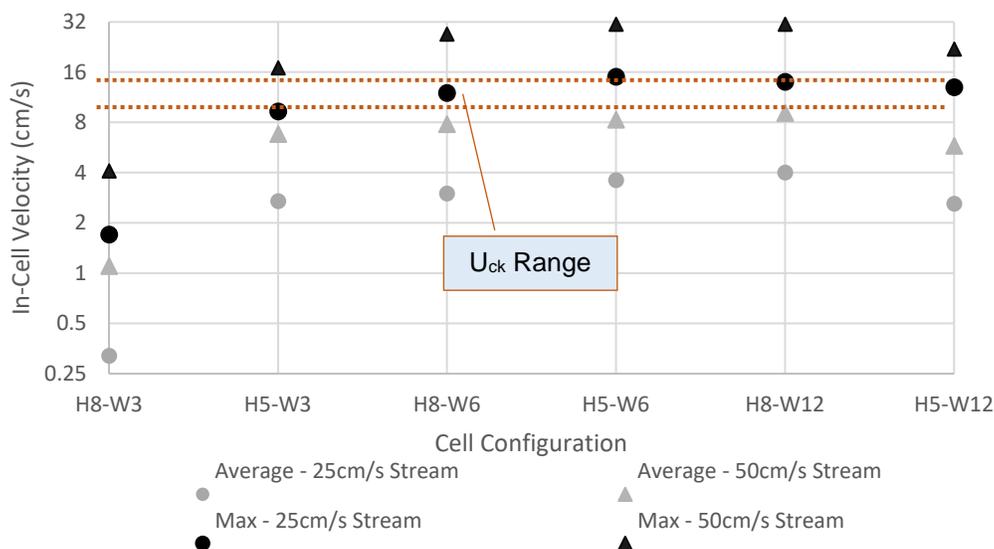
Figure 50 - Comparison of in-cell and channel/stream

The relationship between U_{ck} and in-cell velocities capable of dislodging a particular sediment size is not straightforward, involving complex and dynamic interaction between the sediment surface and confinement cells. Qin's method was not developed for conditions such as the ones tested in the lab, but rather those emulated in natural streams. Discrepancies can possibly be related to this limitation on the applicability of Qin's method. The above relationship would suggest that particles that we observed in the Mastersizer were indeed statistically likely to be observed based on Qin's equations.

5.7. POTENTIAL USE OF CELLULAR CONFINEMENT IN DRAINAGE DITCHES

Cellular confinement for protection from resuspension is a new concept that was initially brought forth in the context of sediment basins. However, there may be potential uses for this technology outside the strict scope of a sediment basin within the scope of sediment control. Cellular confinement may potentially be useful in drainage ditches that traditionally use riprap as a means of energy dissipation and initial sediment control. The following discussion provides a preliminary assessment of a potential use for cellular confinement in a swale, channel, or ditch.

This design assumes the replacement of traditional riprap with a version of cellular confinement already commercially available, and compares the associated general costs. It is assumed that the cost of earthwork and necessary geotextile fabric will not change between the two alternatives, as riprap and cellular confinement installation would require both. The primary cost differences will arise from the purchase and installation costs of riprap as opposed to cellular confinement products.

Riprap has well documented and studied uses and design criteria (Brown and Clyde 1989; NRCS 2004, ALDOT 2014). Brown and Clyde (1989) and NRCS (2004) provided support for the following design. The riprap-lined ditch designed was 50m long and 2.5 meters in breadth. The design included a longitudinal slope of 5% and channel side slopes of 2:1 with a trapezoidal cross-section.

The riprap size chosen was class II which has a mean D_{50} spherical diameter of 485mm. The riprap thickness should be 1.5* D_{max} of 500 mm which equates to a thickness of 750 mm (VDOT 1992). A flow depth of 0.5 meters was assumed throughout the ditch. Figure 51 presents the cross section of the designed ditch and the various areas therein:
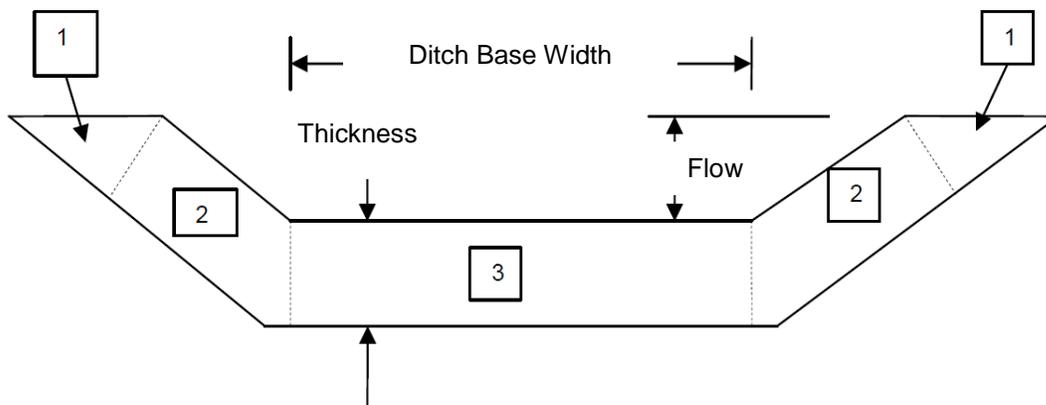
Figure 51 – Ditch cross-section assumed in this section (NRCS 2004)

The following series of equations were used in the volume of stone needed for the channel where the channel is broken into the different areas for simpler calculation (NRCS 2004).

$$A_1 = \frac{(Z^2 + d^2)t}{2}$$ **Equation 10**

$$A_2 = (t^2 + d^2)^{0.5}t$$ **Equation 7**

$$A_3 = b * t$$ **Equation 8**

$$A_T = (2 * A_1) + (2 * A_2) + A_3$$ **Equation 9**

Where,

$$A_{ck} \text{ equals to the ditch cross section area, m}^2$$
$$Z = \text{Ditch wall slope, m/m}$$
$$d = \text{Ditch depth, m}$$
$$b = \text{Ditch base width, m}$$
$$t = \text{Ditch thickness, m}$$
$$A_T = \text{ Total area of cross section in m}^2$$

The use of the above equations yields an A_1 of 1.6 m², an A_2 of 0.68 m², an A_3 of 1.88 m². Combining these values for the total cross-sectional area of A_T yields 6.44 m². With a channel length of 50-m, a volume of 322 m³ of stone will be required. It is estimated that this volume results in a total weight of 842 tons of riprap. Averages from ALDOT projects in 2016 for unit costs of class II riprap are approximately $58 per ton of rock, which translates to $48,854 (ALDOT 2016).

The alternative design using cellular confinement involved absence of the center section of rock, and in its place, applying a cellular confinement product. A thin layer of 0.1-m of rock remained in the base of the channel around the longitudinal perimeter of the cellular confinement product, and 0.5-m of rock remained on the upstream and downstream ends to avoid scouring at the perimeter of the cellular confinement, as illustrated in Figure 52.
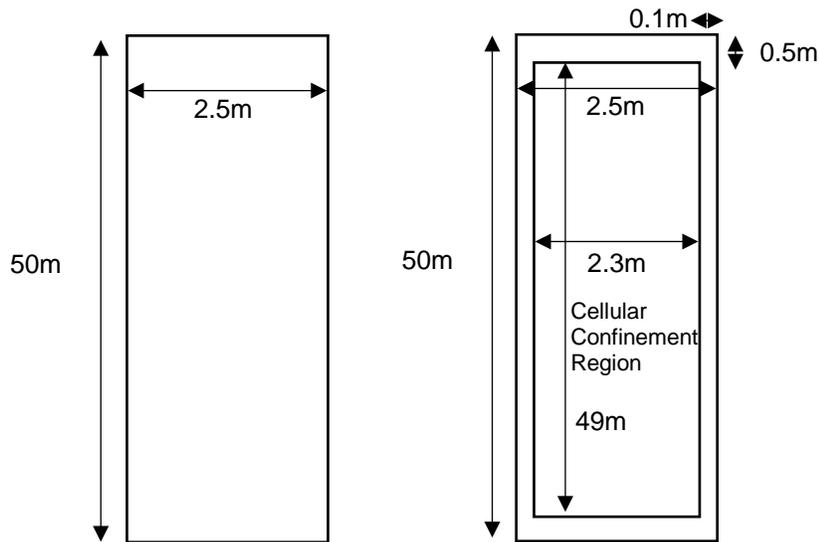
Figure 52 - Proposed channel design with cellular confinement

The cost of rock for the configuration with cellular confinement involves only a fraction of the traditional riprap. At the downstream end, an additional 2.0 x 0.5 x 0.5 m³ volume of riprap is placed to aid in additional energy dissipation. This rock volume, along with the perimeter rock, is included in the estimate. The total volume of rock is 30 m³, with an associated weight of 78.5 tons, and purchasing cost of $4,600 for a $58/ton riprap unit cost.

The commercially available cellular confinement product that was assumed in these calculations was Geocells. Presto Geosystems manufactures the Geocells product that has a cell depth of 200mm, and individual cell areas of 290cm^3 (Presto 2015). Unit prices for the Geocells average $275 per unit (Texas Forest Service 2006). These units require minimal installation that includes simply stretching them out from the tightly bundled package, and stapling them together. The product is shipped in sheets of approximately 2.4m x 6m sheets. A similar application for the product is displayed in the Figure 53.

Figure 53 - Cellular confinement used to stabilize a riprap lined channel. Reference: Prestogeo, 2016

The designed channel for our consideration has an approximate length of 50m, which would require at least 8 consecutive single sheets. The approximate cost of this material is $2,200 without the inclusion of installation. A conservative installation time of three hours, with a three-person team payed $100/hr for labor, the final cellular cost would be $3,100. This sum, in addition to the price of the needed rock for the design yielded a total estimated cost of $7,700, which is a fraction of the cost of the riprap alternative of $48,854. Thus, it may be worthwhile to explore this application in greater detail, using large-scale testing in controlled conditions to assess whether cellular confinement could be used as a replacement for traditional riprap ditches.

5.8. STATISTICAL ANALYSIS RESULTS

Additional statistical analysis was performed in addition to the brief Student's t-test outlined in Chapter 3.4. The experimental program undertaken involved 14 different testing configurations across 2 flow velocities. These tests were repeated a minimum of 3 times. Below in Table 8 and Table 9, configuration repetitions are displayed as well as other key test data. The peak NTU displayed in the tables below are averaged peaks from all of the configuration repetitions and not a single peak value. The average NTU is the averaged turbidity of all repetitions for the entire test duration. The standard deviation of peak NTU is the deviations from one repetition's peak NTU to another. The standard deviation of average NTU is the deviation of one repetitions averaged turbidity to all other repetitions of the same configuration.

Table 8 - 50cm/s Statistical Results

Config.	Repetitions	Peak NTU	Avg. NTU	Std. Dev. Of Peak NTU	Std. Dev. Of Avg. NTU
UP-50	6	912.5	209.3	78.45	33.95
H5-W12-50	3	451.3	201.7	39.02	9.26
H8-W12-50	3	376.0	174.8	21.00	28.68
H5-W6-50	3	316.0	137.7	135.65	20.94
H8-W6-50	4	117.7	71.5	42.58	28.39
H5-W3-50	6	49.0	27.0	11.65	7.88
H8-W3-50	5	29.9	10.5	20.61	6.11

Table 9 - 25 cm/s Statistical Results

Config.	Repetitions	Peak NTU	Avg. NTU	Std. Dev. Of Peak NTU	Std. Dev. Of Avg. NTU
UP-25	3	98.1	28.3	50.67	7.92
H5-W12-25	3	111.0	30.9	4.58	5.37
H8-W12-25	3	139.0	28.2	23.52	4.00
H5-W6-25	3	61.9	18.0	8.37	0.97
H8-W6-25	3	74.5	15.1	16.47	2.02
H5-W3-25	3	66.5	13.2	21.11	4.05
H8-W3-25	4	29.1	7.4	4.32	0.98

In order to avoid familial data set errors by using repeated unpaired t-test results, an analysis of variance (ANOVA) test was carried out twice, 1 for each flow velocity test set. Each test included the UP configuration and all the confinement configurations for that particular flow velocity. The one-way ANOVA test provides an ANOVA F-value that corresponds to a p-value. This p-value indicates whether the data sets are significantly different from one-another or not. For a 95% confidence interval, the p-value must be less than 0.05 to indicate significance. For the 50 cm/s test series, a p-value of 0.0071 was obtained indicating significance. For the 25 cm/s test series, a p-value of 0.39 was obtained which indicates statistical insignificance between data sets (e.g. too much noise or randomness).

Beyond the ANOVA test, post-hoc analysis was completed by means of the Tukey honest significant difference (HSD) test. This analysis provides pair-by-pair significance of treatments, or configuration data sets. Each pair included the UP configuration, and one confinement cell configuration, making the UP the control variable. Below in Table 10 and Table 11, the Tukey HSD results are shown, along with the reputations each configuration was tested in the channel and other relevant data.

Table 10 - 50 cm/s ANOVA and post-hoc results

Config.	Tukey HSD P-Value	Stat. Sign.	ANOVA p-Value for Data Set
UP-50	-	-	
H5-W12-50	0.899	No	
H8-W12-50	0.899	No	0.0071
H5-W6-50	0.899	No	**.0071% Null Hypothesis Correct for all 50cm/s Data**
H8-W6-50	0.338	No	
H5-W3-50	0.084	No	
H8-W3-50	0.0442	Yes	

Table 11 - 25 cm/s ANOVA and post-hoc results

Config.	Tukey HSD P-Value	Stat. Sign.	ANOVA p-Value for Data Set
UP-25	-	-	
H5-W12-25	0.899	No	
H8-W12-25	0.899	No	0.39
H5-W6-25	0.899	No	**39% Null Hypothesis Correct for all 25cm/s Data**
H8-W6-25	0.899	No	
H5-W3-25	0.876	No	
H8-W3-25	0.608	No	

5.9. SUMMARY

Chapter 5 presented and discussed experimental results collected over the course of the present research. The velocity data from the ADV sensor confirmed desired flow rates of 50 cm/s and 25 cm/s within the channel. Turbidity data revealed varying degrees of sediment protection, according to effluent turbidity, corresponding to the configuration of the confinement cells. A dimensionless resuspension parameter, R_p, was proposed to combine geometry and flow characteristics to predict effectiveness of confinement cells in limiting the peak turbidity during intense shear flows in the channel.

Particle size distribution results indicated a trend of more sediment particles of larger diameter in the effluent, and fewer fine particles in the effluent as time progresses in the H8-W6-50 configuration. Bedforms were displayed across the testing conditions, that showed the effect of vortices within the confinement cells, and the scouring of the unprotected sediment surface. The numerical results were consistent with observations of intra-cell scouring during experiments. Incipient motion was then explored through the use of Qin's equation in order to attempt drawing similarities from observed laboratory conditions, and conditions predicted by a set of equations, of which no strong ties seem to be present. A

generalized outline of a design comparison was made for a potential application for the confinement cells – a ditch, in which the confinement cells proved substantially more economical. Statistical analysis was then performed across the data pairs of the two flow velocities showing statistical significance of the 50 cm/s data set, and specifically the UP-50 vs. the H8-W3-50 pair showed a Tukey HSD p-value of 0.0442, giving quantifiable significance to confinement cell protection. Lastly, linear regression analysis was completed which revealed a significant correlation between cell H:W ratios and average turbidity, a plot was then made with test data and R^2 values of best-fitting power curves exceeded 0.9 for both flow velocity conditions.

CHAPTER 6 - CONCLUSIONS AND RECOMMENDATIONS

Consistently throughout this experimental program, the data collected from turbidity measurements proved that cellular confinement is a viable and effective process for reducing the turbidity of channel effluent created by resuspension. Protection from scour and resuspension increased first as a function of cell area, and then as a function of cell height. The reduced flow tests (v = 25 cm/s) revealed similar trends as the full-flow tests, but turbidity reduction was not as substantial. With the exception of the H8-W12-25 and the H5-W12-25 configurations, which performed similar to the UP-25 (unprotected) configuration, the other protected cases generally saw sequentially lower turbidities as protection increased. The fully protected H8-W3-25 configuration, saw a decrease in peak and average turbidities of 71% and 73%, respectively, when compared with the UP-25 test.

The least protective cellular confinement configuration tested under full-flow conditions (v = 50 cm/s), the H5-W12-50, yielded peak turbidities that were 51% less than corresponding values experienced by the unprotected configuration (UP-50). The most protected configuration under full flow conditions, the H8-W3-50 configuration, when compared to the UP-50 test, saw a 96% decrease in peak turbidity, and a 95% decrease in average turbidity of experimental apparatus effluent. For the full-flow series of tests, every intermediate increased protection configuration in terms of progressively smaller cell widths, then larger cell height, saw a decrease in both peak turbidity, and average turbidity measured with the cellular confinement in place. Across all tests, the geometric parameter that most influenced turbidity was the cell width. The resuspension parameter, Rp, also decreased substantially as protection levels increased. Paired with the peak turbidity and cell geometry, Rp provided a useful method to characterize protection.

The success of the cellular confinement arrangements, most noticeably under conditions with high flow rates, indicates that cellular confinement strategies may have good applicability to the mitigation of sediment resuspension within sediment basins, ditches, and channels.

The results from the particle size distribution tests were also a clear indication of the ability of the cellular confinement structures to limit particles from escaping the construction site with the effluent. As per Stokes Law, which predicts larger particles settling first, it was noticed that finer sediments settled later and formed a layer on top of the coarser particles within each individual cell. This process, along with their increased mass, made it more difficult for the larger particles to be resuspended when compared with the smaller particles. Relative to the unprotected configuration, the samples taken from the effluent for PSD analysis with cellular confinement in place had substantially lower particle counts and accompanying lower turbidity as a result of reduced resuspension. The H8-W6-50 configuration examined for PSD was substantially less turbid than the UP-50 case, and the PSD analysis revealed that of the fewer particles that were resuspended from inflows, more were smaller in diameter in comparison. Fewer large particles were resuspended with the cellular confinement in place, comparatively. This finding indicates that, as the tests

progressed, the UP condition quickly resuspended the fines on the top layer of the bed while the H8-W6-50 condition protected these fine sediments for a longer period of time, as they continued to be sampled over the weir for the duration of the test.

The incipient motion calculations showed critical average velocities that were greater than the average velocity results yielded by the CFD model created by Jue (2017). The Uck parameter, for our tests, over-predicted the average critical velocity. The in-cell average velocity based on the CFD model was less than, or near to, the average critical velocity put forth by Qin. It was interesting to note, however, that the velocities experienced within the cellular confinement cells for the H8-W6 case were less than 16% of the free-stream velocities experienced in the channel. This finding, coupled with a direct correlation between velocity and incipient motion, aided in the demonstration of a quantifiable advantage of the use of cellular confinement, though correlation to the mathematical model still needs further work. The maximum velocities that were modeled within the cells, exceeded Qin's average velocity values in most configurations, and some of the particles detected by the Mastersizer in our sample may have been dislodged during such high-velocity sweeps. The applicability of Qin's model may be limited to natural streams and not extend to cellular confinement in a laboratory.

Statistical analysis of the present work yielded two key conclusions. Firstly, between the most protective case, H8-W3-50, and the control, UP-50, there exists a statistically significant difference within a 95% confidence interval. This difference quantitatively confirms the hypothesis that confinement cells act as a means to limit sediment resuspension. Secondly, for both flow velocity conditions of 25, and 50 cm/s, a linear regression test yielded a statistically significant positive correlation, within 95% confidence intervals, between cell H:W ratios and average turbidity normalized by the unprotected configuration. This result confirms that, with our soil and up to our geometric limit of 2.5, an increase in H:W will decrease the average experienced turbidity in effluent. Further regression testing with a power curve of the data, yielded R^2 values of greater than .9 for both flow velocity conditions.

6.1. RECOMMENDATIONS FOR FUTURE WORK

While the present work yielded consistent conclusions, it was limited by its small scale. There is a need for the full-scale testing of such cellular confinement technology within sediment basins and within swales, ditches, and drainage areas for further data. There would also be enormous benefit from the creation of a 3-D computational model for both observational purposes, and insight into the changes in hydrodynamic forces, such as vortices and eddies, that provide shielding within the confinement cells. This 3-D model would allow comparison of experimental data and computational results that would prove helpful in better understanding the nature of protection that confinement cells offer. It would also be useful to have more data for incipient motion analysis and PSD analysis. The nature of our instruments limited our testing to a single PSD test condition, and testing many more cell geometries would be helpful in forming more detailed conclusions.

An additional field for further study would be the optimization of the geometry of the cells themselves. In the tests discussed in this document, all cells were rectangular and sat perpendicular to the

sediment bed. Cells also were limited to a maximum H:W ratio of 2.5, higher ratios should be observed in future work. Exploration of cells that are shaped similar to lamella settlers, or confinement systems that are comprised of many varying cell sizes instead of a single, repeated cell size, may also yield interesting results. These efforts could result in the commercial use of cellular confinement as a means of sediment resuspension prevention in construction sites.

REFERENCES

Adrian, R. J., and Z. C. Liu. (2002). Observation of vortex packets in direct numerical simulation of fully turbulent channel flow, J. Visualization, 5(1), 9–19.

Alabama Department of Environmental Management, "Construction General Permit." Available online: http://www.adem.state.al.us/programs/water/constructionstormwater.cnt. (Accessed May 11, 2017).

Alabama Department of Transportation. (2016). Tabulation of Bids. Available online: alletting.dot.state.al.us/BidTabs/Bidtab_2016.html (accessed on 29 November 2016).

Alabama Department of Transportation. (2010). "ALDOT Sedimentation Basin Recommendations." Montgomery, AL.

Alabama Department of Transportation (2014). "Handbook for Erosion Control, Sediment Control and Stormwater Management on Construction Sites and Urban Areas." Alabama Soil and Water Conservation Committee. Montgomery AL.

Andreotti, B., Philippe C., Olivier D., Orencio D., and Antoine F., (2012)."Bedforms in a turbulent stream: ripples, chevrons and antidunes." Journal of Fluid Mechanics 690: 94-128.

Arulanandan, K., Loganathan, P., and Krone, R. B. (1975). ''Pore and eroding fluid influences on surface erosion of soil.'' J. Geotech. Engr., ASCE, 101(1), 51–66.

Aryal, R. K. & Lee, B. K. (2009). Characteristics of suspended solids and micropollutants in first-flush highway runoff. Water, Air, & Soil Pollution: Focus 9 (5–6), 339–346.

Ashley, G. M. (1990). "Classification of large scale subaqueous bedforms: a new look at an old Problem". J. Sedim. Res. 60, 161–172.

Bentzen, T. R., Larsen, T., and Rasmussen, M. R. (2009). "Predictions of resuspension of highway detention pond deposits in interrain event periods due to wind-induced currents and waves." J. Environ. Eng., 10.1061/(ASCE)EE.1943-7870.0000108, 1286–1293.

Benson, John. "Reynolds." NASA. NASA, 12 June 2014. Web. 07 Nov. 2016.

Bhaduri, B.L., Harbor, J.M., Maurice, P. (1995). "Chemical trap efficiency of a construction site stormwater retention basin". Phys. Geogr. 16, 389–401.

Bidelspach, D. A., and Jarrett, A. R. (2004). "Electro-mechanical outlet flow control device delays sediment basin dewatering." Appl. Eng. Agric., 20(6), 759–763.

Brown, Scott A., and Eric S. Clyde. (1989). "Design of riprap revetment."

Brush, L. M., Jr., Einstein, H. A., Simons, D. B., Vanoni, V. A., Kennedy, J. F. (1966). "Nomenclature for bed forms in alluvial channels." Proc. Am. Soc. Civil. Engrs., J. Hydraulics Div., 92, 5 1-64

Buffington, J. M., W. E. Dietrich, and J. W. Kirchner. (1992). "Friction angle measurements on a naturally formed gravel streambed Implications for critical boundary shear stress," Water Resour. Res., 28, 411-425.

Chen, Charng-Ning. (1975)."Design of sediment retention basins." In Proceedings of the National Symposium on Urban Hydrology and Sediment Control, July 28-31, 1975., no. UKY BU109.

Culp, G., Hansen, S., and Richardson, G. (1968). "High rate sedimentation in water treatment works." J. Am. Water Works Assn., 60(6), 681.

De Oliveira, R., Pearson, H.W., Silva, J.V.N., Sousa, J.T., Leite, V.D., Lopes, W.S. (2011). "Baffled primary facultative ponds with inlets and outlets set at different levels treating domestic wastewater in northeast Brazil." Water Sci. Technol. 63 (6), 1183.

Di Stefano, C., V. Ferro, V. Pampalone, and F. Sanzone. (2013). "Field investigation of rill and ephemeral gully erosion in the Sparacia experimental area, South Italy." Catena 101: 226-234.

Eadie, Brian J., Richard L. Chambers, Wayne S. Gardner, and Gerald L. Bell. (1984). "Sediment trap studies in Lake Michigan: Resuspension and chemical fluxes in the southern basin." Journal of Great Lakes Research 10, no. 3: 307-321.

Environmental Protection Agency (EPA). (2004). "The use of best management practices (BMPs) in urban watersheds." Rep. No. EPA 600/R-04/184, Office of Research and Development, Washington, D.C.

Environmental Protection Agency – EPA (2012a) National pollutant Discharge Elimination System Home – Construction Site Stormwater Runoff Control, EPA Office of Water, Washington DC, 2012.

Environmental Protection Agency – EPA (2012b). 5.5 Turbidity. In Water: Monitoring & Assessment. Retrieved from http://water.epa.gov/type/rsl/monitoring/vms55.cfm

Fennessey, L. A. J., and A. R. Jarrett. (1977). "Influence of principal spillway geometry and permanent pool depth on sediment retention of sedimentation basins." Transactions of the ASAE 40, no. 1: 53-59.

Fan, C., Field, R., and Lai, F. (2003). "Sewer-Sediment Control: Overview of an Environmental Protection Agency Wet-Weather Flow Research Program." J. Hydraul. Eng., 10.1061/(ASCE)0733-9429(2003)129:4(253), 253-259.

Fang, X., Zech W., and Logan C., (2015). "Stormwater Field Evaluation and Its Challenges of a Sediment Basin with Skimmer and Baffles at a Highway Construction Site." Water 7, no. 7: 3407-3430.

Farjood, A, Melville B, and Shamseldin A., (2015). "The effect of different baffles on hydraulic performance of a sediment retention pond." Ecological Engineering 81: 228-232.

Garofalo, G. (2012). "Physical and Computational Fluid Dynamics Modelling of Unit Operations Under Transient Hydraulic Loadings". University of Florida.

Goldman, S. J., Jackson, K., and Bursztynsky, T. A. (1986). "Erosion and Sediment Control Handbook", McGraw-Hill, New York, NY.

Grayson, R. B., Brian L. Finlayson, C. J. Gippel, and B. T. Hart. (1996). "The potential of field turbidity measurements for the computation of total phosphorus and suspended solids loads." Journal of Environmental Management 47, no. 3: 257-267.

Graf, W. H. 1971. "Hydraulics of Sediment Transport". New York, N.Y.: McGraw−Hill.

Gippel, Christopher J. (1989). "The use of turbidimeters in suspended sediment research." In Sediment/Water Interactions, pp. 465-480. Springer Netherlands.

Harbor, J., Snyder, J., Storer, J. (1995). "Reducing nonpoint source pollution from construction sites using rapid seeding and mulching." Phys. Geogr. 16, 371–388.

Harbor, Jon. (1999) "Engineering geomorphology at the cutting edge of land disturbance: erosion and sediment control on construction sites." Geomorphology 31, no. 1: 247-263.

Hazen, Allen. (1904) "On sedimentation." Trans. ASCE 53, no. 980: 45-88.

He, Cheng, and Jiri Marsalek. (2009). "Vortex plate for enhancing particle settling." Journal of Environmental Engineering 135.8: 627-635.

He, C. and Marsalek, J. (2014). "Enhancing Sedimentation and Trapping Sediment with a Bottom Grid Structure." J. Environ. Eng., 10.1061/(ASCE)EE.1943-7870.0000774, 21-29.

Holland, A. F., (2004). "Linkages between tidal creek ecosystems and the landscape and demographic attributes of their watersheds." J. Exp. Mar. Biol. Ecol., 298 (2), 151–178.

Hunt, C. and Grow, J. (2001) "Impacts of Sedimentation to a Stream by a Non-Compliant Construction Site". Bridging the Gap: pp. 1-10. doi: 10.1061/40569(2001)20.

Hurther, D. (2001), 3-D "Acoustic Doppler Velocimetry and turbulence in open-channel flow", Ph.D. dissertation, Ecole Polytech. Fed. de Lausanne, Lausanne, France.

Jackson, R. G. (1976), "Sedimentological and fluid-dynamic implication of the turbulent bursting phenomenon in geophysical flows", J. Fluid Mech., 77, 531–560, doi:10.1017/S0022112076002243.

Jadhav, R.S., and S.G. Buchberger. (1995). "Effects of vegetation on flow through free water surface wetlands." Ecol. Eng. 5:481–496.

Jarrett, A. R. (1996). "Sedimentation basin evaluation and design improvements." Final completion report. Hillsborough, N.C.: Orange County Board of Commissioners.

Booth J.G., Miller R.L., McKee B.A., Leathers R.A. (2000). "Wind-induced bottom sediment resuspension in a microtidal coastal environment." Cont. Shelf Res., 20, pp. 785–806.

Kang, J., Scott K., and Richard M., (2016). "Flocculated sediments can reduce the size of sediment basin at construction sites." Journal of Environmental Management 166: 450-456.

Kennedy, J. F. (1963). The mechanics of dunes and antidunes in erodible-bed channels. J. Fluid Mech., 16, 521-44.

Khan, S., Melville, B.W., Shamseldin, A. (2013). "Design of storm-water retention ponds with floating treatment wetlands." J. Environ. Eng. 139 (11), 1343–1349 (United States).

King, J.K., and Blanton, J. O. (2011). "Model for predicting effects of land-use changes on the canal-mediated discharge of total suspended solids into tidal creeks and estuaries." J. Environ. Eng. 10.1061/(ASCE)EE.1943-7870.0000395, 920-927.

Knapen, A., Poesen J., Govers G., Gyssels G., and Nachtergaele J., (2007). "Resistance of soils to concentrated flow erosion: A review." Earth-Science Reviews 80, no. 1: 75-109.

Krone, R. B. (1979). "Sedimentation in San Francisco Bay System." San Francisco Bay: The Urbanized Estuary, California Academy of Sciences, San Francisco, Calif.

Langendoen, Eddy J. (2000). "CONCEPTS-Conservational channel evolution and pollutant transport system." Research Rep 16.

Lelouvetel, J., F. Bigillon, D. Doppler, I. Vinkovic, and J.-Y. Champagne. (2009), Experimental investigation of ejections and sweeps involved in particle suspension, Water Resour. Res., 45, W02416, doi:10.1029/2007WR006520.

Madaras, J. S., and Jarrett, A. R. (2000). "Spatial and temporal distribution of sediment concentration and particle size distribution in a field scale sedimentation basin." Trans. ASABE, 43(4), 897–902.

Marchioli, C., and Soldati, A. (2002). "Mechanisms for particle transfer and segregation in a turbulent boundary layer." J. Fluid Mech., 468, 283–315.

Marsh, N. A., Western, A. W., & Grayson, R. B. (2004). "Comparison of methods for predicting incipient motion for sand beds." Journal of hydraulic engineering, 130(7), 616-621.

McLaughlin, R.A., Hayes, S.A., Clinton, D.L., McCaleb, M.M., Jennings, G.D. (2009). "Water quality improvements using modified sediment control systems on construction sites." Trans. ASABE 52, 1859-1867.

Meisner, J. E., and Robert F. Rushmer. (1963). "Eddy formation and turbulence in flowing liquids." Circulation Research 12, no. 5: 455-463.

Mehta, A. J., Hayter, E. J., Parker, W. R., Krone, R. B., and Teeter, A. M. (1989). "Cohesive sediment transport. Part I: Process description." J. Hydraul. Eng., 115 (8), pp. 1076-1093.

Mehta, A.J., W.H. McAnally, E.J. Hayter, A.M. Teeter, D. Schoellhamer, S.B. Heltzel, W.P. Carey. (1989). Cohesive Sediment Transport II: Application Journal of Hydraulic Engineering, Vol. 115 (No. 8), pp. 1094–1112.

Millen, J. A., A. R. Jarrett, and J. W. Faircloth. (1997). "Experimental evaluation of sedimentation basin performance for alternative dewatering systems." Trans. ASAE 40(4): 1087−1095.

Miller, R. T., and R. J. Byrne (1966). "The angle of repose for a single grain on a fixed rough bed." Sedimentology, 303-314.

Moore, Walter B., and Bruce A. McCarl. (1987). "Off-site costs of soil erosion: a case study in the Willamette Valley." Western Journal of Agricultural Economics: 42-49.

National Pollutant Discharge Elimination System Permit—General Permit. Available online: http://adem.alabama.gov/programs/water/waterforms/ALR10CGP.pdf (accessed on 8 November 2016).

Natural Resources Conservation Service – Maryland. (2004) Design Guide MD#6 RipRap Design Methods. Available online: https://efotg.sc.egov.usda.gov/references/public/MW/Design_Guide_6.pdf (accessed on 29 November 2016).

Natural Resources Conservation Service. (2010) "Sediment Basin." Conservation Practice Standard Design Guide. Code 350.

Nachtergaele, J, Poesen, J. (2002). "Spatial and temporal variations in resistance of loess-derived soils to ephemeral gully erosion." European Journal of Soil Science, 53, pp. 449–463.

Osman, Akode M., and Colin R. Thorne. (1988). "Riverbank stability analysis. I: Theory." Journal of Hydraulic Engineering 114.2: 134-150.

Pedinotti, S., Mariotti, G., and Banerjee, S. (1992). "Direct numerical simulation of particle behavior in the wall region of turbulent flow in horizontal channels." Int. J. Multiphase Flow, 18, 927–941.

Petterson, T. J. R., German, J., and Svensson, G. (1999). "Pollutant removal efficiency in two stormwater ponds in Sweden." Proc., 8th Int. Conf. on Urban Storm Drainage, Institution of Engineers, Sydney, Australia, 866–873.

Perez, M. (2014) "Evaluation of Inlet Protection Practices (IPPs) Using Large-Scale Testing Techniques." MS Thesis. Auburn University, 2014. Web. May 15, 2017.

Posthumus, H., L. K. Deeks, R. J. Rickson, and J. N. Quinton. (2015). "Costs and benefits of erosion control measures in the UK." Soil use and management 31, no. S1: 16-33.

Poesen, J., Vandaele, K., Van Wesemael, B. (1996). Contribution of gully erosion to sediment production in cultivated lands and rangelands. IAHS Publications 236,251–266.

Presto Geosystems Geoweb Specification Summary. (2015). Available online: http://www.prestogeo.com/downloads/xUa0XErk5aGnhYQLI9QU3XBrd7H2FW93rZ3EejpZ0vDhKTsTR0/geoweb_spec_summary.pdf (accessed on 1 December 2016).

Ravisangar, V., Dennett, K., Sturm, T., and Amirtharajah, A. (2001). "Effect of Sediment pH on Resuspension of Kaolinite Sediments." J. Environ. Eng., 10.1061/(ASCE)0733-9372(2001)127:6(531), 531-538.

Robinson, S. K. (1991), "Coherent motions in the turbulent boundary layer." Annu. Rev. Fluid Mech., 23, 601–639, doi:10.1146/annurev.fl.23.010191.003125.

Rohrer, C., Roesner, L., and Bledsoe, B. (2004). "The Effect of Stormwater Controls on Sediment Transport in Urban Streams. Critical Transitions in Water and Environmental Resources Management: pp. 1-13. doi: 10.1061/40737(2004)71.

Serio, Melissa, and Rebecca Kauten. (2014). "Stormwater Sampling, Water Quality Monitoring and Active DOT Construction Sites: Lessons Learned from Two Years of Data."

Shields, A. (1936). "Anwendung der Aehnlichkeitsmechanik und der Turbulenzforschung auf die Geschiebebewegung." Preussischen Versuchsanstalt für Wasserbau.

Sojka, R.E., Bjorneberg, D.L., Entry, J.A., Lentz, R.D., Orts, W.J. (2007). "Polyacrylamide in agriculture and environmental land management." Adv. Agron. 92, 75-162.

Su, T.-M., Yang, S.-C., Shih, S.-S., Lee, H.-Y. (2009). "Optimal design for hydraulic efficiency performance of free-water-surface constructed wetlands." Ecol. Eng. 35 (8), 1200–1207.

Texas Forest Service. Best Management Practices Product and Vender Guide. (2006). Available online: Ftexasforestservice.tamu.edu%2FuploadedFiles%2FSustainable%2Fbmp%2Fbmp_product_vendor_guide.pdf&usg. (accessed on 1 December 2016).

Thaxton, C. S., Joseph Calantoni, and R. A. McLaughlin. (2004). "Hydrodynamic assessment of various types of baffles in a sediment retention pond." Transactions of the ASAE 47, no. 3: 741.

The City of Calgary. (2011). "Stormwater management and design manual." Calgary. Available from: http://www.calgary.ca/PDA/pd/Documents/urban_development/bulletins/2011-stormwater-management-and-Design.pdf.

Thorne, C.R. (1982). "Effects of vegetation on riverbank erosion and stability. In: Thornes, J.B. (Ed.), Vegetation and Erosion." Wiley, Chichester. pp. 125-143.

United States Geological Survey. (2016). "What Is a Watershed." USGS. US Department of the Interior, United States Geological Survey. Web. 14 Dec. 2016.

United States Environmental Protection Agency. (1999)." Constructed wetlands treatment of municipal wastewaters." (EPA 625-R-99-010). USEPA, Washington, DC.

Utley, B. and Wynn, T. (2008). "Cohesive Soil Erosion: Theory and Practice." World Environmental and Water Resources Congress 2008: pp. 1-10. doi: 10.1061/40976(316)289.

Viola, J. and Leutheusser, H. (2004). "Experiments on Unsteady Turbulent Pipe Flow." J. Eng. Mech., 10.1061/(ASCE)0733-9399(2004)130:2(240), 240-244.

Yager, P. L., Nowell, A. R. M., and Jumars, P. A. (1993). "Enhanced deposition to pits: A local food source for benthos." J. Mar. Res., 51, 209–236.

Yang, C.T., (1972). "Unit stream power and sediment transport." Proc. Am. Soc. Civil Eng. 98, 1805–1826.

Yao, K. M. (1973). "Design of high-rate settlers." J. Environ. Eng. 99(5). 621–637.

Wang, J., (2017). "Characterization of unsteady multiphase flows in stormwater management applications." PhD proposal to Auburn University.

Wu, W. (2007). "Computational River Dynamics." Center for Computational Hydroscience and Engineering. University of Mississippi. Taylor and Francis e-Library.

APPENDICES

Appendix A: Raw averaged data from turbidity measurements

Appendix B: Raw data from turbidity measurements

Appendix C: Particle size distribution data

APPENDIX A - RAW AVERAGE DATA FROM TURBIDITY MEASUREMENTS

Time (Seconds)	15	30	
UP-50	424.8	912.5	10
UP-25	24.4	98.1	2
H8-W3-50	4.2	29.9	1
H8-W3-25	4.6	29.1	1
H8-W6-50	18.7	65.5	10
H8-W6-25	6.9	74.5	1
H8-W12-50	39.3	56.3	26
H8-W12-25	16.0	139.0	2
H5-W3-50	15.9	28.6	4
H5-W3-25	6.4	66.5	1
H5-W6-50	23.2	81.7	16
H5-W6-25	12.5	61.9	2
H5-W12-50	173.3	451.3	43
H5-W12-25	19.6	111.0	3

APPENDIX B - RAW DATA FROM TURBIDITY MEASUREMENTS

H8-W3-50

Sample	Seconds	Turbidity Level					
		Run 1	Run 2	Run 3	Run 4	Run 5	AVG
1	15	3.74	2.01	6.54	4.51		4.2
2	30	10.07	27.4	18.5	29.4	64.1	29.894
3	45	6.54	18.2	7.84	17.3	37.3	17.436
4	60	5.45	26.5	7.48	8.81	22	14.048
5	75	4.2	16.8	5.42	4.8	10.9	8.424
6	90	2.5	7.49	4.28	2.76	13.8	6.166
7	105	1.49	8.31	2.96	7.35	10.6	6.142
8	120	2.47	5.47	2.9	3.06	12.3	5.24
9	135	3.79	2.64	2.17	3.12	4.4	3.224

H8-W3-25

Sample	Seconds	Turbidity Level				
		Run 1	Run 2	Run 3	Run 4	AVG
1	15	5.64	5.30	2.82	4.59	4.59
2	30	25.10	27.10	35.10	29.10	29.10
3	45	5.69	14.00	14.60	11.43	11.43
4	60	6.86	5.86	6.23	6.32	6.32
5	75	3.34	5.03	4.10	4.16	4.16
6	90	2.61	6.22	3.47	4.10	4.10
7	105	2.91	2.75	2.13	2.60	2.60
8	120	1.67	2.28	1.81	1.92	1.92
9	135	3.14	3.10	1.64	2.63	2.63

H5-W3-50

Sample	Seconds	Turbidity Level						
		Run 1	Run 2	Run 3	Run 4	Run 5	Run 6	AVG
1	15	19.20	20.20	2.84	2.71	26.80	23.50	15.88
2	30	22.70	22.70	36.40	34.30	25.90	29.80	28.63
3	45	45.00	51.50	44.60	50.70	52.20	49.90	48.98
4	60	74.40	67.50	40.10	38.10	28.70	31.50	46.72
5	75	58.50	64.60	13.60	12.20	44.70	39.70	38.88
6	90	29.40	32.00	7.44	6.81	26.30	24.80	21.13
7	105	28.40	24.30	7.04	7.17	24.10	23.80	19.14
8	120	20.60	19.10	4.83	4.22	6.86	8.22	10.64
9	135	21.40	18.10	6.18	5.46	14.30	11.18	12.77

H5-W3-25

Sample	Seconds	Turbidity Level			
		Run 1	Run 2	Run 3	AVG
1	15	4.56	4.75	10.00	6.44
2	30	51.70	57.20	90.70	66.53
3	45	17.80	6.73	23.00	15.84
4	60	7.21	5.61	14.80	9.21
5	75	6.21	5.80	6.10	6.04
6	90	3.70	4.29	4.97	4.32
7	105	3.49	3.99	4.11	3.86
8	120	3.64	3.87	3.66	3.72
9	135	2.46	2.88	3.57	2.97

H8-W6-50

Sample	Seconds	Turbidity Level				
		Run 1	Run 2	Run 3	Run 4	AVG
1	15	28.30	21.60	6.27		18.72
2	30	57.80	61.60	53.60	88.90	65.48
3	45	84.60	78.60	84.80	180.00	107.00
4	60	84.30	108.00	98.50	180.00	117.70
5	75	74.10	92.60	84.10	177.00	106.95
6	90	48.90	54.80	66.70	105.00	68.85
7	105	46.20	55.80	55.70	109.00	66.68
8	120	34.70	44.20	47.20	78.90	51.25
9	135	41.60	37.10	40.50	44.00	40.80

H8-W6-25

Sample	Seconds	Turbidity Level			
		Run 1	Run 2	Run 3	AVG
1	15	10.00	7.17	3.67	6.95
2	30	59.80	92.30	71.40	74.50
3	45	16.40	18.90	6.99	14.10
4	60	11.90	15.70	9.08	12.23
5	75	7.89	4.96	12.20	8.35
6	90	7.26	8.30	4.16	6.57
7	105	8.64	2.03	4.51	5.06
8	120	5.65	3.09	5.24	4.66
9	135	5.25	3.19	2.45	3.63

H5-W6-50

Sample	Seconds	Turbidity Level			
		Run 1	Run 2	Run 3	AVG
1	15	6.44	38.80	24.30	23.18
2	30	60.30	102.00	82.80	81.70
3	45	302.00	168.00	26.20	165.40
4	60	298.00	190.00	460.00	316.00
5	75	247.00	160.00	225.00	210.67
6	90	119.00	133.00	235.00	162.33
7	105	103.00	91.00	170.00	121.33
8	120	97.20	90.90	103.00	97.03
9	135	48.60	59.60	76.70	61.63

H5-W6-25

Sample	Seconds	Turbidity	Level		
		Run 1	Run 2	Run 3	AVG
1	15	11.20	10.20	16.00	12.47
2	30	63.80	52.70	69.10	61.87
3	45	26.60	22.90	14.10	21.20
4	60	10.30	34.40	26.00	23.57
5	75	13.90	9.93	6.61	10.15
6	90	18.00	5.25	16.70	13.32
7	105	6.36	4.14	6.21	5.57
8	120	7.98	8.94	6.56	7.83
9	135	4.21	4.00	8.58	5.60

H8-W12-50

Sample	Seconds	Turbidity Level			
		Run 1	Run 2	Run 3	AVG
1	15	21.50	31.00	65.30	39.27
2	30	53.80	33.50	81.70	56.33
3	45	283.00	221.00	291.00	265.00
4	60	400.00	361.00	367.00	376.00
5	75	290.00	247.00	330.00	289.00
6	90	196.00	176.80	262.00	211.60
7	105	139.00	127.90	203.00	156.63
8	120	76.50	73.50	152.00	100.67
9	135	76.20	63.90	95.80	78.63

H8-W12-25

Sample	Seconds	Turbidity Level			
		Run 1	Run 2	Run 3	AVG
1	15	16.90	14.30	16.70	15.97
2	30	112.00	150.00	155.00	139.00
3	45	21.30	30.90	16.50	22.90
4	60	19.10	19.20	14.50	17.60
5	75	23.90	28.00	18.20	23.37
6	90	8.94	12.70	22.87	14.84
7	105	9.87	4.71	9.60	8.06
8	120	4.97	4.96	9.89	6.61
9	135	7.75	3.93		5.84

H5-W12-50

Sample	Seconds	Turbidity Level			
		Run 1	Run 2	Run 3	AVG
1	15	182.00	168.00	170.00	173.33
2	30	402.00	515.00	437.00	451.33
3	45	478.00	434.00	392.00	434.67
4	60	204.00	262.00	287.00	251.00
5	75	151.00	203.00	187.00	180.33
6	90	110.00	121.00	157.00	129.33
7	105	63.90	71.90	67.40	67.73
8	120	96.80	59.90	61.00	72.57
9	135	46.90	66.40	53.00	55.43

H5-W12-25

Sample	Seconds	Turbidity Level			
		Run 1	Run 2	Run 3	AVG
1	15	16.00	16.70	22.40	19.55
2	30	105.00	108.00	114.00	111.00
3	45	34.10	36.60	41.00	38.80
4	60	16.60	18.90	33.50	26.20
5	75	16.90	19.60	34.30	26.95
6	90	14.20	16.40	29.10	22.75
7	105	15.60	6.97	24.60	15.79
8	120	13.00	6.65	11.50	9.08
9	135	7.33	5.59	10.40	8.00

UP-50

Sample	Seconds	Run 1	Run 2	Run 3	Run 4	Run 5	Run 6	AVG
					Turbidity Level			
1	15	156.00	664.00	554.00	338.00	412.00	425.00	424.83
2	30	896.00	854.00	1014.00	808.00	989.00	914.00	912.50
3	45	86.60	73.30	123.00	88.00	101.00	155.00	104.48
4	60	89.30	88.00	144.00	55.00	88.00	260.00	120.72
5	75	46.70	66.70	108.40	78.60	89.00	101.00	81.73
6	90	77.40	56.30	77.10	84.20	56.60	147.00	83.10
7	105	50.00	46.70	57.10	82.50	65.10	47.90	58.22
8	120	19.30	70.10	46.10	54.30	46.80	77.30	52.32
9	135	18.50	51.50	76.40	25.70	45.80	55.70	45.60

UP-25

Sample	Seconds	Run 1	Run 2	Run 3	AVG
			Turbidity Level		
1	15	36.20	22.20	14.80	24.40
2	30	156.00	62.00	76.20	98.07
3	45	28.40	48.30	12.00	29.57
4	60	37.60	33.90	13.80	28.43
5	75	18.50	19.90	22.90	20.43
6	90	8.66	24.90	15.10	16.22
7	105	9.15	18.20	9.33	12.23
8	120	11.00	15.90	9.63	12.18
9	135	18.30	13.50	7.73	13.18

APPENDIX C - PARTICLE SIZE DISTRIBUTION DATA

H8-W6-50 30 seconds	Size (µm)	% Volume In
	0.01	0
	0.0123	0
	0.015	0
	0.0184	0
	0.0226	0
	0.0277	0
	0.0339	0
	0.0415	0
	0.0509	0
	0.0624	0
	0.0765	0
	0.0937	0
	0.115	0
	0.141	0
	0.173	0
	0.211	0
	0.259	0
	0.318	0
	0.389	0
	0.477	0
	0.585	0
	0.717	0.14
	0.878	0.32
	1.08	0.36
	1.32	0.41
	1.62	0.55
	1.98	0.75
	2.43	1.01
	2.98	1.27
	3.65	1.6
	4.47	1.04
	5	0.95

Size (µm)	% Volume In
5.48	2.44
6.72	3.14
8.23	3.94
10.1	5.04
12.4	6.29
15.2	7.43
18.6	8.39
22.8	8.67
27.9	8.28
34.2	7.24
41.9	5.87
51.4	4.26
63	3.03
77.2	1.97
94.6	1.3
116	0.83
142	0.49
174	0.28
213	0.15
262	0.15
321	0.24
393	0.41
481	0.61
590	0.88
723	1.14
886	1.4
1090	1.62
1330	1.73
1630	1.66

H8-W6-50 60 seconds	Size (µm)	% Volume In
	0.01	0
	0.0123	0
	0.015	0
	0.0184	0
	0.0226	0
	0.0277	0
	0.0339	0
	0.0415	0
	0.0509	0
	0.0624	0
	0.0765	0
	0.0937	0
	0.115	0
	0.141	0
	0.173	0
	0.211	0
	0.259	0
	0.318	0
	0.389	0
	0.477	0
	0.585	0
	0.717	0
	0.878	0
	1.08	0
	1.32	0
	1.62	0.09
	1.98	0.14
	2.43	0.19
	2.98	0.24
	3.65	0.3
	4.47	0.19
	5	0.18

Size (µm)	% Volume In
5.48	0.45
6.72	0.58
8.23	0.74
10.1	0.96
12.4	1.23
15.2	1.5
18.6	1.79
22.8	1.97
27.9	2.05
34.2	1.98
41.9	1.8
51.4	1.46
63	1.08
77.2	0.62
94.6	0.23
116	0
142	0
174	0
213	0
262	0
321	0
393	0
481	0
590	0
723	0
886	0
1090	0
1330	0
1630	0

H8-W6-50 120 seconds	Size (µm)	% Volume In
	0.01	0
	0.0123	0
	0.015	0
	0.0184	0
	0.0226	0
	0.0277	0
	0.0339	0
	0.0415	0
	0.0509	0
	0.0624	0
	0.0765	0
	0.0937	0
	0.115	0
	0.141	0
	0.173	0
	0.211	0
	0.259	0
	0.318	0
	0.389	0
	0.477	0
	0.585	0
	0.717	0
	0.878	0
	1.08	0
	1.32	0
	1.62	0.03
	1.98	0.12
	2.43	0.16
	2.98	0.2
	3.65	0.25
	4.47	0.16
	5	0.15

Size (µm)	% Volume In
5.48	0.37
6.72	0.47
8.23	0.58
10.1	0.73
12.4	0.92
15.2	1.11
18.6	1.31
22.8	1.45
27.9	1.53
34.2	1.53
41.9	1.46
51.4	1.29
63	1.07
77.2	0.75
94.6	0.42
116	0.1
142	0
174	0
213	0
262	0
321	0
393	0
481	0.01
590	0.61
723	2.63
886	6.57
1090	11.91
1330	16.13
1630	17.79

Raw Soil Pre-test	Size (µm)	% Volume In		Size (µm)	% Volume In
	0.01	0		5.48	2.05
	0.0123	0		6.72	2.35
	0.015	0		8.23	2.65
	0.0184	0		10.1	3.04
	0.0226	0		12.4	3.47
	0.0277	0		15.2	3.88
	0.0339	0		18.6	4.29
	0.0415	0		22.8	4.54
	0.0509	0		27.9	4.69
	0.0624	0		34.2	4.71
	0.0765	0		41.9	4.68
	0.0937	0		51.4	4.64
	0.115	0		63	4.64
	0.141	0		77.2	4.62
	0.173	0		94.6	4.55
	0.211	0		116	4.39
	0.259	0		142	4.18
	0.318	0		174	4.04
	0.389	0		213	3.98
	0.477	0		262	3.96
	0.585	0.06		321	3.8
	0.717	0.27		393	3.3
	0.878	0.39		481	2.55
	1.08	0.42		590	1.48
	1.32	0.48		723	0.59
	1.62	0.64		886	0.01
	1.98	0.85		1090	0
	2.43	1.1		1330	0
	2.98	1.32		1630	0
	3.65	1.56			
	4.47	1.83			

UP-50 30 seconds	Size (µm)	% Volume In
	0.01	0
	0.0123	0
	0.015	0
	0.0184	0
	0.0226	0
	0.0277	0
	0.0339	0
	0.0415	0
	0.0509	0
	0.0624	0
	0.0765	0
	0.0937	0
	0.115	0
	0.141	0
	0.173	0
	0.211	0
	0.259	0
	0.318	0
	0.389	0
	0.477	0
	0.585	0.04
	0.717	0.25
	0.878	0.43
	1.08	0.49
	1.32	0.55
	1.62	0.74
	1.98	1
	2.43	1.34
	2.98	1.68
	3.65	2.08
	4.47	2.54

Size (µm)	% Volume In
5.48	2.99
6.72	3.62
8.23	4.29
10.1	5.2
12.4	6.23
15.2	7.2
18.6	8.09
22.8	8.49
27.9	8.43
34.2	7.88
41.9	7.07
51.4	6.03
63	5.09
77.2	3.96
94.6	2.72
116	1.4
142	0.17
174	0
213	0
262	0
321	0
393	0
481	0
590	0
723	0
886	0
1090	0
1330	0
1630	0

UP-50 60 seconds	Size (µm)	% Volume In		Size (µm)	% Volume In
				5.48	2.05
	0.01	0		6.72	2.52
	0.0123	0		8.23	3.07
	0.015	0		10.1	3.87
	0.0184	0		12.4	4.87
	0.0226	0		15.2	5.93
	0.0277	0		18.6	7.13
	0.0339	0		22.8	7.97
	0.0415	0		27.9	8.52
	0.0509	0		34.2	8.55
	0.0624	0		41.9	8.19
	0.0765	0		51.4	7.46
	0.0937	0		63	6.69
	0.115	0		77.2	5.74
	0.141	0		94.6	4.66
	0.173	0		116	3.34
	0.211	0		142	1.73
	0.259	0		174	0.34
	0.318	0		213	0
	0.389	0		262	0
	0.477	0		321	0
	0.585	0		393	0
	0.717	0.11		481	0
	0.878	0.27		590	0
	1.08	0.32		723	0
	1.32	0.37		886	0
	1.62	0.49		1090	0
	1.98	0.66		1330	0
	2.43	0.89		1630	0
	2.98	1.12			
	3.65	1.39			
	4.47	1.75			

UP-50 120 Seconds	Size (μm)	% Volume In
	0.01	0
	0.0123	0
	0.015	0
	0.0184	0
	0.0226	0
	0.0277	0
	0.0339	0
	0.0415	0
	6+0.0509	0
	0.0624	0
	0.0765	0
	0.0937	0
	0.115	0
	0.141	0
	0.173	0
	0.211	0
	0.259	0
	0.318	0
	0.389	0
	0.477	0
	0.585	0
	0.717	0.07
	0.878	0.2
	1.08	0.25
	1.32	0.29
	1.62	0.38
	1.98	0.51
	2.43	0.69
	2.98	0.89
	3.65	1.12
	4.47	1.4

Size (μm)	% Volume In
5.48	1.67
6.72	2.08
8.23	2.59
10.1	3.37
12.4	4.41
15.2	5.54
18.6	6.8
22.8	7.69
27.9	8.3
34.2	8.44
41.9	8.2
51.4	7.57
63	6.88
77.2	6.07
94.6	5.29
116	4.33
142	2.96
174	1.63
213	0.38
262	0
321	0
393	0
481	0
590	0
723	0
886	0
1090	0
1330	0
1630	0